Odd Ivar Levik

Thermophysical and Compositional Properties of Natural Gas Hydrate

Thesis submitted in partial fulfillment
of the requirements for the degree of
Doktor Ingeniør of the
Norwegian University of Science and Technology
Department of Petroleum Engineering and Applied Geophysics

September 2000

Abstract

Thermophysical properties (dissociation enthalpy, heat capacity, metastability) and compositional properties (hydrate number, free water and fractionation) of natural gas hydrate were studied experimentally on samples that contained large amounts of ice. Methods for continuous hydrate production and sampling, and for quantification of the properties were developed. Hydrate was produced from a natural gas of ethane (5 %mol) and propane (3 %mol) in methane.

A low temperature scanning calorimetry method was developed to measure dissociation enthalpy, heat capacity, hydrate number and free water (ice). During the analysis, the hydrate samples were pressurized to 1.7 MPa with methane and the system operated between the hydrate equilibrium curves of methane and the hydrate forming natural gas. A sample conditioning procedure eliminated thermal effects of desorption as the ice melted. Desorption occurred since the samples were produced and refrigerated to 255 K under a natural gas pressure of 6-10 MPa, but were analyzed and melted under a methane pressure of 1.7 MPa.

A low temperature isothermal calorimetry method was developed to quantify the metastability properties. Metastability was confirmed for temperatures up to 268 K and quantified in terms of the low dissociation rate.

Fractionation data were obtained in the range 3.0 to 7.5 MPa and for subcoolings between 2 and 16 K. High pressure and large subcooling is desirable to suppress fractionation. A fractionation model was proposed. The model coincides with the van der Waals-Platteeuw model for zero subcooling. No fractionation is assumed for hypothetical hydrate formation at infinite driving force (subcooling). Between these two extremes an exponential term was used to describe the fractionation. The model predicted fractionation with an accuracy of about 1%abs corresponding to 1-10%rel.

Acknowledgments

First of all I thank my supervisor, Professor Jón Steinar Gudmundsson, who gave me the opportunity to learn and with whom I discussed matters far more important than hydrates.

Then I thank Vibeke Andersson, my friend and fellow Dr.Ing. student during the last few years, who always knew what I did not.

Associate Professor Mahmut Parlaktuna, who came from the Middle East Technical University, I thank for all his help in laboratory, for sharing his experiences and for saying "let's do it".

I thank Professor Jean-Pierre Monfort of the National School of Chemical Engineering in Toulouse for his countless efforts in my interest and for setting the standard of hospitality.

Engineers Ivar Bjerkan, Gunnar Bjerkan, Åge Sivertsen and Roger Overå at the workshop played important roles, especially during construction periods, but also in everyday operations.

I also thank other members of Professor Gudmundsson's group, notably Dr.Ing. student Elling Sletfjerding and Post-Doc. fellow Ismail Durgut, who touched the keyboard in all the secret places, so that the computer ERROR messages went away for a while. Dr.Ing. student Aftab Ali Khokhar too was a member of our group, but carried out most of his work at the Colorado School of Mines. Our discussions always brought me one step ahead.

Dr. William R. (Bill) Parrish of Phillips Petroleum is sincerely thanked for support and valuable discussions on calorimetry.

Mr. Jean-Louis Peytavy of Elf E&P in Pau gave valuable help by providing necessary equipment to the fractionation laboratory.

Dr.Ing. Geir Ultveit HaUgEn was sort of affiliated to the Gudmundsson group too, in the evenings. Good for me.

Aker Engineering is especially thanked for the three-year stipend I received to study at NTNU. TOTAL Norge is especially thanked for the one-year stipend I received to study at the National School of Chemical Engineering in Toulouse.

The present work was given financial support by the partners of the *NGH at NTNU* joint industry project; Aker Engineering, Amerada-Hess, Atlantic Richfield, Fortum Petroleum, Phillips Petroleum, Shell International Exploration & Production and TOTAL Norge. The Nordic Energy Research Program gave me the opportunity to visit the Technical University of Denmark.

But still I would have reached nowhere without my parents Maj and Martin who supported, encouraged and loved me whatever I wanted to do (Well..., I was not allowed to eat *Karlson's Glue* and to dive from "M/T Fenborg" in the Pacific Ocean). I will try to be an equally good father for little Annastina. I thank my brother Anders for cheering me up and for the good talks and for all those tunes and lyrics.

And to my wife Evy: Thank you for your concern and patience - I look forward to catching up.

We did have some real good times
I remember them

Quotation from one of Anders' songs

Contents

List of Tables

List of Figures

Nomenclature

Latin letters

a	Clausius-Clapeyron slope, $a \equiv \frac{-\Delta \ln P}{\Delta 1/T}$ (K)
$a_0, a_1, \ldots$	empirical constants
B	second virial coefficient (m^3/mol)
C	normalized concentration (%mol)
$C_{i,diss}$	normalized concentration of component i in the gas liberated from a completly dissociated hydrate sample (%mol)
$C_{i,reac}$	normalized concentration of component i in the reactor gas pocket (%mol)
C_{ji}	Langmuir constant for i-type component in j-type cage (Pa^{-1})
c_p	specific heat capacity at constant pressure (J/gK, J/molK)
D	diameter (m)
f	amount of free water (%mass)
f	fugacity (Pa)
G	Gibbs free energy (J/mol)
ΔH_{diss}	enthalpy of dissociation (J)
Δh_{diss}	specific enthalpy of hydrate dissociation (J/kg, J/mol)
Δh°_{diss}	standard (1 atm) enthalpy of hydrate dissociation (J/mol)
Δh_{vap}	specific enthalpy of vaporization (J/mol)
K	calorimeter calibration constant (J/s^2K)
k	empirical fractionation model constant (K)
L	lenght (m)
M	molecular mass (g/mol)
m	mass (kg)
n	hydrate number (-)
n	amount of substance (mol)
n_g	amount of gas in hydrate (mol)
n_{ideal}	hydrate number when all cages are occupied (-)

n_w	amount of hydrate water in a hydrate sample (mol)
$n_{w,ice}$	amount of (free) water present as ice in a hydrate sample (mol)
$n_{w,tot}$	total amount of water (hydrate water and free water) in a hydrate sample (mol)
$\dot{q}$	specific heat flow (W/kg)
Q	accumulated heat (J)
$\dot{Q}$	heat flow (W)
R	gas constant, $R = 8.314$ J/molK
r	radius (m)
r_{diss}	rate of dissociation (1/s)
t	time (s)
T	temperature (K)
ΔT	subcooling, driving force (K)
v	molar volume (m^3/mol)
V	volume (m^3)
x	mole fraction (-)
y	mole fraction (-)
z	compressibility factor (-)

Greec letters

α	degree of dissociation (-)
λ	thermal conductivity (W/Km)
μ	chemical potential (J/mol)
μ_h	chemical potential of hydrate (J/mol)
μ_β	chemical potential of hypothetical empty hydrate lattice (J/mol)
ν_j	number of j-type cages per water molecule (-), j=(l,s)
ρ	mass density (kg/m^3)
θ_i	fraction of occupied cages that are occupied by i-type guests
θ_j	fraction of j-type cages occupied (-), j=(l,s)
θ_{ji}	fraction of j-type cages occupied by i-type guests

Subscripts

abs	absolute
amb	ambient
$diss$	dissociation
eq	equilibrium
exp	experimental

f	final
g	gas
H	hydrate
h	hydrate
i	initial
i	component type
j	cage type
L	liquid
l	large cage
p	pressure is constant
rel	relative
s	small cage
tot	total
w	water
1.7MPa	pressure is 1.7 MPa

Acronyms and abbrevations

C1	methane
C2	ethane
C3	propane
CAPEX	CAPital EXpenditures
CSMHYD	Colorado School of Mines HYDrate code
CSTR	Continuous Stirred Tank Reactor
DSC	Differential Scanning Calorimeter
DSC	Differential Scanning Calorimetry
G	Guest molecule
g	gas
h	hydrate
h-l-g	hydrate-liquid-gas
h-i-g	hydrate-ice-gas
NG	Natural Gas
NGH	Natural Gas Hydrate
NTNU	Norwegian University of Science and Technology
RPM	Rotations Per Minute (min^{-1})
sH	hydrate structure H
sI	hydrate tructure I
sII	hydrate tructure II
w	water

Chapter 1

Introduction

1.1 Background

1.1.1 Storage and Transport of Natural Gas Using Hydrate

The most important technologies for storage and transport of natural gas (NG) are liquefied natural gas (LNG), pipelines, compressed natural gas (CNG) and conversion of the gas to handle it in the form of more valuable products, such as synthetic crude (syncrude) or methanol. Reinjection of the gas for later production is also an alternative. These are proven technologies.

The present work is related to the development of hydrate technology for storage and transport of natural gas. Storage of natural gas in the form of hydrate at elevated pressure was proposed in the 1940's (Berecz and Balla-Achs 1983). Gudmundsson (1990) proposed storage at ambient pressure and not far below 0 °C, which are conditions where the hydrate is thermodynamically unstable. The hydrate may be in the form of a powder (dry hydrate concept) or dispersed in condensate or crude to form a pumpable hydrate-in-oil slurry (hydrate slurry concept) (Gudmundsson et al. 1998).

Natural gas hydrate (NGH) contains up to 182 Sm^3 NG per m^3 hydrate, or 182 Sm^3/m^3. It has been demonstrated that natural gas hydrate with ice can be stored at -15 °C at ambient pressure without a significant loss of gas. At these conditions of pressure and temperature the hydrate is thermodynamically unstable, but is regarded metastable (Gudmundsson et al. 1994).

Natural gas hydrate may be produced at 60-90 bar and 2-10 °C. The hydrate can then be cooled to for example −15 °C, while an elevated pressure is maintained. Next, the system is depressurized to ambient pressure while appreciable temperature increase is not allowed. The hydrate is then stored and transported under ambient pressure and about −15 °C. Upon heating above 0 °C, the hydrate readily dissociates to yield natural gas and water. The hydrate technology has two important characteristics:

Ambient pressure. Storage and transport of natural gas in the form of hydrate is carried out at ambient pressure. This gives large savings, since pressure equipment has relatively high capital expenditures (CAPEX). Maintenance and operation of high pressure equipment are more involved and the equipment is heavy, so the operation expenditures are high too, compared to unpressurized operation.

No active cooling. The hydrate is cooled down to the storage temperature in the hydrate production plant. During storage and transport it is not necessary to actively provide cooling. Passive insulation is sufficient. This permits cheap systems for storage and transport units.

A hydrate chain with production, transport and melting of hydrate is technically and economically feasible (Gudmundsson and Børrehaug 1996). The process schemes include traditional units such as stirred tank reactors, heat exchangers and pumps. It is believed that a hydrate process can be designed using mostly standard equipment. Hydrate specific technology may be necessary in hydrate separation for the dry hydrate concept.

When hydrate technology becomes commercially available it will be an economic question which storage and transport solution is preferred in each case. But as examples, comparing in terms of CAPEX per transport distance, the hydrate chain is cheaper than the pipeline option except for short transport distances (< 1000 km) and cheaper than the syncrude option except for very long transport distances (> 12000 km). Hydrate technology is cheaper than LNG technology regardless of distance (Gudmundsson et al. 1998).

1.1.2 Emerging Scenarios

Stranded gas is a collective term which includes gas from fields that are small or remote and smaller amounts of associated gas in oil fields. Stranded gas

is expected to play a more important role in the future as focus is put on marginal fields. Efficient ways to transport this gas to the market will become important.

The growing interest in energy sources that are environmentally friendly compared to fuel oil and coal makes gas attractive. But to develop marginal fields it is necessary to have cheap and effective technical solutions for the storage and transport. The present work is a contribution in this respect. Focus is put on the fundamental properties of natural gas hydrate.

1.2 Topics

1.2.1 Problem Statements

The major contribution of the present work was construction of laboratories and development of experimental techniques. However, these activities sprung out from some fundamental topics: *Thermophysical and compositional properties* of NGH, such as specific heat capacity, heat of dissociation, hydrate number and amount of free water or ice (Chapters 2 and 6). *Metastability* at ambient pressure and below 0 °C is a thermophysical property that is treated separately (Chapters 3 and 7). *Fractionation*, that is how different components partition between the hydrate phase and the gas phase, is related to the compositional properties and is treated separately too (Chapters 4 and 8).

Thermophysical and compositional properties have to be measured. It is desirable to correlate thermophysical properties to hydrate composition and in turn to the hydrate production conditions. Developing the method to measure thermophysical and compositional properties is a key issue in the present work. The starting point was that calorimetry could probably be used, referring to the numerous works by Handa, for example (Handa 1988b). Calorimetric analysis of natural gas hydrate samples that contain a lot of free water (ice) is difficult. An important task in the present work was to develop a method to do such analyses.

Metastability as a phenomenon needs to be understood better. The role of ice and how it affects metastability is an important issue. It is also necessary to expand the quantitative knowledge about metastability. It is desirable to map the metastability region; that is, to correlate the metastable behavior to storage conditions.

Fractionation is not desirable in the hydrate process, but can not be completely avoided (Holder and Manganiello 1982). It is necessary to have more quantitative knowledge about how hydrate production conditions, primarily pressure and temperature, affect the fractionation.

Method development is a major challenge in the present work. This includes production, separation, sampling and analysis of hydrate at elevated pressures. The main challenge was to develop the method to determine thermophysical and compositional properties.

The present work could have relevance for in situ hydrates in permafrost regions and hydrate plugs in pipelines. Permafrost hydrate is subject to conditions that are not very different from storage conditions in the dry hydrate concept. Hydrate plugs may undergo Joule-Thompson cooling to form a mixture of hydrate and ice which resembles the composition of the samples used in this work.

Dry samples of sII hydrate with ice was used in the present work. Andersson (1999) studied rheological properties of hydrate slurries. Khokhar (1998) studied storage properties of sH hydrate and reported that hydrate promotors act as hydrate stabilizers. It was also found that below 0 °C there is a satisfactory agreement between estimated hydrate dissociation enthalpies from the Clausius-Clapeyron equation and calorimetric measurements.

1.2.2 Scopes of Work

The scopes of the present work were:

- Develop equipment and methods for continuous production and sampling of NGH (Sections 5.2 and 6.2).
- Develop a calorimetric method to determine thermophysical properties; enthalpy of dissociation and specific heat capacity, and compositional properties; hydrate number and amount of free water (Section 6.3).
- Develop equipment and methods to quantify metastability properties of NGH at different temperatures and compositions of the surrounding atmosphere (Sections 5.5 and 7.2).
- Develop equipment and a method to quantify the effect of driving force on fractionation in NGH formation (Sections 5.6 and 8.2).

Chapter 2

Thermal and Compositional Properties - Literature Study

This chapter covers hydrate composition and differential scanning calorimetry (DSC). It is shown how DSC may be used to determine thermal properties; specific enthalpy of hydrate dissociation (Δh_{diss}), hydrate number (n), amount of free water (f) and specific heat capacity (c_p). Literature measurements are reviewed, as are existing models and correlations. Enthalpy of hydrate dissociation is given broad attention. Composition of the hydrated gas is treated separately in Chapter 4.

2.1 Hydrate Composition

Sloan (1998, Chapter 2) gave a summary of hydrate compositional properties. Hydrates are crystalline solids. The crystal lattice is made of hydrogen bonded water molecules. The water molecules are oriented such that they form polyhedra, or cages, which share faces. Only a few kinds of cages may form. These arrange into three different structures known as structure I (sI), structure II (sII) and structure H (sH). sI is built from two different cages. The smallest is made from twelve pentagonals, a 5^{12} cage. The largest is made from twelve pentagons and two hexagons, a $5^{12}6^2$ cage. In a sI unit cell there are two 5^{12} cages and six $5^{12}6^2$ cages. sII too is made from two different cages. The smallest is the 5^{12} cage. The largest is made from twelve pentagons and four hexagons, a $5^{12}6^4$ cage. In a sII unit cell there

are sixteen 5^{12} cages and eight $5^{12}6^4$ cages. Cages in sI and sII are illustrated in Figure 2.1. sI hydrate has 46 water molecules per unit cell while sII hydrate has 136. sH is made from three different cages. The smallest is the 5^{12} cage. The medium sized cage is made from three squares, six pentagons and three hexagons, a $4^3 5^6 6^3$ cage. The largest is made from five pentagons and eight hexagons, a $5^{12}6^8$ cage. In a sH unit cell there are three 5^{12} cages, two $4^3 5^6 6^3$ cages and two $5^{12}6^8$ cages (Sloan 1998).

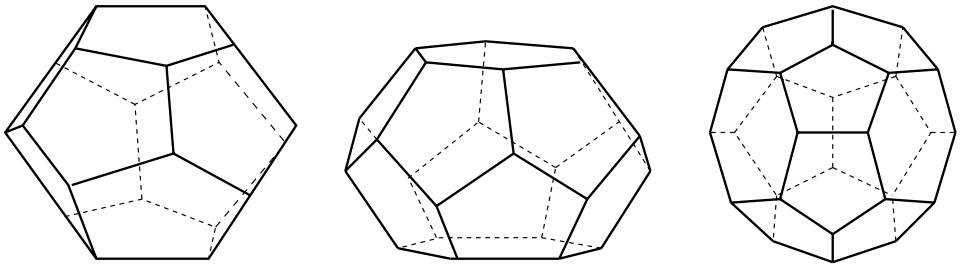

Figure 2.1: The different cages in sI and sII hydrate. (a) the 5^{12} cage, (b) the $5^{12}6^2$ cage and (c) the $5^{12}6^4$ cage (Sloan 1998).

The cages may be empty or contain one guest molecule.[1] An empty hydrate structure with no guest in any of the cages is hypothetical since it will collapse, or actually never form. A certain portion of the cages must contain a guest molecule to stabilize the structure. The guest molecules and the water molecules interact via van der Waals forces. The guest must be non-polar and small enough to fit into a cage. For sI and sII this limits the potential alkane hydrate formers to methane, ethane, propane and isobutane. Normal-butane is too large, but it may form sH hydrate. Other hydrate formers are Ar, Kr, N_2, O_2, Xe, H_2S and CO_2. sI and sII may form in binary systems (one guest in addition to water). sH is different since it only forms in ternary (or higher) systems. Examples of sI formers are CH_4 and CO_2. Examples of sII formers are C_3H_8 and iso-C_4H_{10}. Hydrates with only one type of guest molecule are called single hydrates. If there are more than one type of guest the hydrate is called a mixed hydrate. sH is always a mixed hydrate. sI and sII may be mixed or single hydrates.

Because of size differences between guests and cages it is not possible for just any guest to stabilize just any cage. If the diameter of a guest is larger

[1] There are rare cases with two guests per cage.

than the diameter of a cage there is no room for the guest. If the diameter of the guest is less than about a fraction 0.76 of the cage diameter, then the attractive forces between the guest molecule and the water molecules in the lattice are too small to contribute to the stabilization. This applies to He, H_2 and Ne which do not form hydrate. A selection of diameter ratios is found in Table 2.1. It is seen that methane may enter both cages in sI and the smallest cage in sII. Methane is too small to stabilize the largest sII cage. Ethane enters the largest cages in both sI and sII. Propane is so large it can only fit into the largest sII cage, just as iso-butane. Because propane and iso-butane only fit into the largest sII cage, natural gases will usually form sII. Molecules with a diameter less than 0.35 nm are too small to form hydrate. If the diameter is larger than 0.75 nm the molecule is too large.

Table 2.1: Ratios of guest diameter to cage diameter for selected sI and sII hydrate formers, extracted from Sloan (1998, p. 47). Superscript * indicates the cage(s) occupied in simple hydrates.

Guest	Guest diameter (nm)	sI small	sI large	sII small	sII large
CH_4	0.436	0.855*	0.744*	0.868	0.655
C_2H_6	0.550	1.08	0.939*	1.10	0.826
C_3H_8	0.628	1.23	1.07	1.25	0.943*
i-C_4H_{10}	0.650	1.27	1.11	1.29	0.976*

The hydrate number, n, is defined as the ratio of water molecules to gas molecules in the hydrate, $n = n_w/n_g$. If all cages in a hydrate structure were occupied then the ideal hydrate numbers would result; $5\frac{3}{4}$ and $5\frac{2}{3}$ for sI and sII, respectively. If all cages in a sII hydrate formed from a natural gas were occupied, then each volume of hydrate would contain 182 volumes of gas at standard conditions, 182 Sm^3/m^3 at 1 bar and 15 °C. But gas hydrates are non-stoichiometric, meaning that not all of the cages are occupied. In addition, the fraction of cages that are occupied is system dependent. It may well be that 95% of the largest cages are occupied while only 50% of the smallest cages are occupied. To calculate the hydrate number from the fractional occupancies, the following equations may be used:

$$n_{sI} = \frac{46}{2\theta_s + 6\theta_l} \tag{2.1}$$

$$n_{sII} = \frac{136}{16\theta_s + 8\theta_l} \tag{2.2}$$

van der Waals and Platteeuw (1959) developed a statistical thermodynamic model of the fractional occupancies of different guests in different cages. The reduction in chemical potential, $\Delta\mu$, when hydrate forms may be expressed as:

$$\Delta\mu = \mu_\beta - \mu_h = -RT(\nu_s \ln(1-\theta_s)) - RT(\nu_l \ln(1-\theta_l)) \qquad (2.3)$$

where μ_β is the chemical potential of the hypothetical empty lattice and μ_h is the chemical potential of the hydrate with guests at the temperature T. ν_s and ν_l are constants equal to the number of small and large cages, respectively, per water molecule in the lattice. $\nu_s = \frac{16}{136} = \frac{2}{17}$ and $\nu_l = \frac{8}{136} = \frac{1}{17}$ for sII hydrate. θ_s and θ_l are the fractional occupancies of small and large cages, respectively. According to the model, if θ_s or θ_l approaches unity, then the chemical potential reduction becomes infinite. This is not possible, and consequently a fractional occupancy less than 1 of both cages is predicted (Holder and Manganiello 1982).

An important question is; what is the smallest hydrate number or the largest fractional cage occupancy that is possible in practical operations? It is shown later (Table 2.3, page 16) that a hydrate number of 5.95 has been measured for sII natural gas hydrate. The fractional cage occupancy is then 5.67/5.95=0.953 and the gas content is 173 Sm^3/m^3. Handa (1986c) produced methane hydrate (sI) and reported a hydrate number of 6.00±0.01. The fractional cage occupancy is then 5.75/6.00=0.958. Handa (1986a) measured hydrate numbers for single hydrates of Kr (n=6.10) and Xn (n=5.90). The ideal hydrate numbers are 5.67 and 5.75 for Kr and Xn, respectively (Sloan 1998). The fractional occupancies then become 0.930 for Kr and 0.975 for Xn. In these works by Handa, efforts were made to obtain high cage occupancies. Irrespective of the hydrate former, it seems that a fractional occupancy of about 0.95 must be regarded a high value. One way to reduce the hydrate number and increase the cage occupancy is to produce the hydrate under excess pressure (Handa 1986a).

2.2 Heat Flow DSC

Tian (1923) constructed a calorimeter with two main advantages; high sensitivity towards temperature changes ($< 10^{-4}$ K) and the possibility of isothermal operation. Calvet and Prat (1963) modified Tian's calorimeter. Important developments were the ability to do correct measurement of the heat flow without the necessity of stirring and that two calorimeter cells were used instead of only one. This made it possible to determine a

differential signal, hence the term differential scanning calorimetry (DSC). This type of calorimeter is often called a Tian-Calvet heat flow calorimeter and is illustrated in Figure 2.2.

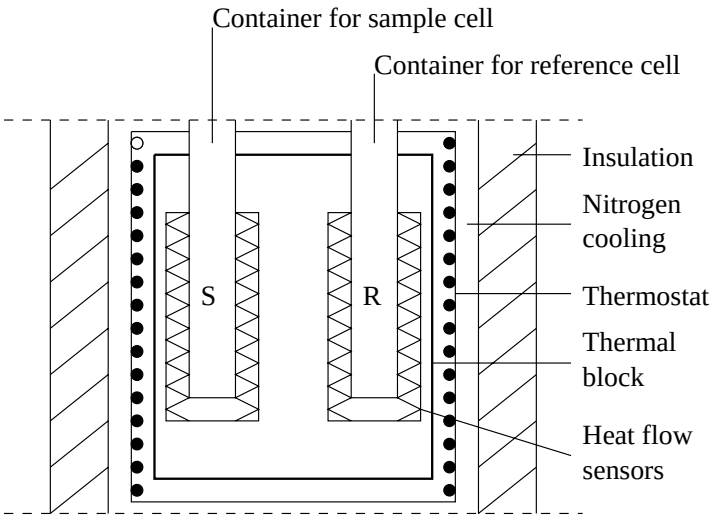

Figure 2.2: Sketch with the main items of a Tian-Calvet heat flow calorimeter (not to scale).

The two cells are placed in a thermal block. One of the cells is the sample cell. The other is the reference cell, which may contain a reference sample or be empty. Both cells are surrounded by up to 1000 heat flow sensors. The heat flow signal for both cells are registered. The output heat flow is the difference between the signals of the two cells, hence the term *differential*. The cells are thermally decoupled, i.e. heat is only transfered between a cell and the thermal block - there is no heat flow from one cell to the other. For calorimeters with cylinder type cells (disc type is also available) the sample volume is relatively large, which may be an advantage. But the thermal interia is large too and quick heating or cooling is not possible.

It is impossible to make two identical cells, so a portion of the total signal is due to the difference between the cells. This portion may be relatively small and ignored, or it may be corrected by subtracting the signal of a blank run, where both cells were empty. This type of correction is relevant for very precise measurements, like when the signal from the reacting system is weak (Höhne et al. 1996).

A DSC curve (thermogram) typically has the heat flow, $\dot{Q}$ (W), on the ordinate and time on the abscissa. Temperature may be plotted along a secondary ordinate axis or on the abscissa instead of time, see Figure 2.3. The differential heat flow is proportional to the temperature difference, ΔT, between the sample cell end the reference cell:

$$\dot{Q} = K\Delta T \tag{2.4}$$

where K is a calibration constant. The area of a peak is the area between the base line and the heat flow signal. The area, Q (J), is found by integrating $\dot{Q}$ over time:

$$Q = \int \dot{Q} dt = K \int \Delta T \, dt \tag{2.5}$$

The baseline is not measured in the peak range. Thus, to integrate a peak, the baseline has to be interpolated over the temperature or time interval covered by the peak. The interpolated baseline is the line which in the range of a peak is constructed such that it connects the measured curve before and after the peak as if there was no peak. This is illustrated in Figure 2.3. It is desirable that the interpolated baseline accounts for any change in the heat capacity on the temperature interval of interest. It is not obvious how this can be done, but for a change of the baseline between initial and final temperatures T_i and T_f, respectively, a good approximation of the interpolated baseline, $\dot{Q}_{bl}$, is to assume that

$$\dot{Q}_{bl} = (1 - \alpha)\dot{Q}_{i_{ex}} + \alpha \dot{Q}_{f_{ex}} \tag{2.6}$$

where α is the degree of reaction or transition. $\dot{Q}_{i_{ex}}$ and $\dot{Q}_{f_{ex}}$ are the segments of the measured curve extrapolated into the peak range from the initial (i) and final (f) end, respectively. $\dot{Q}_{i_{ex}}$ and $\dot{Q}_{f_{ex}}$ need to be expressed as polynomials and these polynomials extrapolated into the peak range. The $\dot{Q}$ slopes in the points T_i and T_f should not differ very much (Höhne et al. 1996).

The enthalpy is equal to the (accumulated) heat for a process at constant pressure; $\Delta H = Q$. Specific enthalpy, Δh (J/mol), of a peak is found by dividing the total enthalpy change, ΔH (J), by the amount of substance, n (mol), thus $\Delta h = \frac{\Delta H}{n}$. Mass basis could also be used.

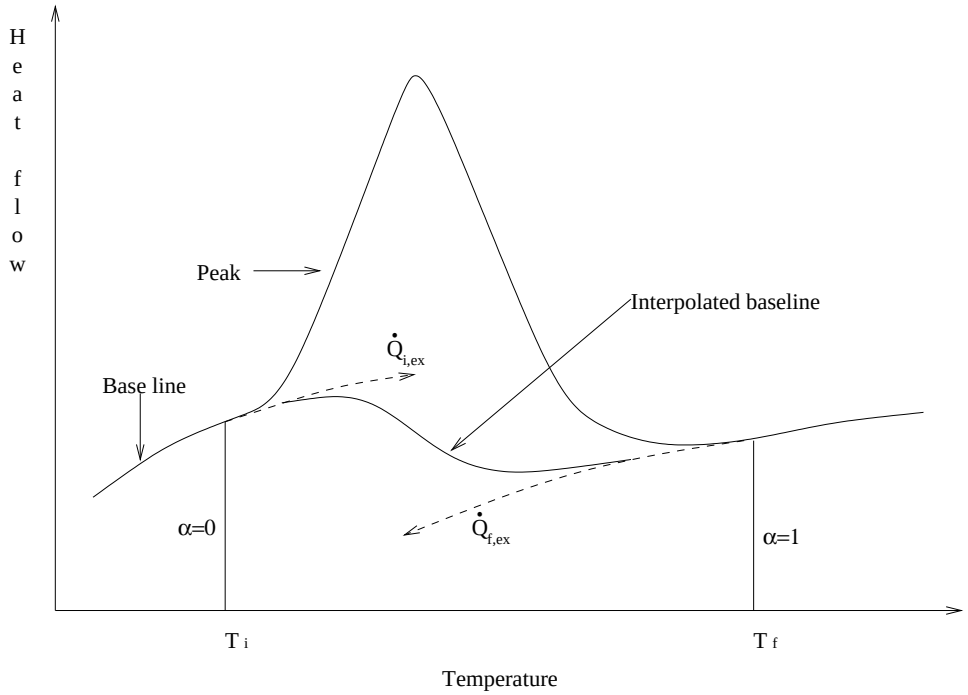

Figure 2.3: Construction of the baseline in the peak region (Höhne et al. 1996). α is the degree of reaction of conversion.

The specific heat capacity at constant pressure, c_p (J/gK), may be determined by calorimetry in different ways. The classical procedure is to heat the sample at a constant rate over the temperature interval of interest. The resulting curve is corrected by subtracting a blank run. It is then possible to express the corrected enthalpy change, ΔH (J), by a best fit expression. By definition, c_p is the derivative with respect to temperature of this fitted expression when referred to the amount of sample. On mole basis (Höhne et al. 1996):

$$c_p = \frac{d\Delta H}{ndT} = \frac{d\Delta h}{dT} \tag{2.7}$$

2.3 Dissociation Enthalpy, Hydrate Number and Free Water Measurements by Calorimetry

The dissociation of hydrate may follow two schemes:

$G \cdot nH_2O(h) = nH_2O(s) + G(g)$ for $T < 273.15$ K

or

$G \cdot nH_2O(h) = nH_2O(l) + G(g)$ for $T > 273.15$ K

where G is the guest gas. In addition the hydrate may contain free water (ice) which melts:

$H_2O(s) = H_2O(l)$

The difference in enthalpy between the two first reactions is assumed to be the enthalpy of ice melting (Handa 1986a). After dissociation, there is also the possibility of gas desorption;

$G(aq) = G(g)$

The enthalpy of desorption does not contribute to the dissociation enthalpy. But it may become important when measuring apparent or overall enthalpies of consecutive processes.

Calorimetric methods are used to measure the specific enthalpy of hydrate dissociation, Δh_{diss}, in units J/mol or J/g. Such measurements are intimately related to the hydrate number (n) and the amount of free water (f) through the mass and energy balances. The measurements are difficult, since the hydrate system is reactive and since it is difficult to make hydrate samples which do not contain any free water. Still, there have been made a number of measurements on *single* hydrates. Few data are available for *mixed* hydrates, such as natural gas hydrate, and no reliable measurements of the *standard* enthalpy of natural gas hydrate dissociation, Δh°_{diss}, were found. This is an important motivation for the present work.

The Δh_{diss} units may seem ambiguous. To clarify, in the unit J/mol, "mol" refers to a base of 1 mol hydrate with the unit formula $G \cdot nH_2O$. Thus, a system which contains m moles of hydrate also contains m moles of hydrated gas. The molar mass of the hydrate is $M_G + 18n$ where M_G is the molar mass of the guest, n is the hydrate number, and 18 is the molar mass of water. In the unit J/g, "g" refers to a base of 1 g hydrate.

2.3.1 Measurements by Handa et al. (Δh°_{diss}, n and f)

Calorimetry Procedure

Handa et al. (1984) and Handa (1986a) described a Tian-Calvet heat flow calorimeter which was modified such that the sample could be pressurized with gas, see Figure 2.4. A calorimetric procedure was given to find h°_{diss}, n and f for single hydrates from xenon and krypton with 1 to 8 %mass of free water (ice). Two runs are necessary.

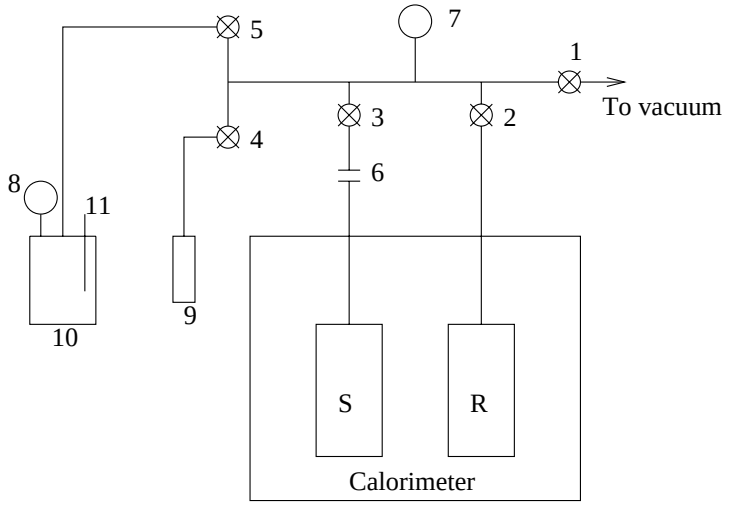

Figure 2.4: Block diagram of Handa's calorimeter (Handa 1986a). S and R: sample and reference cells. 1, 2, 3, 4 and 5: high-pressure high-vacuum valves. 6: High-pressure high-vacuum quick-connect-disconnect coupling. 7 and 8: Pressure transducers. 9: Gas cylinder. 10: Expansion chamber. 11: Thermometer.

In the first run the sample is heated from 270 K to about 275 K at a rate of $8.3{\cdot}10^{-4}$ K/s (0.05 K/min). The pressure is equal to the equilibrium pressure at about 277 K. The purpose is to melt any ice in the sample, to determine the amount of free water. Valve ⊗3 is open and ⊗2 is closed.

To prepare for the second run, the temperature is brought down to 78 K and the pressure reduced to less than 1 kPa. Valves ⊗3 and ⊗5 in Figure 2.4 are left open. The sample is then heated at a scanning rate of $2.8{\cdot}10^{-3}$ K/s (0.168 K/min) to 290 K while recording the system pressure and the tem-

perature in the expansion chamber (10). The purpose is to dissociate the hydrate. The large volume of the expansion chamber causes the pressure to stay low. This ensures smooth dissociation. When all of the hydrate is dissociated the pressure is usually between 80 and 100 kPa (Handa 1986a).

Raw Data Processing

The amount of hydrated gas, n_g, is calculated from PVT data obtained during the second run:

$$n_g = \frac{(P_f - P_i - P_w)(V_{tot} - V_w)}{RT_g + B(P_f - P_i - P_w)} \tag{2.8}$$

where P_f is the pressure at the end of the second run and P_i is the pressure just before dissociation started. P_w is the water saturation vapor pressure at the cell temperature T_c at the end of the second run. V_{tot} is the total system volume and V_w is the volume of liquid water in cell S (found by weighing as the water density is known). B is the second virial coefficient of the gas (Dymond and Smith 1980). T_g is the volume-weighted average temperature of the gas,

$$T_g = \frac{V_1 T_r + 0.5 V_2 (T_c + T_r) + T_c (V_S - V_w)}{V_{tot} - V_w} \tag{2.9}$$

where V_1 is the volume enclosed by valves $\otimes$1, $\otimes$2, $\otimes$3 and $\otimes$4 with $\otimes$5 open. T_r is the room temperature. The volume V_2 is enclosed by $\otimes$3 and the *top* of the sample cell (S). The temperature of the gas in V_2 was assumed to be the average of the cell temperature, T_c, and the room temperature, T_r. V_S is the volume of the sample cell. The effect on n_g because of gas absorbed by the water is negligible for Kr hydrate with 2-8 %mass ice and Xn hydrate with 1 %mass ice.

The amount of hydrate water, n_w, is found by subtracting the amount of free water, $n_{w,ice}$, found in the first run, from the total amount of water, $n_{w,tot}$, found by weighing after the second run:

$$n_w = n_{w,tot} - n_{w,ice} \tag{2.10}$$

The hydrate number is then calculated using:

$$n = \frac{n_w}{n_g} \tag{2.11}$$

Results

Results from Δh_{diss} and n measurements are collected in Table A.1. A selection of the more recent and reliable data at standard conditions (Δh°_{diss}) are given in Table 2.2. The measurements are accurate to about ±1%.

It is seen how the dissociation enthalpy is substantially higher for temperatures above 275.15 K than below this temperature. The explanation is that above 273.15 K the hydrate dissociates into gas and liquid water, while below it dissociates into gas and ice. Additional heat is required to form liquid water instead of ice.

Table 2.2: Standard (P=101,325 Pa) enthalpies of hydrate dissociation, Δh°_{diss}. The natural gas hydrate labeled NGH8 contained (%mol): methane (99.93), ethane (0.01), propane (0.01), iso-butane (0.05) and was retrieved during the Deep Star Drilling Project. Sample NGH9 was retrieved from the Gulf of Mexico and its Δh°_{diss} is only an estimate since the composition of the hydrate could not be determined precisely (Handa 1988b).

Guest	Δh°_{diss} kJ/mol	n -	T K	Remark	Reference
sI NGH8	17.50	$CH_4 \cdot 5.91H_2O$	273	h→i+g	(Handa 1988b)
sII NGH9	27.8-33.1	0-20 %mass ice	220-260	h→i+g	(Handa 1988b)
CH_4	18.13±0.27	6.00±0.01	160-210	h→i+g	(Handa 1986c)
C_2H_6	25.70±0.37	7.67±0.02	190-250	h→i+g	(Handa 1986c)
C_3H_8	27.00±0.33	17.0±0.1	210-260	h→i+g	(Handa 1986c)
i-C_4H_{10}	31.07±0.20	17 assumed	273.15	h→i+g	(Handa 1988a)
CH_4	54.19±0.28	6.00±0.01	273.15	h→w+g	(Handa 1986c)
C_2H_6	71.80±0.38	7.67±0.02	273.15	h→w+g	(Handa 1986c)
C_3H_8	129.2±0.4	17.0±0.1	273.15	h→w+g	(Handa 1986c)
i-C_4H_{10}	133.2	17 assumed	273.15	h→w+g	(Handa 1988a)

2.3.2 Other Measurements (Δh_{diss})

Maksimov (1996) reviewed a number of Russian publications and summarized works by Groisman (1985), Groisman and Savvin (1988) and Chersky et al. (1982). They made an adiabatic casing in which a measurement cell with constant heat supply was placed. Δh_{diss} were measured for sII NGH samples in the pressure range 1.1 to 14 MPa. The Δh_{diss} values are in the range 500 to 540 J/g for n in the range 5.95 to 6.7. In the present work these data were converted to cover the range 68.8 to 77.3 kJ/mol, see Table 2.3.

Table 2.3: Enthalpies of hydrate dissociation, Δh_{diss}, reproduced from Maksimov (1996). The data were originally published by Chersky et al. (1982) and Groisman (1985) at pressures of 1.1-14 MPa, i.e. not standard state, for the transition h→w+g. The composition of the samples are given in Table A.2.

Sample	Δh_{diss}(kJ/mol)	n	P(MPa)	T(K)
sII NGH1	77.3	6.7	1.1	273
sII NGH2	72.5	6.6	2.2	278
sII NGH3	72.1	6.3	4.1	283
sII NGH4	73.9	6.2	5.9	286
sII NGH5	70.9	6.1	7.6	288
sII NGH6	71.4	6.1	8.5	289
sII NGH7	68.8	5.95	14.0	293

Kobayashi and Lievois (1988) built a Tian-Calvet heat flow calorimeter which was specially designed to study hydrate. The cells were large, 1.158 dm^3. The cells featured magnetic stirrers. Methane hydrate was formed in the sample cell by operating it as a stirred batch reactor. Having formed a sufficient amount of hydrate the system was left to equilibrate for the base line to establish. The obtained value for the specific enthalpy of methane hydrate dissociation to gas and water at 278 K and 4.34 MPa (close to equilibrium) was Δh_{diss}=13,090 cal/gmole$_{CH_4}$. In SI units: Δh_{diss}=54.769 kJ/mol. The hydrate number was about 6.0, so the values transform into 441.7 J/g.

Rueff et al. (1988) also used DSC technique to determine Δh_{diss} of methane hydrate. For six different samples Δh_{diss} varied between 421.23 and 436.66 J/g with n=6.15. They also measured c_p for methane hydrate.

2.3.3 Non-calorimetric Techniques to Measure n

With Raman spectroscopy, n can be measured and it is possible to determine how the guests partition between the different cages. This can not be done by calorimetry. Sum et al. (1996) were the first to use Raman spectroscopy on hydrates of natural gas components. Among the systems studied were CH_4, C_3H_8 and CD_4+C_3H_8. The measurements compared well to predictions from the statistical thermodynamic model of van der Waals and Platteeuw (1959). For methane hydrate, Sum et al. found that the hydrate number increases if pressure and temperature increase. It should also be noted that Raman spectroscopy may be used to quantify the content of gas in the free water under hydrate forming conditions or at equilibrium.

Uchida et al. (1999) analyzed naturally occurring hydrate ($CH_4 > 99$ %mol) from Blake Ridge (leg 164) and synthetic methane hydrate. They concluded that the hydrate number is constant at about 6.2 ± 0.2 ($n_{ideal} = 5.75$). It does not change as a function of formation conditions (P=3.0-8.1 MPa, T=273.2-278.4 K) or depend on the amount of free water. This is a different conclusion than Sum et al. (1996) reached. The large cage was occupied to a fraction of 0.976-0.981 and the small to a fraction of 0.715-0.857.

Ripmeester et al. (1988) demonstrated that ^{13}C NMR can be used to measure n. The original paper and the summary by Sloan (1998, pp. 310-312) are referred to for the details.

2.4 Dissociation Enthalpy Models and Correlations

The Clausius-Clapeyron equation is the most widely used model to calculate enthalpy of hydrate dissociation, Δh_{diss}. Handa (1988b) points this out, although he refers to the Clapeyron equation - an example that the terminology is somewhat loose. The Clausius-Clapeyron equation is treated in Section 2.4.1. Models that represent alternatives to the Clausius-Clapeyron equation are treated in Sections 2.4.2 to 2.4.4.

2.4.1 The Clausius-Clapeyron Equation

By equating Gibbs free energies, $G_A(P,T) = G_B(P,T)$, and combining basic thermodynamic relations, the Clapeyron equation is derived:

$$\frac{dP_{saturation}}{dT} = \frac{\Delta h_{AB}}{T\Delta v_{AB}} = \frac{\Delta s_{AB}}{\Delta v_{AB}} \tag{2.12}$$

for the *equilibrium* between *two phases A and B* of a *pure substance* (Barrow 1979). h, v and s are the molar enthalpy, volume and entropy, respectively. The equation expresses the P-T relation along a phase transition line for a pure substance. The Clapeyron equation is exact and applies to liquid-gas, solid-fluid and solid-solid phase equilibria.

For *liquid-gas equilibria* at *low pressures* the Clapeyron equation simplifies to the Clausius-Clapeyron equation where P is the saturation pressure:

$$\frac{d\ln P}{d\frac{1}{T}} = \frac{-\Delta h_{vap}}{R} \tag{2.13}$$

which upon integration and rearrangement yields:

$$\ln P = \frac{-\Delta h_{vap}}{R} \cdot \frac{1}{T} + C \tag{2.14}$$

P is the vapor pressure of a pure liquid, Δh_{vap} is the specific enthalpy of vaporization and C an integration constant. Plotting $\ln P$ as a function of $1/T$ yields a straight line. The enthalpy of vaporization is determined by the slope of the line, a:

$$a \equiv \frac{\Delta \ln P}{\Delta\frac{1}{T}} = \frac{-\Delta h_{vap}}{R} \tag{2.15}$$

thus the heat of vaporization is:

$$\Delta h_{vap} = -aR \tag{2.16}$$

The Clausius-Clapeyron equation is not exact, but is based on two assumptions: $v_{gas} \approx v_{idealgas}$ and $v_{liquid} \ll v_{gas}$ where v indicates molal volumes of the different phases.

The Clausius-Clapeyron equation has been extended from one component vapor-liquid systems into hydrate systems. The model is widely referred to in hydrate papers, for instance by Fleyfel and Sloan (1991), Groisman and

Savvin (1988) and Parent (1948). The equation enables the calculation of the heat of hydrate dissociation, as the hydrate dissociation process is assumed analogous to liquid vaporization. Accordingly, the enthalpy of vaporization is replaced by the enthalpy of dissociation, Δh_{diss}. To account for non-ideal gas behavior, the original equation is modified by the introduction of the compressibility factor, z:

$$\Delta h_{diss} = -zaR \tag{2.17}$$

An underlying assumption is that Δh_{diss} is independent of temperature. Δh_{diss} is not a very strong function of the temperature, so for narrow temperature intervals the assumption is reasonable. Correlations that account for temperature dependency are given in Section 2.4.4. Comparison between calculated Δh_{diss} values and calorimetry measurements has proven the Clausius-Clapeyron method accurate within 1-5% for hydrates of some single guests; methane, ethane, propane and iso-butane. The Clausius-Clapeyron equation has been discussed in the literature and agreement has been reached that the Clausius-Clapeyron equation is only valid for univariant systems like Hydrate $\rightleftharpoons$ Water + Gas and with three restrictions (Sloan and Fleyfel 1992):

- The fractional occupancy of each cage is about constant.
- The volume change of the condensed phase is negligible compared to the gas volume.
- The gas consumption is about constant.

Handa (1986a) states that in general the Clapeyron equation results in large errors. One reason is the poor quality of most dissociation pressures reported in the literature. Such errors propagate through calculations to result in correspondingly large errors in values of dissociation enthalpy. As a result, many of the Δh_{diss} values reported in the literature are questionable. On the other hand, Maksimov (1996) refers to the works by Chersky et al. (1982) and Groisman (1985) and points out that the difference between Clausius-Clapeyron estimates and measured Δh_{diss} values for sII natural gas hydrate does not exceed 3%. This is acceptable for engineering applications.

When doing Clausius-Clapeyron calculations, one has to assess a value to the independent variable z. Should it be desirable to take pressure and temperature effects on z into account, this rises a separate modeling question. The standard procedure is to determine $z(P,T)$ by solving a cubic equation of state. Rueff et al. (1988) in a paper on hydrate dissociation refer to the Peng-Robinson equation of state. To calculate dissociation enthalpies at standard conditions it will usually be a good approximation to assume that $z = 1$. The step-by-step procedure for Clausius-Clapeyron calculations are:

1. Perform hydrate dissociation experiments to record the equilibrium pressures, at different temperatures.
2. Plot the pressure-temperature pairs in a coordinate system with $\ln P$ on the ordinate axis and $\frac{1}{T}$ on the abscissa axis.
3. Calculate the slope, a.
4. Assess a value to z.
5. The enthalpy of dissociation is now: $\Delta h_{diss} = -zaR$.

Khokhar (1998) used the Clausius-Clapeyron equation to calculate Δh_{diss} below 273.15 K for hydrates of different compositions and for different structures. Among different sII hydrates, he found that Δh_{diss} does not vary a lot even if the composition varies, see Table 2.4. The implication is that Δh_{diss} is about the same for a wide range of gas compositions. The mixtures methane + propane and methane + n-butane can be said to represent natural gases. The average Δh_{diss} below 273.15 K for the corresponding hydrates were 27.85 kJ/mol. 27.8-33.1 kJ/mol was the Δh_{diss} interval measured[2] by Handa (1988b) on a naturally occurring sample of sII natural gas hydrate. The correspondence is good.

2.4.2 Guest Size Dependent Enthalpy Estimation

Sloan and Fleyfel (1992) suggested that to an approximation, Δh_{diss} is determined by the type of cage occupied, which in turn is determined by the size of the guest(s). Δh_{diss} is independent of the guest type - only the *size* of the

[2] This was for measurements on the sample referred to as NGH9 in Table 2.2. A unique value could not be found and the interval is based on assumptions of no ice in the sample (27.8 kJ/mol) and 20 %mass ice (33.1 kJ/mol).

Table 2.4: Clausius-Clapeyron calculations below 273 K for different sII hydrates (Khokhar 1998).

Guest(s)	Slope (1/K)	Δh_{diss} (kJ/mol)
Propane	−3583.62	28.96
i-Butane	−3544.45	28.64
Methane + propane	−3361.48	27.53
Methane + n-butane	−3533.02	28.17

guest matters. To support the hypothesis a number of Clausius-Clapeyron plots were presented for single and mixed hydrates. The overall observation was that hydrates of the same structure and with the same types of cages occupied had about the same Δh_{diss}.

For example, single hydrates of propane and iso-butane are sII hydrates and only the largest cavities are occupied. The slope in Clausius-Clapeyron plots are −15100 K and −15700 K for propane and iso-butane, respectively. The difference is about 4%. Double sII hydrates with both cages occupied show the same resemblance. For example, a mixture of 1 %mol propane in methane and a mixture of 36.2 %mol propane in methane have the same slopes (within the experimental error); −9802 K. The overall results are presented in Table 2.5.

The size dependent model was disputed by Skovborg and Rasmussen (1993) who claimed that the grouping of components according to Sloan and Fleyfel is not possible. For example it was pointed out that the slope, and thus Δh_{diss}, depends on the hydrate number. For the slope to be constant, z too must be constant over the pressure and temperature range of interest.

Table 2.5: The guest size dependent model for Δh_{diss} prediction above 273 K by Sloan and Fleyfel (1992). It assumes that for a given structure (sI or sII) Δh_{diss} is determined by which cages are empty (e) and which are occupied (o).

Structure	Large	Small	$\approx \Delta h_{diss}$ (kJ/mol)
sI	o	o	54-57
sI	o	e	71-74
sII	o	o	79
sII	o	e	126-130

2.4.3 Chemical Potential Model

Handa (1986a) derived a model for Δh_{diss} as follows:

For the 3-phase (h-l-g) equilibrium at T and P we have:

$$\mu_h = n\mu_w + \mu_g \tag{2.18}$$

where μ is the chemical potential of hydrate (h), liquid water (w) and hydrate former (g). n is the hydrate number. Pure solid, pure liquid and pure ideal gas at 273.15 K and 101,325 Pa were taken as standard states for solid, liquid and gas, respectively. This yields:

$$\mu_h = \mu_h^\circ + \int_{P^\circ}^{P} v_h dP \tag{2.19}$$

$$\mu_w = \mu_w^\circ + \int_{P^\circ}^{P} v_w dP + RT \ln a_w \tag{2.20}$$

$$\mu_g = \mu_g^\circ + RT \ln \frac{f}{f^\circ} \tag{2.21}$$

where superscript $^\circ$ refers to the standard state, (101,325 Pa), v_h is the molar volume of hydrate, v_w is the partial molar volume of water, a_w is the activity of water and f is the equilibrium fugacity of the hydrate forming gas. n is a function of P leading to the assumption that the hydrate in its standard state has a hydrate number as it would have at P.

When the gas solubility in the water is low, $\ln a_w \approx -x_g$ and $v_w \approx v_w^*$ where superscript * denotes *pure*. The effect of P on the volumetric properties of the condensed phases is assumed neglectible, yielding the model equation:

$$\Delta\mu^\circ = -nx_g RT + RT \ln \frac{f}{f^\circ} + (P - P^\circ)(n_w^* - v_h) \tag{2.22}$$

where

$$\Delta\mu^\circ = \mu_h^\circ - n\mu_w^\circ - \mu_g^\circ \tag{2.23}$$

For the (h-i-g) equilibrium, the standard state functions are obtained from the model equation by introducing $x_g = 0$ and $v_w^* = v_{ice}$. It is indicated how the chemical potential model may be developed further and used to find h°_{diss}.

Compared to the Clausius-Clapeyron equation, Handa's model is difficult to use and there is nothing to gain regarding accuracy, which is about $\pm 5\%$. The chemical potential model is not persuied further in the present work.

2.4.4 Correlations

Holder et al. (1988) wrote a comprehensive review on phase behaviour in systems containing clathrate hydrates. An empirical correlation was proposed for Δh_{diss} (J/mol). The correlation includes constants c and d for different guests and temperature intervals. The constants are given in Table 2.6. Note that the correlation yields the dissociation enthalpy at the equilibrium pressure and not at standard pressure.

$$\Delta h_{diss} = 4.18(c + dT) \tag{2.24}$$

Table 2.6: Coefficients for calculating Δh_{diss} according to the correlation $\Delta h_{diss} = 4.18(c + dT)$ (Holder et al. 1988).

Gas	Structure	c	d	T range (K)
CH_4	I	6,530	-12.0	248-273
		13,500	-4.0	273-298
C_2H_6	I	8,460	-9.6	248-273
		13,300	15.0	273-287
C_3H_8	II	7,600	-4.9	248-273
		37,750	-250.1	273-278
CO_2	I	9,290	-12.9	248-273
		19,200	-15.0	273-284
N_2	I	493,400	-9.0	248-273
		6,190	18.4	273-298
H_2S	I	8,490	-7.8	248-273
		6,780	31.5	273-298

Based on the Clausius-Clapeyron equation, Selim and Sloan (1990) gave correlations to calculate Δh_{diss} for natural gas hydrate in sediment, below and above 273 K. The correlations have the same form as the one by Holder et al. (1988).

$\Delta h_{diss} = 215.59 \cdot 10^3 - 394.945T$ (J/kg) for $T = 248$-273 K
$\Delta h_{diss} = 446.12 \cdot 10^3 - 132.638T$ (J/kg) for $T = 273$-298 K

Zakrzewski and Handa (1993) studied dissociation of tetrahydrofuran hydrate in confined geometries. The enthalpy of hydrate dissociation was suppressed as much as 36.9% compared to bulk dissociation. This demonstrates that Δh_{diss} correlations for sediment hydrate, as the one by Selim and Sloan (1990), may not apply to bulk hydrate. On the other hand, these particular correlations are based on Clausius-Clapeyron calculations ("modified Clapeyron equation"), which *do* apply to bulk hydrate.

2.4.5 Dissociation Enthalpy Comparison

A number of dissociation enthalpy measurements and have now been referred, along with different ways to predict such values. Now, the different values are compared for two cases; methane and natural gas.

Methane

Figure 2.5 shows five different dissociation enthalpies, labeled a-e, for methane. Clausius-Clapeyron calculations overestimate the experimental values by about 4%. The guest size dependent model by Sloan and Fleyfel (1992) shows a aimilar overestimate. This is not unexpected since the model is justified by a number of Clausius-Clapeyron calculations. The correlation by Holder et al. (1988) underestimates by about 5%.

Natural Gas

Figure 2.6 shows three different Clausius-Clapeyron lines. They are based on the Mastahskoe gas composition given is Section 2.5.2. The data points reproduced from Maksimov (1996) are near-equilibrium velues of pressure and temperature. The other two lines are based on qeuilibrium simulations using CSMHYD and PVTsim.

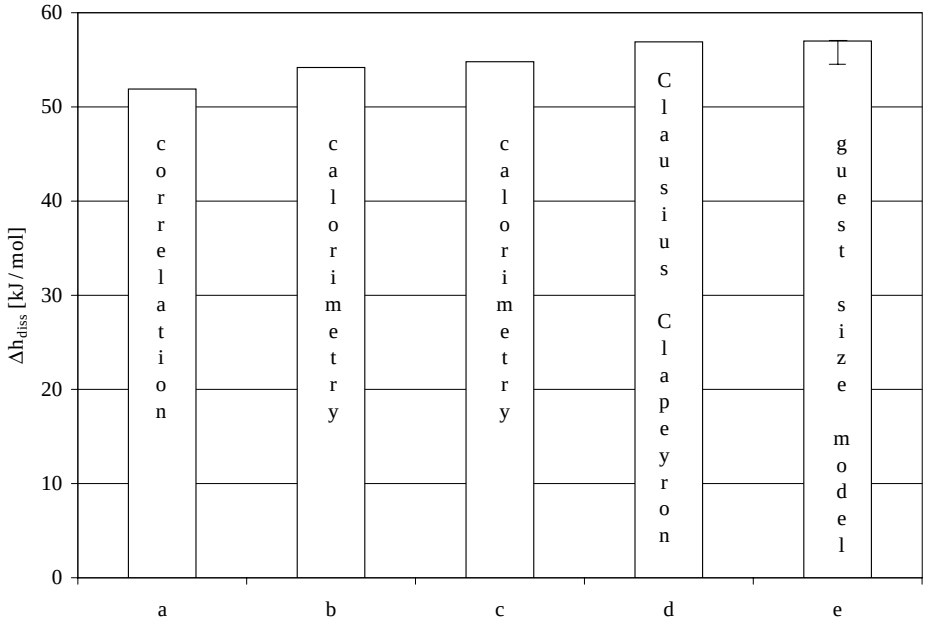

Figure 2.5: Comparison of measurements (col. b,c) and predictions, of enthalpy of methane hydrate dissociation. a: Correlation by Holder et al. (1988), b: Calorimetric measurement by Handa (1986c), c: Calorimetric measurement by Kobayashi and Lievois (1988), d: Clausius-Clapeyron calculation by Sloan and Fleyfel (1992), e: Guest size dependent model by Sloan and Fleyfel (1992).

Figure 2.7 shows enthalpies of natural gas hydrate dissociation from the Clausius-Clapeyron calculations, and enthalpies according to the guest size dependent model by Sloan and Fleyfel (1992) and the correlation by Selim and Sloan (1990). The guest size dependent model gives about the same value as Clausius-Clapeyron calculations. The Clausius-Clapeyron calculations overestimate the calorimetric measurments between 5% and 17%. Similar deviations were seen for methane, but the deviation between Clausius-Clapeyron calculations and measurements are larger for natural gas than for methane. The correlation by Selim and Sloan (1990) deviate -18% from the experimental value. This is corresponding to the observation by Zakrzewski and Handa (1993) who found that the correlation significantly underestimates enthalpies of bulk dissociation.

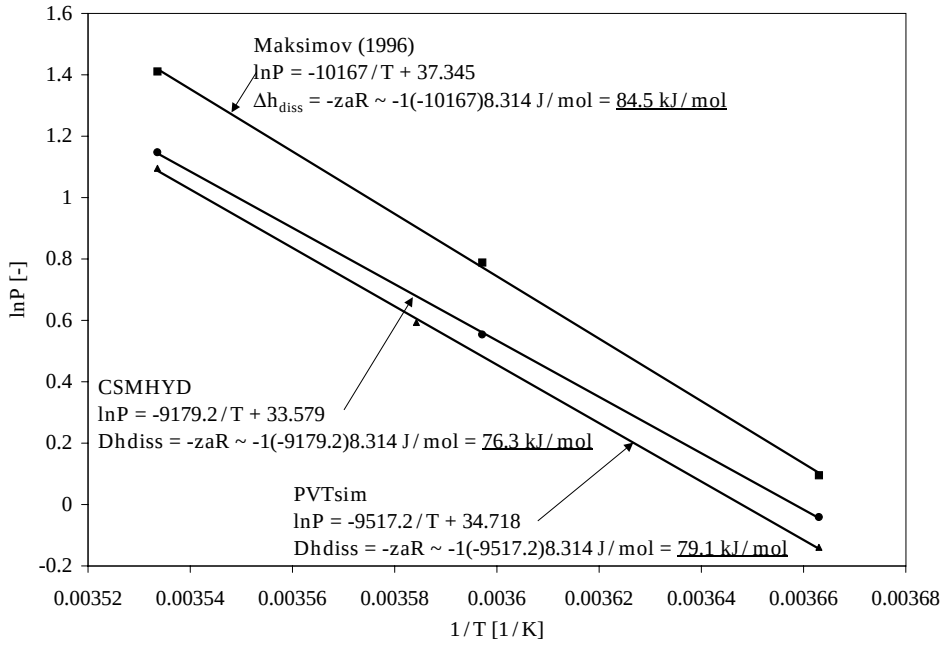

Figure 2.6: Clausius-Clapeyron plot of Mastahskoe gas. Maksimov (1996) provided experimental P and T values, while those obtained by CSMHYD and PVTsim are equilibrium simulations based on the gas composition.

2.5 Specific Heat Capacity

2.5.1 Measurements

To determine c_p of Kr and Xn hydrates, Handa (1986a) used the classical method described in Section 2.2. The measurements were corrected by subtracting the signal of a blank run. Heat capacity for hydrate was obtained by correcting for any ice in the sample while it was assumed that the heat capacities of hydrate and ice were additive. c_p for hydrate are given in units of J/molK where mol refers to the hydrated gas. Selected results for temperatures not too far below 273 K are given in Table 2.7. Groisman (1985) measured c_p of natural gas hydrate, and reported values of 2.14-2.88 J/gK for temperatures of 213-275 K.

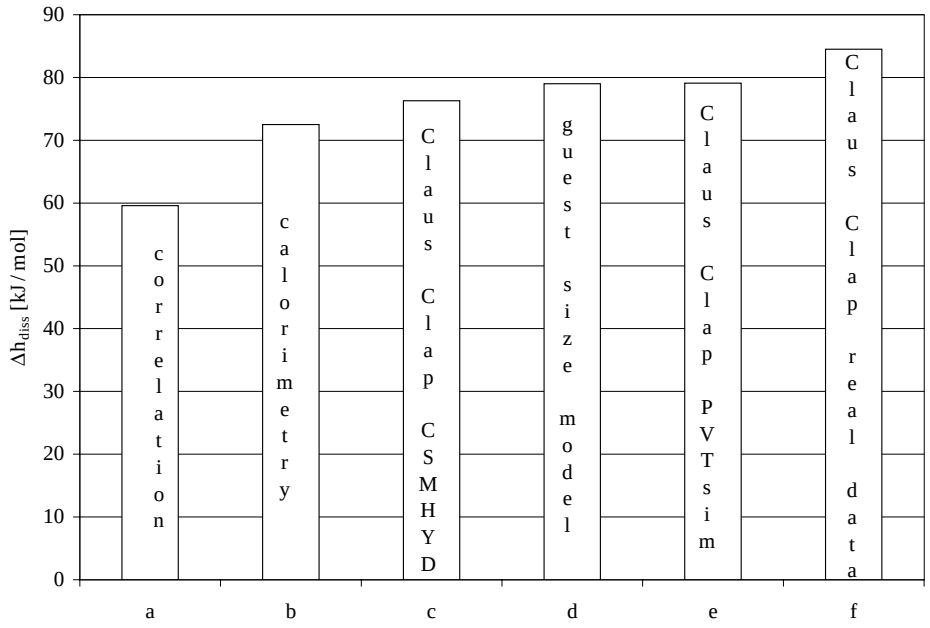

Figure 2.7: Comparison of measurements (col. b) and predictions, of enthalpy of Mastahskoe gas hydrate dissociation. a: Correlation by Selim and Sloan (1990), b: Calorimetric measurements reproduced from Maksimov (1996), c: Clausius-Clapeyron calculation from CSMHYD equilibrium simulations, d: Guest size dependent model by Sloan and Fleyfel (1992), e: Clausius-Clapeyron calculation from PVTsim equilibrium simulations and f: Clausius-Clapeyron calculation from experimental data taken from Maksimov (1996).

2.5.2 Models and Correlations

Maksimov (1996) reviewed Russian works. With reference to Groisman (1985) the following model was given with unit J/gK:

$$c_{p,NGH} = \frac{4.5R + 18n(2.3 + 8.4732 \cdot 10^{-3}(T - 273.15))}{M_{NG} + 18n} \tag{2.25}$$

where R is the universal gas constant, n is the hydrate number, T is absolute temperature and M_{NG} is the molecular mass of the hydrated natural gas. A comparison of measurements and model calculations showed an error of $\pm 5\%$.

Table 2.7: Selected measured values of c_p for single hydrates.

Guest	c_p (J/molK)	n	T (K)	Reference
CH_4	233.7	6.00	240	(Handa 1986c)
CH_4	257.6	6.00	270	(Handa 1986c)
C_2H_6	310.9	7.67	240	(Handa 1986c)
C_2H_6	337.8	7.67	260	(Handa 1986c)
C_3H_8	644.0	17.0	240	(Handa 1986c)
C_3H_8	710.2	17.0	260	(Handa 1986c)
Kr	217.9	6.10	240	(Handa 1986a)
Kr	243.3	6.10	270	(Handa 1986a)
Xn	218.8	5.90	240	(Handa 1986a)
Xn	242.4	5.90	270	(Handa 1986a)

The measurements were made on synthetic hydrate made from natural gas produced at the Mastahskoe field in Yakutia. The composition was (%mol): CH_4 (91.509), C_2H_6 (3.942), C_3H_8 (1.220), i-C_4H_{10} (0.454), n-C_4H_{10} (0.140), i-C_5H_{12} (0.147), n-C_5H_{12} (0.051), H_2 (2.0) and O_2 (0.4). This yielded an average molecular mass of 17.63 g/mol. The composition of the hydrate was not specified.

Maksimov (1996) with reference to the original work by Istomin and Yakushev (1992) assumed that c_p of gas hydrates may be modeled in terms of additive contributions from the lattice and the guest(s). c_p (J/molK) of the empty lattices of Xe and Kr compare well to c_p of ice Ih in the range 240-270 K. The difference is about $\pm 4\%$.

The following model was proposed to calculate c_p (J/molK):

$$c_p = nc_\beta + \sum_i c_i x_i \tag{2.26}$$

where c_β is the heat capacity of the empty lattice ($c_\beta \approx c_{iceIh}$), c_i is the molar heat capacity of the hydrated gas of type i which is present to a fraction x_i in the hydrated gas. c_p may be converted from J/molK to J/gK by dividing the c_p value from Equation 2.26 by $(M_G + 18n)$. Empirical c_p correlations for single hydrates are given in Table 2.8. The error is about $\pm 1\%$.

Table 2.8: Empirical correlations of specific heat capacity for single hydrates.

c_p correlation (J/molK)	T (K)	Reference
$c_p(CH_4 \cdot 6.00H_2O) = 6.6 + 1.4538T - 0.3640 \cdot 10^{-2}T^2 + 0.6312 \cdot 10^{-5}T^3$	85-270	(Handa 1986c)
$c_p(C_2H_6 \cdot 7.67H_2O) = 22.7 + 1.8717T - 0.5358 \cdot 10^{-2}T^2 + 1.076 \cdot 10^{-5}T^3$	85-265	(Handa 1986c)
$c_p(C_3H_{10} \cdot 17.0H_2O) = -37.6 + 4.8606T - 1.625 \cdot 10^{-2}T^2 + 3.291 \cdot 10^{-5}T^3$	85-265	(Handa 1986c)
$c_p(Xe \cdot 5.90H_2O) = 2.12 + 1.3516T - 3.232 \cdot 10^{-3}T^2 + 5.622 \cdot 10^{-6}T^3$	85-270	(Handa 1986a)
$c_p(Xe \cdot 6.29H_2O) = 36.0 + 0.77505T$	150-230	(Handa 1986b)
$c_p(Kr \cdot 6.10H_2O) = -4.76 + 1.4345T - 3.398 \cdot 10^{-3}T^2 + 5.391 \cdot 10^{-6}T^3$	85-270	(Handa 1986a)

2.6 Thermal Conductivity and Expansivity

Sloan (1998) and Maksimov (1996) reviewed measurements of thermal conductivity, λ, for hydrate. Not much seems to be reported. Two methods are in use; the transient method and the steady state method. Accuracies range between 8 and 12%. Data are given in Table 2.9.

Table 2.9: Collection of experimental data for thermal conductivity (λ) for clathrate hydrates. The reference by Istomin and Yakushev (1992) refers to other original publications of the data.

Guest/structure	λ (W/Km)	T (K)	Reference
Ice	2.23	263	(Sloan 1998, p. 60)
sI	0.49±0.2	263	(Sloan 1998, p. 60)
sII	0.51±0.2	263	(Sloan 1998, p. 60)
Methane	0.45	216.2	(Cook and Leaist 1983)
Methane	0.393	275.15	(Stoll and Bryan 1979)
Methane	0.45	213	(Istomin and Yakushev 1992)
Propane	0.39	275.15	(Stoll and Bryan 1979)
Xenon	0.36	245	(Handa and Cook 1987)
Ethylenoxide	0.49	263	(Istomin and Yakushev 1992)
Tetrahydrofuran	0.51	260	(Istomin and Yakushev 1992)
1,3-dioxane	0.51	260	(Istomin and Yakushev 1992)

Groisman (1985) studied the thermal conductivity for NGH from a gas mixture containing C1 to C5 alkanes, hydrogen and oxygen. Average molecular mass of the gas was 17.63 g/mol (gravity 0.61). It was found that λ_{NGH} increases with temperature in the range 223 to 275 K and with pressure in the range 2.1 to 10.0 MPa. Pressure dependancy was weak. λ_{NGH} was mainly determined by the density in the range 300 to 700 kg/m^3.

The thermal conductivity of hydrate is conciderably lower than that of ice. This difference can be used to quantify the amount of hydrate in a hydrate-ice sample (Sloan 1998).

Much research remains regarding hydrate thermal conductivity. But it is indicated that neither the type of guest molecule nor the structure type have appreciable effect on the thermal conductivity. Groisman (1985) arrived at an empirical ralation between NGH thermal conductivity (W/mK) and densities in the range 300 to 700 kg/m^3:

$$\lambda_{NGH} = -0.21 + 8.33 \cdot 10^{-4} \rho_{NGH} \tag{2.27}$$

Sloan (1998, p. 64) reviewed measurements of thermal expansivity, $\frac{dl}{ldT}$, for hydrate and ice. Values for hydrate are not very different from those of ice and are given in Table 2.10.

Table 2.10: Thermal expansivities at 200 K of hydrate and ice. Superscript * indicates directional differences.

Structure	dl/ldT (K^{-1})
sI	$77 \cdot 10^{-6}$
sII	$52 \cdot 10^{-6}$
sH	$^*(59\text{-}67) \cdot 10^{-6}$
ice	$^*(56\text{-}57) \cdot 10^{-6}$

2.7 Important Findings

- Accurate measurements of Δh°_{diss} for single hydrates are reported in the literature.
- No accurate measurements of Δh°_{diss} for sII natural gas hydrate seem to be reported in the literature. This is an important motivation in the present work.
- Δh_{diss} may be estimated from phase equilibrium P-T data using the Clausius-Clapeyron equation. The accuracy for single hydrates is about 1-5 %. For mixed hydrates the accuracy may be poorer.
- The most accurate way to obtain Δh°_{diss} for natural gas hydrate is to do calorimetric measurements.

- c_p measurements and correlations for sII natural gas hydrate exist.
- A calorimetric method to measure thermophysical properties (enthalpy of dissociation and specific heat capacity) and compositional properties (hydrate number and free water) exists. A limitation of the method seems to be that samples can not contain large amounts of free water.

Chapter 3

Metastability - Literature Study

3.1 Metastability Concepts

Glasstone and Lewis (1960) use the term metastable equilibrium. Metastable refers to "a definite equilibrium which is, nevertheless, not the most stable equilibrium at the given temperature". The change to stable equilibrium occurs spontaneously *or* upon addition of the stable phase. For example, the addition of a small amount of solid substance to a supercooled liquid of the same substance, will usually result in solidification. Also, the temperature of the system increases up to the liquid-solid phase line in the PT phase diagram. A system may exist in a state of metastable equilibrium indefinitely. Metastable equilibrium is a *thermodynamic* concept. Sonntag and van Wylen (1982) note that there is a possibility of metastable state for any phase transition.

Debenedetti (1996) addressed the lifetime of metastable liquid systems. The lifetime, τ, must be longer than the observation time, τ_{obs}, to study a metastable system. To carry out measurements of a given quantity, it is also necessary that its characteristic molecular relaxation time, τ_{rel}, is much shorter that the system lifetime. The observation time scale has to be intermediate, such that $\tau > \tau_{obs} > \tau_{rel}$. Only then is a given property of a metastable liquid measurable and reproducible. Metastable systems will eventually evolve towards a condition of greater stability, which makes this

a *kinetic* concept. The lifetime τ of metastable systems is a proper way to describe the kinetics.

According to Chao and Greenkorn (1975), the state of a system is said to be stable if the system tents to reduce displacements imposed on it. The system is said to be unstable if it tends to increase such displacements. If the system is stable toward infinitesimal displacements but unstable toward finite displacements, it is said to be metastable.

Physiochemical metastability in thermodynamic and kinetic terms have analogies in mechanical systems. An analogy to thermodynamic metastability is a slim iron rod standing upright on a flat end. This is a metastable situation. Upon a finite displacement the rod will tip over, and end up lying down in a stable state. An analogy to kinetic metastability is the same slim iron rod standing on a flat end, only now it is submerged in a very viscous fluid. Upon a finite displacement the rod will again tip over and end up lying down, but because it has to fall through the viscous fluid it will take a very long time.

3.2 Hydrate Metastability Measurements

Handa (1986a) dissociated Xn and Kr hydrates using a Tian-Calvet heat flow calorimeter. Powder samples dissociate in one step below 273 K. But bigger samples dissociate in two steps. In the first step ($T < 273$ K) the surface undergoes dissociation; Hydrate $\rightarrow$ Ice + Gas. The surface gradually becomes covered by ice, which prevents further dissociation until the second step ($T \approx 273$ K) where the ice begins to melt.

Yakushev and Istomin (1991) demonstrated the self preservation effect of hydrates. sI hydrate from methane as well as sII hydrate from a methane-propane mixture were studied. When hydrate is stored at 0.1 MPa and temperatures below 273 K and below the PT region of thermodynamic hydrate stability, the hydrate can still exist for long times without large losses of gas. Other samples decomposed rapidly, for example needle crystals (2-6 days) and massive fine-porous samples (2-14 days).

Ershov and Yakushev (1992) reported that hydrate in rocks at initial temperatures of about 273-278 K can cause the temperature to drop below 273 K as an effect of partial dissociation, since hydrate dissociation is an endothermic process. After some time (minutes) the surface of the sample

becomes covered by an ice layer. Dissociation stops and the sample temperature increase to the initial temperature. It was shown how the humidity of the surroundings affect the stability properties. Four differently confined samples were stored at 260 K. The more air circulation (less confinement), the higher the rate of sublimation and the poorer was the stability. The results are collected in Table 3.1. The effect of electromagnetic radiation was investigated. A lamp (40 W) at a distance (2 m) lit half of samples. The lit halfs disappeared in 0.25-0.33 h, while the halfs in the shadow lasted for 3-5 h. Sharp edges that form when samples are broken become covered by ice early compared to smooth, flat areas, indicating different stability properties. It was also seen that samples stored at a relatively high temperature develops an ice layer more rapidly than samples stored at a relatively low temperature. It was noted that as the samples dissociated they turn white.

In summary, the works by Yakushev et al. show that the stability depends on environmental humidity and the possibility for ice sublimation, specific surface area, electromagnetic influence, temperature and mechanical impacts.

Table 3.1: Effect of confinement on the rate of dissociation at 260 K.

Confinement	Life time (h)	Remarks
Open air	40	Control sample of ice
Open air	36	No ice layer formation
Open little box	80	0.1-0.2 mm ice layer
Closed cellophane pocket	200	0.3-0.5 mm ice layer
Hermetic	> 3600	$\approx 30\%$ loss of gas

Gudmundsson and Parlaktuna (1992) and Gudmundsson et al. (1994) stored metastable NGH at ambient pressure and temperatures of 268, 263 and 255 K for up to 10 days without appreciable changes in gas content or gas composition. Hydrate was made in a stirred batch reactor. Water conversion was 27 to 44%. The samples contained comparable and large amounts of ice. During storage the hydrate lost some gas depending on the temperature: 11.3% (268 K), 3.4% (263 K) and 0.33-0.85% (255 K). The gas was lost during the first day of storage. Different samples were equally stable and behaved alike during dissociation. The role of ice was not studied further.

Ebinuma et al. (1999) did measurements on methane hydrate particles in polycrystalline ice. A volume fraction of about 0.85 of the samples were hydrate. Thin section samples at 258 K were observed using polarized light microscopy. The ice surrounding the hydrate particles suppressed dissociation at 258 K and ambient pressure even though the measured equilibrium temperature at this pressure was 195 K

Buffett and Zatsepina (1999) considered systems at temperatures above 273.15 K. They suggested that gas hydrates can be warmed above the equilibrium temperature, but once gas bubbles start to nucleate, dissociation may become rapid. Experiments on CO_2 hydrate in coarse grain sand suggested that 3-4 K superheating is possible.

Stern et al. (1999) investigated pressure-temperature-time path effects on methane hydrate dissociation kinetics and stability at 0.1 MPa. Different P-T-t paths were followed to bring the samples from post-synthesis conditions (elevated pressure) to 0.1 MPa prior to dissociation. Some samples were *heated slowly* (10 K/h) at 0.1 MPa (temperature-ramping). Other samples were *depressurized rapidly* to 0.1 MPa at temperatures between 205 and 289 K (rapid-depressurization).

In the temperature-ramping experiments the dissociation began at about 200 K, 5 K above the equilibrium temperature. At about 216 K the dissociation had come to a 95% completion.

In the rapid-depressurization experiments at 250-270 K the samples were metastable and existed for more than 25 h. Only minor dissociation was observed. Such samples could be warmed to 273 K where they dissociated giving off about 90% of the initial gas. But when the metastable samples were cooled to 190 K and then heated they dissociated at 198 to 218 K , as in the temperature-ramping experiments. When the rapid-depressurization experiments were tried at lower temperatures (205 K) the samples dissociated steadily at 0.1 MPa.

Stern et al. (1999) concluded that methane hydrate metastability at the higher temperatures is partially due to increased mobility and annealing of grain boundaries. This is believed to block channels where gas may escape to the surroundings. When these channels block, then dissociation is inhibited. It was proposed that ice-hydrate interfaces may play a role in metastable behavior of both hydrate and ice.

3.3 Hydrate Metastability Models

Yakushev and Istomin (1991) explained the self preservation effect by the formation of an ice layer on the hydrate sample. The ice forms from water molecules left behind when the outer hydrate layer on a sample dissociates. It is claimed that the film is impermeable for gas molecules and this prevents

further dissociation. The self preserved system is thus a two-phase system containing hydrate and ice. Using the van der Waals-Platteeuw model it was shown that in certain pressure-temperature regions the hydrate will convert into ice on the surface. For $T < 273$ K a pressure decrease towards ambient pressure causes $\Delta\mu = \mu_\beta - \mu_{ice}$ to decrease and give negative values. μ_β and μ_{ice} is the chemical potential of empty hydrate lattice and ice, respectively.

Gudmundsson and Parlaktuna (1991) considered the mechanical properties of ice and what the implications are on ice-hydrate systems. The following equation, originally proposed by Michel (1978), was used:

$$\sigma = 7.94 \cdot 10^4 \left(\left(1 - \frac{e}{0.285} \right) \frac{1 - 0.9 \cdot 10^{-3} T}{d} \right)^{1/2} \tag{3.1}$$

σ (Pa) is the tensile strength. e is the porosity, defined as $e = 1 - \frac{\rho'}{\rho}$ where ρ' (kg/m^3) is the density of the ice and ρ is the density of pure ice (917 kg/m^3). T is the temperature in °C and d (mm) is the grain diameter. The equation is supported by data for grain sizes in the range 1.4 to 9 mm. Calculations were done for hydrate particles encapsulated in an ice shell. For example, 1 mm shell thickness can maintain a pressure of about 0.5 MPa for a hydrate particle with a diameter of 15 mm. The tensile strength of ice is more sensitive to the grain size than the temperature.

Gudmundsson et al. (1994) considered NGH metastability as a consequence of insufficient supply of heat. Since large amount of heat is required to dissociate the hydrate, the hydrate will persist for long times if it is stored adiabatically in insulated tanks. It is said that the initial dissociation may be responsible for an ice layer which in turn protects the rest of the sample and causes the observed metastability.

Ebinuma et al. (1999) modeled the metastability of methane hydrate particles in polycrystalline ice. They assumed that hydrate particles are uniformally distributed in the ice at ambient pressure and that dissociation is suppressed due to the mechanical strength of the ice. They rely on an analogy to glaciology where the ice contains air bubbles in which the pressure is increased above ambient due to a densification process. Using this analogy, the maximum volume fraction of metastable methane hydrate particles in the ice is estimated as follows:

$$P_{eq} - P_{amb} = \sigma((\frac{L}{2r})^2 - 1) \tag{3.2}$$

where P_{eq} is the temperature dependent equilibrium dissociation pressure of methane hydrate as determined experimentally (empirical correlation): $P_{eq} = \exp(\frac{-2255.1}{T} + 9.1955)$. P_{amb} is the ambient pressure. σ is the tensile strength of polycrystalline ice[1]: $\sigma = 0.06 + 0.02d^{-0.5}$. L is the centre-centre distance between neighbouring methane hydrate particles and r is the radius of these particles.

Ebinuma et al. (1999) concluded that the maximum hydrate volume fraction permitting metastability at ambient pressure increases with decreasing temperature and with decreasing grain size. For example, 1 μm particles at 263 K are stable for volume fractions up to almost 0.9, while 1 mm particles at the same temperature are stable up to less than 0.3 volume fractions. The allowed volume fraction approaches unity as the temperature approaches 195 K, since at this temperature the dissociation pressure equals the ambient pressure.

Buffett and Zatsepina (1999) said the hydrate superheating limit for $T > 273$ K depends on the conditions for bubble nucleation. The limit is reflected in the energy barrier to be overcome when nucleating bubbles in the liquid phase. Metastable hydrates should persist as long as the liquid surrounding the hydrate is supersaturated in the hydrate former. This calls for a distinction between bulk hydrate and hydrate in porous media, since mass transfer is slow in pore water compared to bulk water. Accordingly, hydrate metastability could be more pronounced in pores compared to hydrate dispersed in water. It is suggested that methane hydrate in pores should also persist as long as the supersaturation of the surrounding fluid is maintained.

Istomin (1999) discussed the possibility of superheating of natural gas hydrate, referring mostly to the Russian literature. Temperatures below and above 273 K are considered. The metastable state is interpretated as a superheated state covered by thermodynamic stable protective films. For metastable natural gas hydrate covered by an ice film it is necessary that the film does not sublime. He assumes that for $T < 273$ K an initially pure hydrate sample gradually becomes covered with a thin film of metastable ice, either cubic or amorphous. This ice transforms into hexagonal ice Ih which is the thermodynamically stable ice structure at ambient pressure.

[1] Units not specified. The original reference is (Currier and Schulson 1982).

A zone of metastable ice thus forms between the hydrate and the outer layer of stable hexagonal ice. The only way that guest molecules can escape is by diffusing through the ice layer. This process is slow and accordingly the metastable hydrate may exist for long. It is pointed out that self preservation can also be regarded as hydrate subject to a superheating of as much as 78 K in the case of methane hydrate at 271 K ($T_{eq} = 193$ K).

Istomin (1999) also refers to substantially superheated ice Ih which exists at least for hours when covered with a protective layer of hydrate. In a sense this is the reverse of self preserved hydrate which spontaneously becomes covered with ice. But in the case of hydrate-covered ice, deliberate actions need be taken to form the hydrate. Ii is also proposed that methane hydrate may be metastable at temperatures as high as 283 K at ambient pressure or a moderate gauge pressure (0 - 1 MPa). The requirements are that a hydrate of a heavy guest covers the methane hydrate (or the natural gas hydrate) and that the hydrate cover is thermodynamically stable at relevant pressure-temperature conditions. Such heavy guests may be propane or iso-butane. The heavy guest in its gaseous state needs to surround the hydrate for the outer hydrate layer to be stable. It is admitted that this is a theoretical opportunity, but potential application in hydrate storage and transport operations is mentioned.

3.4 Rate of Solid-Solid Transitions

A solid sample which is undergoing dissociation has its total enthalpy of dissociation, ΔH_{diss}. At some time during a dissociation process, only a portion of the sample will have dissociated. This portion is referred to as degree of transition, α. By the time t, an amount of heat equal to ΔH_t has been supplied to the sample (endothermic dissociation). These quantities relate as follows: $\alpha = \frac{\Delta H_t}{\Delta H_{diss}}$ (definition) where $\alpha \to 1$ and $\Delta H_t \to \Delta H_{diss}$ for $t \to \infty$. The higher the heat flux, $\dot{Q}$ (W), to the sample, the higher is the rate of dissociation. Thus, the rate of dissociation, r, can be calculated from calorimetric measurements, using Equation 3.3 (Zeng et al. 1998).

$$r = \frac{d\alpha}{dt} = \frac{\frac{d\Delta H_t}{dt}}{\Delta H_{diss}} \tag{3.3}$$

This can be used as a method to quantify the dissociation rate of hydrate. Below 273 K, the dissociation rate is so low that the hydrate is regarded metastable. It follows that kinetic metastability may be quantified in terms of the dissociation rate.

Isothermal calorimetry can be used to obtain thermal data to calculate r. But it should be noted that solid-state kinetics is a complex issue. Two laboratories may arrive at very different results even if no "mistake" is made by either. System dependency is strong. The characteristics of isothermal kinetics are often highly dependent on the changing surface geometry of the sample as the degradation proceeds. Edges on the sample tend to round and this reduces the specific surface of the sample. If the system behaves according to a particular rate equation, this does not necessarily provide information about the processes, notably the chemistry, that the sample undergoes (Bamford and Tipper 1980).

NGH metastability may be regarded as a kinetic phenomenon, since given sufficient time the samples will dissociate completely. Special precautions must be taken in calorimetric kinetic experiments on solids. The results are sensible to temperature, scanning rate, heat flow and sample mass. In addition, parameters such as sample type (granulates or powder) and atmosphere are also important. The kinetic parameters obtained from such experiments are usually system dependent and not general compound data (Höhne et al. 1996).

Reactant concentration is a central magnitude in kinetics. But for solid crystalline systems like NGH, "concentration" is a term that bears no definite meaning. In addition, solid reactions do not always proceed uniformly throughout the sample, but often in local zones of enhanced reactivity, such as the surface (Galwey 1985).

Kinetic investigations by calorimetry may be carried out either by scanning procedures or isothermal procedures. When a sample is subject to an isothermal procedure, this is the same as storing the sample in the calorimeter cell while recording the heat flow to the sample. In case of a NGH sample, there will be an endothermic signal if it is undergoing dissociation. If the heat flow to the sample increases, then the rate of dissociation increases proportionally for constant temperature.

3.5 Important Findings

A literature study which focused on metastability of natural gas hydrate below 273 K has been carried out. Measurements and models were reviewed. Important findings were:

- It seems that ice plays an important role in metastable hydrate systems, notably by forming an ice layer from water molecules left behind when the outer hydrate layers dissociate.
- No evidence was found of metastability in pure hydrate systems. Such systems gradually transform into ice-hydrate systems, which may be matastable.
- Metastable behavior is normally promoted by decreasing temperature, but there are examples of an opposite effect too. Humid, confined and dark surroundings promote metastable behavior.
- Thermodynamic metastability and kinetic metastability are to different concepts. There is no evidence of infinite hydrate metastability. Consequently, hydrate metastability is considered a kinetic phenomena.

Chapter 4

Fractionation and Driving Force - Literature Study

4.1 Fractionation

4.1.1 Fractionation Measurements

When hydrate forms from gas mixtures the gas components partition between the hydrate and the gas. Different components partition differently. This is fractionation. Heavy components concentrate in the hydrate phase, and light components tend to stay in the gas phase. The opposite could also be the case, as in some systems with hydrogen sulfide.

Fractionation was reported by Hammerschmidt as early as 1934 (Hammerschmidt 1934). Table 4.1 illustrates how large the compositional differences may be between the hydrate forming gas mixture and the hydrate.

Parlaktuna and Gudmundsson (1991) reported the composition of hydrate produced in a batch reactor. The feed gas contained ethane (5 %mol), propane (3 %mol) and methane to 100 %mol. The composition of the gas that was liberated during hydrate dissociation was very different from the feed gas composition, as showed in Table 4.2.

While fractionation is well known as a phenomenon, there is not much about it in the literature. Happel et al. (1994) noted that previous investigations have been concerned with determining the pressure and temperature

Table 4.1: Compositions of pipeline gas and hydrate (Hammerschmidt 1934).

	Pipe line natural gas		Gas from pipe line snow
	%	%	%
Date sampled	6-8-33	8-28-32	1-3-33
Carbon dioxide	0.20	0.00	0.44
Nitrogen residue	7.19	5.11	6.46
Methane	82.50	82.70	56.95
Ethane	5.99	6.68	5.66
Propane	3.26	4.46	24.97
Isobutane	0.30	0.40	4.69
n-Butane	0.49	0.57	0.83
Pentanes, plus	0.07	0.08	0.00
Total	100.00	100.00	100.00

Table 4.2: Compositions (%mol) of gas in hydrate (Parlaktuna and Gudmundsson 1991). Superscript * indicates that the reactor was repressurized during the hydrate formation period.

$P_{initial}$, P_{final} (MPa)	$T_{initial}$, T_{final} (K)	Methane	Ethane	Propane
2.35 , 1.88	290.8 , 273.2	69.49	15.78	14.73
2.31 , 2.00*	291.8 , 277.0	67.95	13.63	18.42
2.29 , 2.35*	278.0 , 275.5	72.89	16.42	10.70

conditions where natural gas forms hydrate. The composition of the hydrate has been of less or no concern. Happel et al. studied fractionation in methane-nitrogen mixtures. At the time (1994) the authors found only one reference (Jhaveri and Robinson 1965) which had studied the composition of hydrate formed in this system.

Happel's apparatus consisted of a CSTR reactor (1 dm^3) with a turbine agitator and an external circulation loop for hydrate sampling. The pressure was controlled by a back pressure regulator on a purge line. The temperature was controlled by cooling media in a reactor jacket. The methane-nitrogen gas mixture was fed through the reactor bottom at a controlled mass flow rate. Purge gas was sampled from the reactor gas cap during the experiments. The system was operated in steady state, i.e. gas was fed and purged continuously and the composition of the gas in the gas cap was constant.

From information about the hydrate composition and the gas composition they drew isobaric T-x phase diagrams. Fractionation was clearly demonstrated. For instance, at 1040 psia (7.17 MPa) and 275 K the methane content was about 0.37 mole fraction in the gas and and about 0.75 mole fraction in the hydrate.

Ng and Borman (1999) account for one of the the latest contributions in fractionation studies. Composition of hydrate in equilibrium with six different gas mixtures were determined at two different pressures, 300 and 1000 psia (2.07 and 6.89 MPa). Operation temperatures were about 2 K below the equilibrium temperature calculated by the EQUI-PHASE hydrate code. The gas mixtures contained minimum two or maximum six gas components among these six: methane, ethane, propane, iso-butane, normal-butane and carbon dioxide. The apparatus was a stirred batch reactor submerged in a cooling bath. During the experiments the gas pocket was displaced and replaced with fresh charges of the feed gas mixture. Each experiment lasted for about 72 hours to convert most of the water. After that time the hydrate was dissociated in the reactor and the composition determined by gas chromatography. Experimental results compared well to EQUI-PHASE simulations, except for systems with ethane.

van der Waals and Platteeuw (1959) were the first to measure hydrate azeotropes. Hydrate azeotropes are analog to azeotropes in vapor-liquid systems as the composition of the hydrate forming gas is equal to the composition of the hydrated gas. In isothermal P-x phase diagrams, azeotropic hydrate systems exhibit dissociation pressure minima. When hydrate forms at azeotrope pressure no fractionation occurs. The hydrate azeotrope in the system hydrogen sulfide-propane at 270 K was treated. For hydrogen sulfide-propane, propane may concentrate in the hydrate or it concentrates in the gas phase. It depends on the overall composition of the system.

4.1.2 Fractionation Model

van der Waals' and Platteeuw's (1959) paper is known primarily for the statistical thermodynamic model of clathrate solutions. Holder and Manganiello (1982) gave a compact presentation of how this model describes fractionation when hydrate is in equilibrium with the gas phase. The fractional occupancies, θ_j, of the different cages (j=large, small) are given by a Langmuir type adsorption theory,

$$\theta_j = \frac{\sum_i C_{ji} f_i}{1 + \sum_i C_{ji} f_i} \tag{4.1}$$

where C_{ji} is the Langmuir constant for gas component i in a type j cage and f_i is the gas phase fugacity for gas component i. The Langmuir constant expresses the affinity a guest has to a cage. The fraction of j-type cages occupied by the i-type guest is:

$$\theta_{ji} = \frac{C_{ji} f_i}{1 + \sum_i C_{ji} f_i} \tag{4.2}$$

Makogon (1997) gives the fraction of all sII cages which are occupied by i-type guest as:

$$\theta_i = \frac{16\theta_{s,i} + 8\theta_{l,i}}{16 \sum_i \theta_{s,i} + 8 \sum_i \theta_{l,i}} \tag{4.3}$$

If the above equations are are combined with information about the hydrate structure (Section 2.1), then fractionation for a system in equilibrium can be calculated.

f_i is related to the mole fraction of i in the gas, y_i, and to the pressure, P, by

$$f_i = \phi_i y_i P \tag{4.4}$$

where ϕ_i is the fugacity coefficient. C_{ji} is a function of temperature only for a gas component i with its properties fixed. The potential function $w(r)$ describes the gas-water interaction and determines the Langmuir constant,

$$C_{ji} = \frac{4\pi}{kT} \int_0^{R_j - a} \exp \frac{-w_{ji}(r)}{kT} r^2 dr \tag{4.5}$$

where r is the radial position of an i-type gas molecule in a j-type cage which has a radius R_j. $w(r)$ is expressed by the Kihara spherical core function,

$$w(r) = 2z\epsilon \left[\frac{(\sigma^*)^{12}}{R^{11} r} \left(\delta^{10} + \frac{a}{R} \delta^{11} \right) - \frac{(\sigma^*)^6}{R^5 r} \left(\delta^4 + \frac{a}{R} \delta^5 \right) \right] \tag{4.6}$$

where

$$\delta^N = \frac{\left[\left(1 - \frac{r}{R} - \frac{a}{R}\right)^{-N} - \left(1 + \frac{r}{R} - \frac{a}{R}\right)\right]^{-N}}{N} \tag{4.7}$$

and z is the number of water molecules that form the cage (the coordination number). ϵ (energy well depth), σ^* (modified Kihara diameter) and a (core diameter) are the pair potential parameters for gas-water interactions. $\sigma^* = \sigma - a$ where σ is the Kihara diameter, which is where the pair potential is zero. A simple way to do manual calculations of the Langmuir constants is to use the correlation $C_{ji} = \frac{A_{ji}}{T} \exp \frac{B_{ji}}{T}$ where A_{ji} and B_{ji} are empirical constants (Parrish and Prausnitz 1972). The original publications are referred to for detailed explanations.

Holder and Manganiello (1982) used van der Waals-Platteeuw theory to show that hydrate azeotropes (no fractionation) may occur only in ternary mixtures (two guest gases and water), meaning that fractionation is bound to occur in systems with three or more guest gases. But among a selection of gases; methane, ethane, ethene, propane, cyclopropane, iso-butane and hydrogen sulfide, hydrate azeotropes are predicted at 273 K for only a few pairs; methane-propane, methane-cyclopropane, methane-isobutane, hydrogen sulfide-propane, hydrogen sulfide-cyclopropane and hydrogen sulfide-isobutane. These are pairs of molecules where the smallest (methane or hydrogen sulfide) fits well into the smallest sII cavity and the largest molecule fits well into the largest sII cavity. All these pairs form sII due to the size of the larger molecule.

Holder and Manganiello gave the following criterion for azeotrope formation: "In general, hydrates formed from a ternary mixture containing two hydrate forming gases and water will have a dissociation pressure for some mixture which is lower than any dissociation pressure of any binary mixture if and only if one of the gases has a diameter ratio, $\frac{\sigma}{d_2}$, for the *large* cavity very near 0.44 and the other gas has a diameter ratio, $\frac{\sigma}{d_1}$, for the *small* cavity near 0.44." σ is the Kihara diameter and d_i is the cavity diameter for cavity of type i.

4.1.3 Fractionation Simulations

The theory of van der Waals and Platteeuw has been implemented in commercially available computer simulation codes, for example CSMHYD from Colorado School of Mines (U.S.A.) and EQUI-PHASE from DB Robinson Research (Canada). These codes may be used to simulate fractionation when a hydrate is in equilibrium with the gas mixture. Required input is the composition of the gas and either pressure or temperature.

Makogon (1997, pp. 43-47) used EQUI-PHASE to simulate fractionation of natural gas of methane (80 and 99 %vol) and ethane, propane, carbon dioxide and butanes. He noted that the composition of the hydrate is determined mainly by the composition of the hydrate forming gas as well as pressure and temperature. Some conclusions were:

- The amount of a heavy component in the hydrate increases with the molecular weight.
- The amount of heavy components in hydrate decreases and methane content increases when both pressure and temperature increase.
- Hydrate formation pressure has the most significant effect on the propane and iso-butane content in hydrate.
- It is suitable to maintain low pressure and temperature during hydrate-based separation.

4.2 Driving Force

The studies in Section 4.1.1 reported hydrate compositions at or close to phase equilibrium. In the present work focus is on hydrate formation away from the equilibrium curve. The purpose is to study hydrate composition as function of the driving force. No papers which report a similar approach were found. But work has been done on the effects of the driving force on kinetics, notably hydrate nucleation.

The driving force is generally an expression which represents the difference between the equilibrium value end the experimental value of some parameter. Sloan (1998, p. 98) listed different driving force expressions that are in use in nucleation modeling (Table 4.3).

Table 4.3: Driving forces in hydrate nucleation (Sloan 1998, p. 98).

Temperature	$T_{eq} - T_{exp}$
Chemical potential	$\mu_{w(h),exp} - \mu_{w(l),exp}$
Fugacity	$\frac{f_{i,exp}}{f_{i,eq}} - 1$
Free energy	ΔG_{exp}

$T_{eq} - T_{exp}$ is usually referred to as subcooling, as in this work, or as supercooling. Relations between the driving force and the induction time are, without exceptions, stochastic and system dependent. The complexity of hydrate kinetics accounts for the lack of deterministic models in the literature. Instead, correlations and best fits are determined. But the results from one laboratory can not be transferred to another laboratory or to the field to do reliable quantitative predictions (Sloan 1998, pp.98-103).

Sloan (1998) noted that there are few justifications based on equilibrium or non-equilibrium thermodynamics for the driving forces listed above. Thus a general driving force derived from basic principles for T=constant is proposed:

$$\Delta G = v_w(P_{eq} - P_{exp}) + RT \sum x_i \ln \frac{f_{i,eq}}{f_{i,exp}} + v_h(P_{exp} - P_{eq}) \qquad (4.8)$$

The first and last right hand terms are due to Pv differences between experimental (exp) and equilibrium (eq) conditions. Since the molar volume of water (v_w) is within 15% of the molar volume of hydrate (v_h), and since these two terms typically are small compared to the $RT \cdots$ term, these Pv terms effectively cancel.

4.3 Discussion

Fractionation Measurements

Both the apparatus of Happel et al. (1994) and that of Ng and Borman (1999) are well suited to study fractionation, but both could be improved by implementing ideas from the other.

Happel et al.'s apparatus. From the gas entered the reactor at the bottom and till the unconverted portion of the gas reached the liquid surface, there

must have been a shift in the gas composition in the bubbles. Consequently, the composition of the purge gas does not give the full picture - it is an approximation. It may be better to feed the gas into the gas pocket and have the gas sampling point far from the feed point, as in the apparatus of Ng and Borman. Happel et al. took small hydrate samples. Ng and Borman allowed all of the hydrate to dissociate and then collected small gas samples from the gas that evolved. It is easier to collect a representative gas sample than a representative hydrate sample.

Ng and Borman's apparatus. To maintain a "constant" gas composition the gas pocket was from time to time displaced and replaced with fresh gas. Between each displacement-replacement cycle, there must have been a continuous shift in the gas pocket composition. It may be better to have an arrangement with continuous feed and purge, using the arrangement of Happel et al.

Driving force

A suitable driving force is needed for the present work. If the driving force is expressed as subcooling it becomes simple to quantify it. It is necessary to know the pressure and temperature and the hydrate equilibrium curve. Both pressure and temperature are easy to measure directly. The equilibrium curve is readily available with sufficient accuracy from computer simulations for the methane-ethane-propane-water system to be used in the present work. It is then easy to find the driving force, ΔT, simply by taking $\Delta T = T_{eq} - T_{exp}$. If this formulation of the driving force is selected it is also easy to log the driving force during the course of an experiment. This is an important consideration since it is necessary to maintain a driving force that is not only constant but has the desired value as defined in the experiment plan. Another important consideration is that pressure can be regulated rapidly, while temperature regulation is usually much slower. For these reasons it was decided to express the driving force as subcooling, ΔT, with unit K in the present work.

4.4 Important Findings

- van der Waals-Platteeuw theory can be used to calculate the composition of hydrate in equilibrium with the hydrate forming gas. This makes it possible to calculate the fractionation in equilibrium systems.

- Fractionation will always occur for systems with three or more guest gases. Fractionation can only be avoided for a limited number of double hydrates (two guest gases).
- Experimental fractionation data in the literature are few, and only systems allowed to form hydrate close to the hydrate equilibrium curve have been studied. It seems the effect of the driving force on fractionation has not been reported earlier.
- The apparatuses of Happel et al. (1994) and of Ng and Borman (1999) are well suited to do fractionation studies.
- It is argued that subcooling is a suitable way to express the driving force in the present work.

Chapter 5

Apparatuses

5.1 Introduction

Five laboratories were designed and built to study different aspects of natural gas hydrate. The laboratory with the most involved design was the *flow loop laboratory* for continuous hydrate production and sampling (Section 5.2). It had a 9 dm^3 continuous stirred tank reactor (CSTR) and two parallel flow lines where different in-line test units (filters, samplers etc.) were connected. The design pressure was 12 MPa and the flow line inner diameter was 20 mm. The volume of the loop was about 35-40 dm^3, depending on the number and type of test units in use. Hydrate samples removed from the flow loop were prepared in the *cold laboratory* (Section 5.3). In the *climate laboratory* (Section 5.5) for natural gas hydrate storage, temperature and air humidity could be controlled. After hydrate production, sample preparation and storage, samples could be analyzed in the *calorimeter laboratory* (Section 5.4), featuring a low-temperature heat flow calorimeter, capable of operating at sample pressures of 10 MPa. These laboratories were built at NTNU in Trondheim. The *batch reactor laboratory* (Section 5.6) to study fractionation in natural gas hydrate formation featured a 0.6 dm^3 batch reactor and a gas chromatograph. It was built at the National Polytechnical Institute in Toulouse in France. Other presentations of the laboratory facilities are those by Andersson (1999), Petersen (1997) and Gudmundsson et al. (1999).

5.2 Flow Loop Laboratory

5.2.1 Conceptual Design

The purpose of the flow loop laboratory was hydrate production and sampling. To justify the conceptual design it is useful to review the objectives of the laboratory and some basic requirements. The main objectives were to produce hydrate for subsequent analysis of thermophysical properties, and to collect operational experience and data on hydrate slurries and continuous hydrate production. This would provide essential engineering input when upscaling to a pilot plant, as well as constituting fundamental science.

The flow loop was not supposed to imitate the future large scale process. However, the hydrate production conditions had to have relevance to the expected future, and a reasonable pressure for the future large-scale process was assumed to be 6 MPa. A design pressure of 12 MPa, the double of 6 MPa, was defined.

The large-scale process for natural gas hydrate production was, and is still today, likely to be a train with one or more reactors of some kind. The closest thing within the economical constraints was a flow loop with a hydrate reactor. A CSTR with standard design was chosen since performance and upscaling correlations of such reactors are known. A circulation pump was needed to circulate the condensed phase. Heat of hydrate formation had to be removed in a heat exchanger. A separator was necessary to handle unconverted gas. Filters were the first choice for hydrate sampling.

It was desirable to operate the reactor (well) within the hydrate pressure-temperature region while at the same time having the option to operate the rest of the loop nearer the hydrate equilibrium curve at a lower pressure. To boost the pressure at the reactor inlet, the pump had to be the last unit preceding the reactor and a pressure reduction valve the first unit downstream of the reactor. It was desirable to remove gas bubbles before the slurry entered the test sections. Thus the separator would follow downstream of the pressure reduction valve, and then the two parallel test unit lines downstream of the separator. The test sections needed a bypass line. The heat exchanger had the greatest potential for plugging, both because of its internal geometry and since this was where the temperature would be lowest. Being conservative, the heat exchanger was placed after the filter (test section). The heat exchanger was the last unit before the pump. Thus,

the pressure would be relatively low in the heat exchanger, making hydrate formation in the heat exchanger less likely. Having decided about the main units and their order, the basic flow sheet in Figure 5.1 was settled.

Choosing standard type of equipment whenever possible and suitable was settled as a basic rule in the concept phase and remained an important guideline. Standard equipment is less expensive and has a shorter delivery time. Another guideline was to have flexibility in mind during design and modifications. The purpose was to be able to operate the loop in different modes and preparing for tasks that were not foreseen at the time. Realizations of this design philosophy was for example the bypass lines and the numerous blinded tees where tubing or sensors could be connected as needed. Another example is that the reactor and the separator had identical measures except the separator was twice the length of the reactor. Parts that fitted one fitted the other as well. Yet another example is the gas supply system with two parallel gas supply lines. It was possible to change from one gas tank to an other in practically no time. This guaranteed continuous gas supply. It also gave the option of changing from one feed composition to another simply by switching valves.

The flow loop was going to be used with water and petroleum fluids. Salts and low-dosage hydrate promoters would be added in some experiments. Thus it was decided to go for stainless steel in all units as well as in tubing and fittings. For safety reasons it was decided that all electrotechnical and electronic installations in the room should be classified for installation in hazardous areas. All units were mounted on a wheeled skid (HxWxL=2.0x1.0x2.2 m^3).

5.2.2 Room Temperature

To have better control of the temperature, the flow loop was placed in a room where the temperature could be regulated between 273 and 298 K. An oven on the wall provided excessive heating, if needed, and the temperature was regulated by a thermostated air conditioner. The idea was to keep the room temperature at the operation temperature. This gave good control of the temperature in all places in the loop. It was a way of minimizing the temperature gradients in the loop. There were no temperature irregularities which caused hydrate dissociation (hot spots) or hydrate deposition (cold spots).

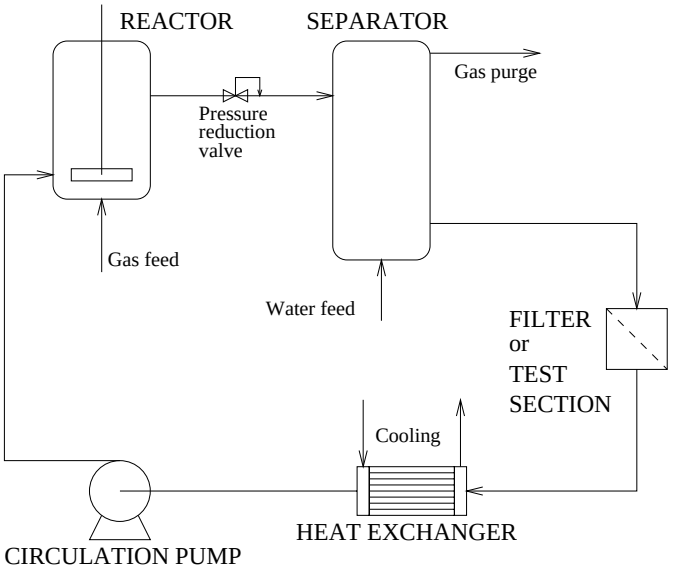

Figure 5.1: Conceptual loop design showing the main units. The second test section line and the test section bypass line are not shown.

After collecting hydrate in a filter, the filter was isolated. If the room temperature had not been close to the operation temperature, hydrate would soon start to dissociate. But since the room temperature was low and the pressure equal to the operation pressure, the hydrate in the isolated filter was thermodynamically stable. There was still no risk of hydrate dissociation when displacing the filtrate (details later). It was also an important requirement in the studies of hydrate slurry rheology, that the temperature of the slurry was well defined and stable (Andersson 1999).

5.2.3 Main Units

Reactor

A CSTR reactor with a standard design was chosen, since the performance and up-scaling of such reactors are well described in the literature. There should be nothing special about the reactor, just baffles, an impeller, inlets and outlets. The only extra thing was the two sparged gas inlets and the view-ports for visual observation and video monitoring. The reactor volume

was settled at 9 dm^3. This volume was 15 times larger than the batch reactor (0.6 dm^3) that had been used previously, and about an order of magnitude smaller than what was regarded as a reasonable reactor volume in a future pilot plant.

The reactor inner length/diameter ratio was $\frac{L}{D} = 378/180$ mm/mm. The baffles extended about $D/10$ from the wall. The impeller diameter was about $D/2.5$ and it was placed $D/2$ above the bottom. The lower inlet and outlet ports were also located $D/2$ above the bottom. The upper ports were located the same distance below the top. The reactor ports could be used for flow inlet or outlet, or they could be used as view-ports or be blinded. There was also the possibility of using the ports for sensors of different kinds. A total of eight ports were symmetrically placed on two levels. The design details were proposed by Proserv who also fabricated the reactor and separator.

The impeller was a straight blade turbine with six blades. It generates radial flow and is especially suited for dispersion of gases in liquids. It was driven by an Autoclave Engineers Magnedrive and could be operated at any speed between 0 and 2500 RPM. The rotation speed was measured and showed on a display.

The gas spargers dispersed the gas, making mass transfer more efficient compared to non-sparged inlets. The two spargers were placed opposite each other, at the same distance from the center of the reactor bottom. This distance was equal to the radius of the impeller. Thus gas was injected at a point close to and just below where the stirring was most vigorous, at the tips of the impeller. The spargers were specially made from small stainless steel cup filters (7 μm) with outer diameter of about 1 cm and a length of about 2 cm. The spargers also held small check-valves to prevent water backflush into the gas feed line.

The reactor liquid (slurry) feed came from the heat exchanger and it was desirable to instantly distribute the feed throughout the reactor. Thus the water or slurry was fed to the reactor through one of the lower ports in the level of the impeller. The outlet line was connected to one of the upper ports.

The unit downstream of the reactor was a Tescom pressure reduction valve. It was only used during some early tests and then dismounted. The performance of the valve was not as desired. The valve had no significance to the work presented here and is not mentioned further.

Separator

The main purpose of the separator was to separate unconverted gas for purging. Its length was twice the length of the reactor. Other dimensions were the same, giving a separator volume of 18 dm^3. It had four upper (lower) ports placed at the same distance from the top (bottom) as in the reactor. Because of the separator length it was given four additional ports in two intermediate levels. The separator volume was about half of the total loop volume.

To avoid gravity separation of hydrate and water in the separator, mixing was provided by a mixing pump. It was a Haskel piston pump which circulated slurry from the bottom of the separator to the top via an external line. Should it be desirable to concentrate the hydrate in the separator separate, the mixing pump was simply not used. Hydrate was then retained in the separator which served as a hydrate holding tank. An exit line for hydrate lean slurry was connected to a lower port. An exit line for hydrate rich slurry was connected to an upper port. The flow sheet in Figure 5.2 only shows the upper exit line.

Test Units

Several types of test units were available. Only cup filters were used in this work. The filter units consisted of the actual filter cup, a perforated support basket for the filter cup and a pressure cell with inlet and outlet valves. Two types of filter cups were used; Köpp porous polymer cups and in-house made cups made from stainless steel mesh. Köpp filter grades of 5, 25 and 80 μm were used. Mesh filter grades were 77 and 510 μm. The inner length and diameter of the polymer cups were 16 and 6 cm, respectively. This yielded a cup volume of about 0.45 dm^3. The mesh filters were somewhat larger. Apart from the filters, a Fras Technology sampler, an in-house tube sampler, a thin-section glass cell and a specially designed tube viscometer were also available and used by Andersson (1999).

The purpose of the support basket was to hold the filter cup in the desired position and to prevent rupture of the filter cloth due to the pressure drop across it. The basket was made from perforated steel plates. The inner dimensions of the support basket fitted closely to the outer dimensions of the filter cup. The basket top flange served as a positioner for the basket and thus for the filter. To direct the slurry through the filter, the flange was designed as a double flange with O-rings at critical places.

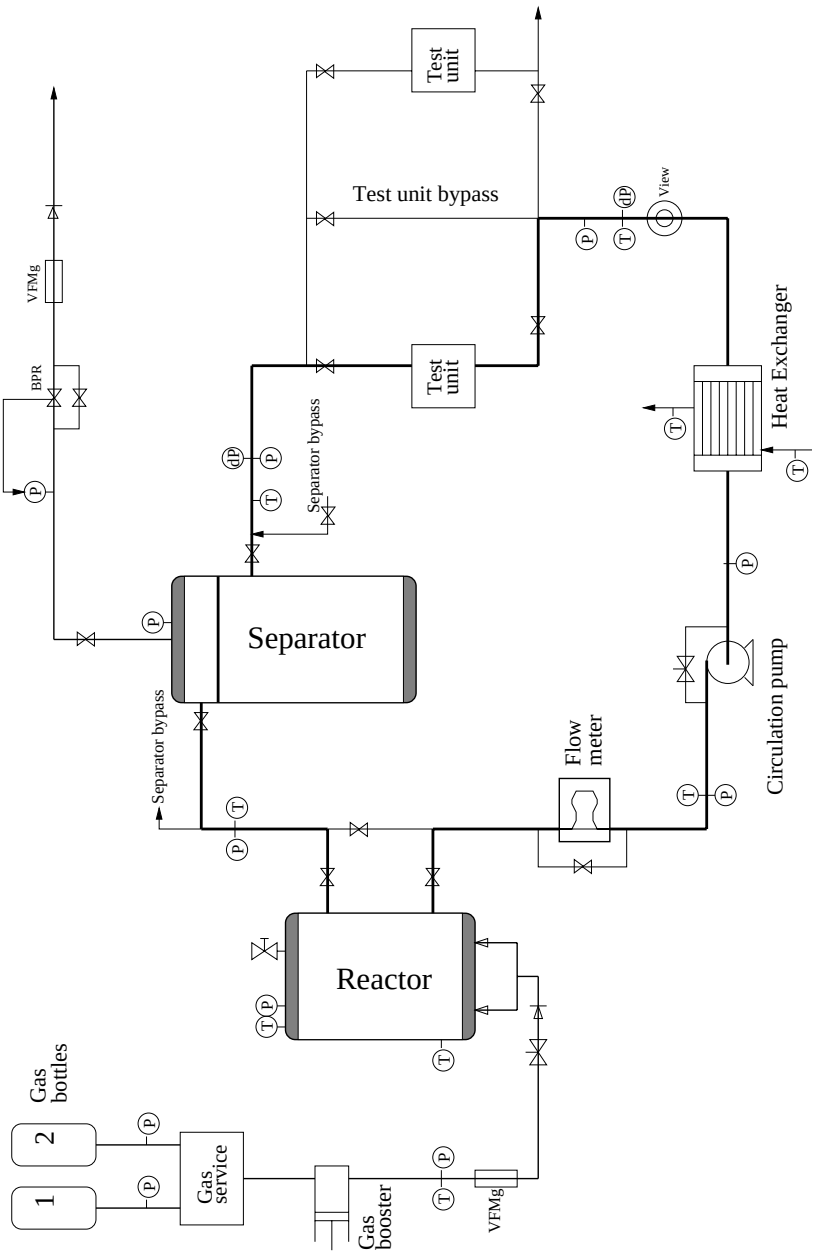

Figure 5.2: Detailed flow sheet of the flow loop laboratory. P and T are pressure transducers and thermocouples, respectively. dP connected to the differential pressure cell. VFM_g are gas flow meters. BPR is the backpressure regulator.

The pressure cell was necessary to enable inline filtration at elevated pressures. The only dimensional requirements were that a filter cup of about one liter should fit into it and it had to withstand the design pressure.

During filtration it was possible to measure the pressure drop across the filter by a differential pressure gauge. After filtration, the annulus between the support basket and the walls of the pressure cell was full of filtrate (water). It was necessary to displace this liquid while maintaining the desired pressure inside the pressure cell. A special valve arrangement was made for the purpose, as illustrated in Figure 5.3. With this arrangement a high-pressure gas of choice could be fed to the pressure cell. The gas flow rate was controlled by the needle valve. As gas was fed through the top, water was displaced through the bottom. The pressure inside the pressure cell was maintained by a relief valve. Upon gas break-trough all of the water had been displaced. The valve arrangement together with the valves permanently mounted on the pressure cell caps constituted a double block and bleed system. This was necessary since the quick connects could not be opened when pressurized. The flow loop also had double block and bleed valves so that test sections could be connected and disconnected while operating the loop.

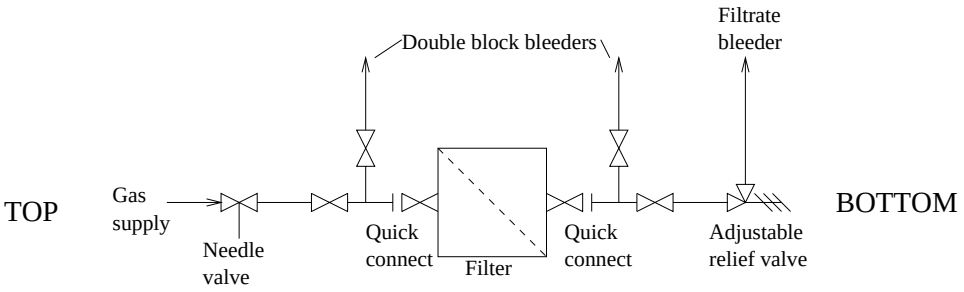

Figure 5.3: Valve arrangement used to displace the filtrate from the filters while maintaining the hydrate production pressure. The double block and bleed arrangement was necessary since the quick connects could not be opened while pressurized.

Heat Exchanger

The purpose of the heat exchanger was to maintain constant temperature in the high-pressure loop. The heat exchanger was a shell-and-tube type, made by Sperre Industri. The main reason for this choice was that the hot

side should have a high design pressure, 12 MPa. For flexibility reasons the heat exchanger was made so that the cold side also could withstand this pressure. The hydrate slurry was on the tube side and the glycol/water cooling media on the shell side. The reason for this configuration was that if hydrate plugging occurred, it would be easier to remove small cylindrical plugs inside the tubes than a larger irregular plug extending throughout most of the shell side and immobilized by the tubes penetrating it.

The cold and hot streams in the shell-and-tube exchanger followed a cross-counterflow pattern. Circulation of cooling media was maintained by a centrifugal pump that worked at constant speed. The duty of the heat exchanger was regulated by a three-way Samson regulating valve. The cooling media flow was constant and the valve directed a proportion of this flow through the heat exchanger. The regulator received temperature signals from one of two optional temperature sensors, one in the reactor and one in the hydrate slurry line line just down-stream of the heat exchanger. To maintain a low temperature in the cooling media, the cooling circuit featured a plate heat exchanger where the cooling media could give away heat to a secondary cooling media (propane). The secondary cooling media exchanged heat with the surroundings in a cooling machine placed out-doors.

If particles or fouling in the cooling circuit should come loose and become trapped in the regulating valve it could malfunction. As a precaution a filter was placed close to the inlet of the regulating valve. For the same reason, and also to prevent poorer heat transfer with time, the cooling media contained a biocide to prevent algae growth. For the regulating valve to function properly there had to be a certain pressure drop in the cooling circuit. By partially closing a ball valve in the cooling circuit extra pressure drop could be generated, if needed. The cooling circuit also had an air trap with a bleed valve at the highest point and a drain valve at the lowest point. A turbine meter in the cooling circuit and temperature sensors to measure the cooling media's temperature increase provided data to accurately calculate the heat exchanger duty.

Circulation Pump

Originally a piston pump identical to the separator mixing pump was used as a circulation pump. It was decided to try this pump type since it was a lot less expensive than the alternatives. After some time of testing it was clear that the pressure pulses that the pump generated made it unsuitable.

The primary reason was that the tube viscometer required non-fluctuating flow.

The pump types that were considered then were monopumps and centrifugal pumps. Both are suitable for slurry pumping and were considered good alternatives. In a monopump particles of considerable size may get through the pump without being crushed. In a centrifugal pump the particles are more likely to be crushed from mechanical impact. Still, a Caster centrifugal pump was chosen for economical reasons. The flow could be regulated between zero and about 100 dm^3/min, depending on the pressure drop through the loop. The pressure drop depended on which units were bypassed and which were not, and the viscosity of the fluid.

5.2.4 Utility Units

Compressor

Gas could be fed to the reactor directly from the gas tanks. But if the tank pressure was below the operation pressure the gas needed boosting. A Haskel piston compressor was used. Pilot valves on the compressor started and stopped the compressor automatically whenever needed.

Water Feed Pump

There were two ways to feed liquid to the loop. Before pressurization, water was usually sucked into the loop after evacuating it. This gave full control of the water volume and air pockets were completely avoided. If it was necessary to inject water while the loop was pressurized, this was done by the water feed pump; a Haskel piston pump. The stroke volume of the pump was small (2.14 cm^3) and one by one stroke could be made through manual operation. This made it suitable as a dosage pump for additives. By adding diluted additives and by performing the injection over a time that was at least as long as the loop circulation time, the additives could be fairly well distributed throughout the slurry volume. The injection point was at the pump inlet to benefit further from the mixing in the volute.

Degasser

To avoid effects from air dissolved in the water, the water was degassed before it was transfered to to the loop. Degassing took place in a specially designed vacuum tank. A filter between the tank and the loop removed particles in the feed water. The main reason for filtering the water was that particles such as sand could damage the valves in the loop. The degasser and its connections are shown in Figure 5.4. The tank was mounted on a rocking skid so that it could be rotated manually almost 360°. Thus the tank was also suitable for preparation of solutions or emulsions in volumes larger than the loop volume. After degassing the tank could be moderately pressurized with a gas, typically methane, and water sucked/displaced into the loop. Alternatively, water could be directed to the water feed pump for high-pressure injection.

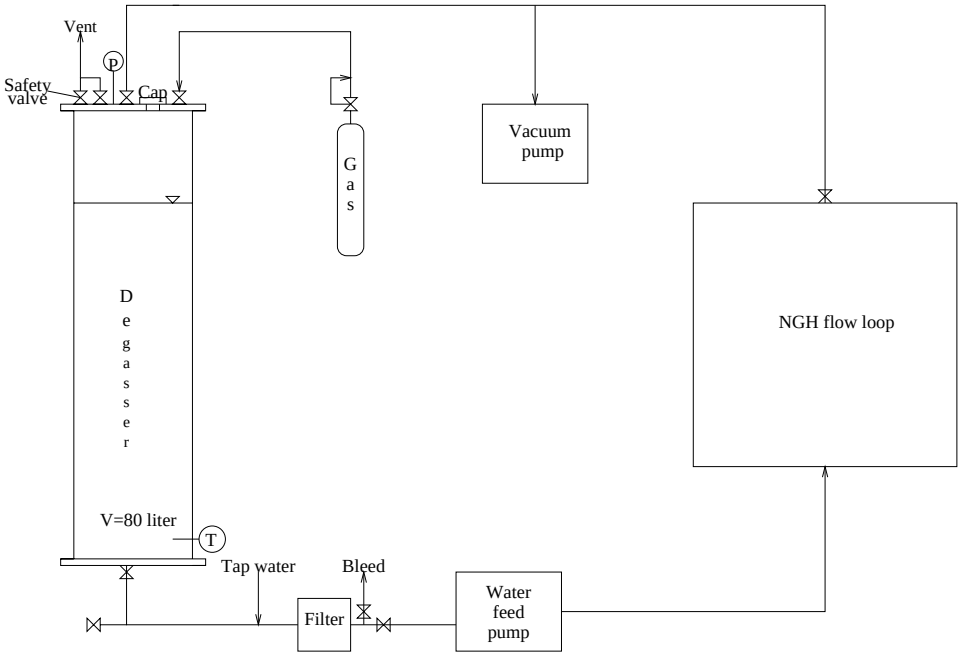

Figure 5.4: The degasser.

Vacuum Pump

The vacuum pump had two uses. It could be used to evacuate the degasser. Consequently the water would give off its dissolved air. Better control with the overall composition of the system in the loop was obtained. After degassing, the degasser could be moderately pressurized with a gas, usually methane.

The other use of the vacuum pump was to evacuate the flow loop. Then the loop could be connected to the degasser and a desired amount of water would flow quickly into the loop. The vacuum pump was made by Leybold and had a final pressure of $< 10^{-2}$ Pa.

View-port

The value of visual observations was expected to be high. Qualitative information could help understanding the system. Thus a view port was placed in the flow loop, downstream of the test sections. It would then be possible to observe the effect of filtration. By bypassing the filters it would also be possible to determine how long it would take to make hydrate particles large enough to be observed visually. This could be a quantitative, although not deterministic, way to describe different systems. Studies of agglomeration and particle size were also among the foreseen uses of the view-port. It had a light opening of 38 mm and with two windows placed on opposite sides of the flow. Thus it was possible to look "through" the slurry and not only "on" the slurry.

Valves, Fittings and Tubing

The main criteria when selecting valves and fittings were that all items had to be made of stainless steel and all items had to be available within the same fitting system. Swagelok fittings and Whitey valves were chosen. The main loop with bypass-lines had 25 mm tubing with 20 mm inner diameter. Gas lines were made from 6 mm tubing. Flexible hoses with quick connects were used between the test units and the rest of the loop. Double block and bleed arrangements were necessary since the quick connects could not be opened while pressurized. Numerous special parts were made at the in-house mechanical workshop.

5.2.5 Instrumentation, Regulation and Logging

Pressure

Pressure was measured by Keller pressure transducers. They were placed upstream and downstream of all main units. For the reactor and separator, the pressure was measured in the units as well. See Figure 5.2. The transducer range was 0 to 10 MPa. Pressures at each measuring point were shown on displays placed on one of the walls in the flow loop laboratory. The pressure profile in the loop could then be monitored in real-time.

There were two ways to regulate the pressure, depending on the mode of operation. Usually, there was a continuous supply of gas that exceeded the gas conversion rate. The excess gas collected in the separator and was purged through a back-pressure regulator to the vent line. Thus constant pressure was maintained. Alternatively, the purge line was closed. Pressure was then regulated by setting the gas supply pressure somewhat higher than the operation pressure and supply gas through a needle valve, as seen on the flow sheet. The pressure drop over the needle valve and the spargers accounted for most of the pressure difference between supply pressure and operation pressure.

Temperature

PT-100 temperature sensors were placed together with the pressure transducers, upstream and downstream of all main units, as well as in the reactor and the separator. There was a display for each temperature sensor so the temperature profile in the loop could be read at any time.

The temperature was regulated by the regulating valve in the cooling circuit, as described earlier. To have even better control with the temperature, the whole flow loop was placed in a thermostated room. Room temperature could then be set at the operating temperature. This gave a flatter temperature profile. There was also a sensor to measure the room temperature.

Differential Pressure

The pressure drop over a test section was measured by a Fuji Electric differential pressure sensor. The main purpose was to monitor the pressure

drop during filtration. This gave information about how the filtration was progressing, as a thick filter cake gives a high pressure drop.

Gas Flow

Bronkhorst gas flow meters were installed on the gas supply line and on the gas vent line. The gas flows were shown on displays on the wall in the flow loop laboratory. The gas flow meters with the displays were necessary to be able to regulate the gas supply rate. Regulation was done manually. The parameters that together determined the gas supply rate was the opening of the needle valve on the gas supply line and also the difference between the gas supply pressure and operation pressure. Gas flow data were also necessary to establish the mass balance, since the difference between supplied gas and purged gas was accounted for by the hydrated gas, the gas pocket in the separator (and gas bubbles) and dissolved gas.

Liquid Flow

The liquid or slurry flow in the flow loop was measured by a Fisher-Rosemont coriolis meter. The flow rate was controlled by manually regulating the speed of the circulation pump.

In the cooling circuit there was a Nixon Instrumentation turbine meter which measured the cooling media flow rate through the heat exchanger. This meter too had a wall-mounted display connected to it. The circulation pump in the cooling circuit worked at constant speed. The flow rate of cooling media through the heat exchanger was regulated automatically by the regulating valve, as described above.

Data Logging

A large number of electronic measuring devices have now been described. Every one of them gave a continuous analog signal that was collected by the data logger installed on a personal computer. LabVIEW was used to collect the data. The user interface displayed the pressure and temperatures at different positions in the flow loop. The pressure drop over the filter (test section) was also displayed, as was the gas flow rate in the supply line and the purge line. Data from every sensor were available, in real-time and in

the log files. The logging frequency was set by the operator and could be changed at any time during an experiment.

5.2.6 Safety

Important safety issues were preventing gas leakages, preventing ignition should there still be a leakage, and preventing the loop pressure to exceed the design pressure. Line rupture valves were mounted on the two parallel gas feed lines as well as at the compressor outlet. If an explosive atmosphere were created after all, the probability of ignition was small since all electrical and electronic installations, sensors and transmitters as well as switches, lightening and air conditioning, were intrinsically safe and classified for installation in hazardous area zone 2 where, by definition, "an explosive gas/air mixture is not likely to occur in normal operation, and if it occurs it will exist only for a short time".

A combustible gas sensor was used routinely to monitor the contents of hydrocarbons in the air. Two ventilation fans were installed, one which drew air from the laboratory and an other which supplied fresh air. A 2 m^2 relief panel was placed on one of the walls.

If there was a malfunction of the gas supply system or the operator made an error, it could be that the pressure would exceed the design pressure. Safety valves relieved excess gas through a vent line. To qualify the flow loop for operation at pressures up to the design pressure it was pressure tested at 15 MPa, a pressure which exceeded the design pressure by 25%. The pressure test was carried out by using the water feed pump to completely fill and pressurize the loop with water. The test pressure was maintained for 30 minutes.

5.2.7 Miscellaneous

Video equipment

A Sony video camera was used to record the slurry passing through the view-port downstream of the filters. A Sony micro camera was small enough (12 mm diameter) to fit into the windows of the reactor and separator, and was used together with the thin-section glass cell too. It had a specially made system for back-lightening. Video images could be exported to the

Optimas image processing software. These facilities were primarily used by Andersson (1999) in the studies of hydrate slurry rheology.

Control Room

The situation in the flow loop laboratory could be monitored from the control room in a neighbouring building. It was necessary to have such a room, since the laboratory was noisy, cold and drafty. In the control room, all logging channels could be read at any time. A video monitor gave qualitative information regarding slurry appearance and hydrate content. If the circulation should stop, this would bee seen immediately.

5.3 Cold Laboratory

The purpose of the cold laboratory was to prepare hydrate samples. The room had temperature regulation down to nearly 250 K and was placed next-door to the flow loop laboratory. The cold laboratory was necessary to freeze the filter cakes, for sample preparation and for placing samples in the calorimeter sample cell. All this had to take place at temperatures equal to or below the hydrate storage temperature, i.e. well below 273 K. The room contained a sturdy working bench with a vise and a saw that were used to cleave the filter cups with the frozen filter cake. A porcelain mortar and a range of sieves (1-10 mm, $\pm$0.2 mm) were available for samples preparation.

A portable glove compartment was available when transferring the calorimeter sample cell from the cold laboratory to the calorimeter laboratory in a neighbouring building. The glove compartment was filled with nitrogen. The idea was to prevent frost deposit on the sample cell as this would be a source of error in the measurements. A balance ($\pm$0.01 g) was used to measure the sample mass.

5.4 Calorimeter Laboratory

The purpose of the calorimeter laboratory was to measure thermophysical and compositional properties of hydrate in the hydrate-ice samples that were obtained from the flow loop laboratory. The calorimeter laboratory featured the main analytical instrument used in this work, a Setaram BT2.15 heat

flow calorimeter. Important requirements when choosing a calorimeter were the possibilities to operate at temperatures well below 273 K and pressurize the sample with a gas of choice. The sample cell volume should be several cm^3, since large samples were desired to suppress effects of sample inhomogenities. Also, a similar calorimeter had been used by (Handa 1986a; Handa 1986b; Handa 1986c) to do experiments that had similarities to what was planned in this work. The calorimeter laboratory was placed in the same room as the climate laboratory.

Figure 5.5 shows the calorimeter and attached units. It contained two identical cells; the sample cell (S) and the reference cell (R). A temperature sensor for measuring the sample temperature was placed near, yet outside, the sample cell. Both cells were placed in a thermal block with heat flux meters surrounding the cells. Electrical heating was supplied if required according to the temperature program (see below). Excessive cooling was continuously provided by saturated nitrogen (77 K). The nitrogen gas was continuously supplied from a liquid nitrogen tank that had a heating element for nitrogen vaporization. Nitrogen that had gone through the calorimeter and absorbed heat was vented to the surroundings.

The tubing arrangement included a pressure transducer, a pressurized gas tank and valves. It was possible to adjust the pressure accurately in the two cells. The arrangement also made it possible to remove undesired gas(es) from the cells, either by evacuation or by pressurization-depressurization cycles. The cell pressure was logged with LabVIEW.

Two modes of operation were possible; scanning mode and isothermal mode. A period with either scanning operation at a constant temperature transient or isothermal operation at a constant temperature is called a sequence. A temperature program is made from one or more sequences. The calorimeter was controlled by the SetSoft computer program which accompanied the calorimeter. The temperature programs were edited in SetSoft which also handled the logging of sample temperature and heat flow as function of time.

Two types of calorimeter cells were used in this work. The one used to analyze hydrate was an open cell with a volume of 8.5 cm^3 and with a tube rod, hence it was possible to control the pressure inside the cells between 0 and 10 MPa. The other type of cell was a closed cell with a volume of 12.5 cm^3 and with a solid rod. It was used in some introductory experiments. A Mettler balance ($\pm$0.002 g) was also available.

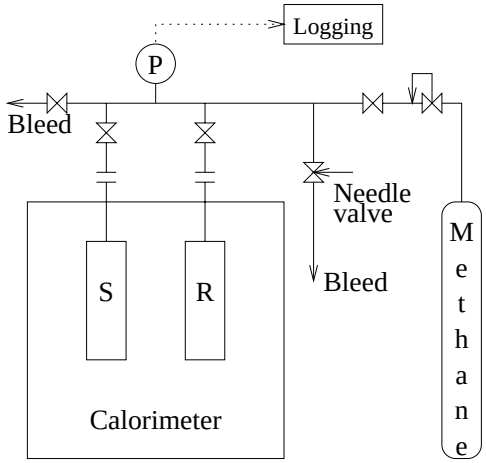

Figure 5.5: The calorimeter with attached units.

5.5 Climate Laboratory

The purpose of the climate laboratory was to store hydrate samples under controlled climatic conditions, including temperature and composition of the atmosphere, notably relative humidity. The climate laboratory was designed for metastable storage of refrigerated hydrate at ambient pressure (1 atm).

It was decided to go for a solution with desiccators and Sanyo laboratory freezers. Hydrate was put in a desiccator and the desiccator in a freezer. The relative air humidity in the desiccator was maintained at about 100 %RH by placing crushed ice in the bottom. Dry air was obtained by using silica gel. It was also possible to add gases, such as methane, to alter the composition of the atmosphere surrounding the hydrate sample. Temperature could be controlled in intervals of 1 K between 224 K and 278 K (± 2 K).

A Vaisala sensor for temperature and relative humidity was placed in one of the desiccators. A pressure transducer was also placed inside the desiccator. The sensors gave continuous logging signals. These were collected by LabVIEW installed on a personal computer. In other desiccators relative humidity and temperature were measured by traditional analog instruments that were read manually. The accuracy of these varied. The relative humidity meter had a larger error for temperatures below 273 K.

One of the freezer cabinets could be used to do storage experiments at differ-

ent temperatures. In the other cabinet filter cakes were kept at the lowest possible temperature, 224 K. Samples could later be prepared from these cakes. One household freezer was available for storage at about 255 K. One household freezer was modified, and had temperature regulation between between 255 K and 273 K.

5.6 Batch Reactor Laboratory

5.6.1 Concept

The purpose of the batch reactor laboratory was to study fractionation when a gas mixture forms hydrate. There were two basic requirements; controlled and repeatable conditions during hydrate production and ability to perform quantitative analysis of gas mixtures. A batch reactor with pressure regulation immersed in a water bath with temperature regulation was the used to produce hydrate (Figure 5.6).

A gas chromatograph with a flame ionization detector was used for gas analysis. The gas chromatograph sampling line could be connected to different gas sample sources, notably a dissociation cell, the reactor or the bottle with calibration gas. A household freezer (252 K) was used to stabilize the hydrate by refrigerating it while it was still in the reactor and at the hydrate production pressure.

5.6.2 Reactor

The assembly for hydrate production is shown in Figure 5.6. The reactor was a stirred batch reactor made of stainless steel. This was the same reactor used by Gudmundsson et al. (1994). Inner diameter was 75 mm and inner length was 140 mm, yielding a volume of about 600 cm^3. The stirrer was a shafted, plastic coated, magnetic bar. Two small bolts on the reactor bottom baffled the water, although their primary function was to fix a rod which served as an upper shaft bearing. The magnetic bar was rotated by a magnetic stirrer placed under the reactor. The reactor had two ports with closing valves on the wall. One port was connected to an Alcatel vacuum pump which gave a final pressure of 5 Pa. The other port was connected to a gas supply line. The top cap of the reactor could be removed to get access to the hydrate. The bottom cap with the stirrer could also be dismounted,

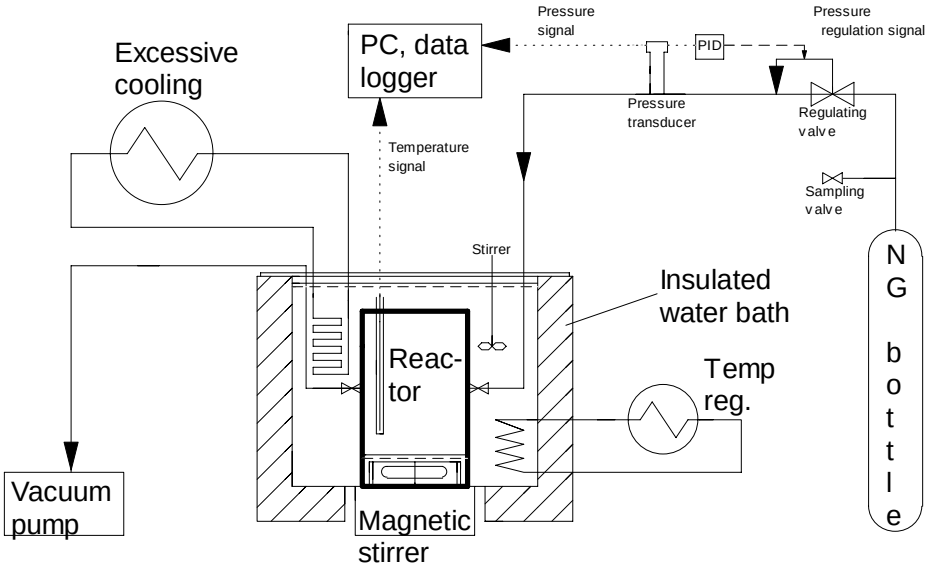

Figure 5.6: Laboratory for hydrate production to study fractionation.

although this was never done during everyday operation.

The reactor was placed in a water bath with good mixing. A cold sink which provided excess cooling exchanged heat with the water bath. Bath temperature was kept constant by a thermostatic heater, thus the reactor temperature was regulated indirectly. It was taken into account that during hydrate production the reactor temperature was typically 0.3 to 0.5 K above the cooling water temperature. The reactor temperature was read by a PT-100 sensor in a thermopocket and the cooling water temperature by a thermocouple. The pressure in the reactor was read by a pressure transducer. Via a PID regulator, the transducer gave a signal to a pressure regulating valve. The reactor was operated within ± 0.5 K of the temperature set point and within ± 0.2 MPa of the pressure set point. Reactor pressure and temperature as well as cooling bath temperature were logged by a personal computer using the Synchronie logging program.

5.6.3 Gas Analysis

The gas samples that were injected to the gas chromatograph were of three different categories; calibration gas, gas from the gas cap in the reactor at the end of the hydrate production period and gas from dissociated hydrate. Calibration gas was injected from the gas bottle. Reactor gas was injected directly from the reactor. Gas from dissociated hydrate was injected from a dissociation cell with a volume of about 80 cm^3. The cell was made from tubular heavy-duty transparent plastic with threaded ends for the caps. It was possible to visually observe the hydrate sample as dissociation proceeded.

An Intersmat IGC 120 DFL gas chromatograph with a loop (0.3 cm^3), a porapak N 80-100 column ($\approx$2 m) and a flame ionization detector was used to make quantitative analysis of methane, ethane and propane. The temperature program had three sequences; an isotherm (351 K, 1.5 min), a ramp (20 K/min) and a final isotherm (403 K) which lasted long enough for propane to elute. The gas in the loop was injected after a static period (6 s) to make the total molar amount of gas in the loop approximately equal in all injections. A Hewlett-Packard HP 3396 series II integrator was used to perform peak integration. Normalized concentrations were calculated from the measured chromatographic areas. Absolute concentrations were not needed.

Chapter 6

Hydrate Sampling and Calorimetry Method

6.1 Introduction

The purpose of the study reported in this chapter was to develop two experimental methods; a method for continuous hydrate production and sampling (Section 6.2) and a method for calorimetric analysis of the hydrate samples (Section 6.3). These methods are the main results presented in this chapter. The apparatus for hydrate production and sampling was described in Section 5.2. The calorimeter was described in Section 5.4.

The calorimetry method can provide data to determine thermophysical properties; specific heat capacity (c_p, J/gK) and specific enthalpy of hydrate dissociation (Δh_{diss}, J/g), and compositional properties; hydrate number (n, -) and amount of free water (f, %mass). Free water is the term used to designate occluded water, meaning water not converted to hydrate. The composition of the hydrated gas is reported separately in Chapter 8.

Hydrate was readily produced in the flow-loop. Sampling was more difficult, and the development the calorimetric method was the biggest challenge to the present work.

6.2 Method for Continuous Hydrate Production and Sampling

The flow loop where hydrate was made is described in Section 5.2. Andersson (1999, pp. 53-56) gave a description of hydrate production which stresses the slurry related issues. The hydrate used in the present work was made from degassed tap-water and a gas mixture containing ethane (5 %mol) and propane (3 %mol) in methane. The water was prepared in the degasser, described in Section 5.2.4. Tap water was degassed by vacuum boiling at about 0.2-1 kPa. After degassing the degasser was pressurized to about 0.3 MPa using methane. The flow-loop was evacuated. The degasser and the loop were connected and water was displaced into the loop. In this manner the loop was filled with any desired amount of water, leaving a gas cap in the separator. Next, the loop was pressurized to just below the hydrate equilibrium pressure for the desired operation temperature. The system was left like this with the reactor stirring, the circulation and the cooling on to presaturate and cool the system before the hydrate production started, usually the next day.

Gas was sparged through the reactor bottom during hydrate production. There were two modes of operation - open system and closed system. In case of an open system, gas was continuously vented from the separator gas cap. This was achieved by applying a feed pressure slightly above the operation pressure, while on the vent line there was a back-pressure regulator which took care of gas venting and pressure regulation. For closed system operation, the vent line was closed. Gas was injected when the pressure in the system had dropped below the set pressure due to hydrate formation.

Hydrate formed readily. The slurry was circulated while injecting gas until the hydrate concentration became appreciable. During hydrate production the test unit bypass line was used (Figure 5.2). To collect hydrate samples the slurry was led through one of the test sections. In this case the test section was an in-line cup filter described in Section 5.2.3. The pressure drop while the slurry was flowing through the test section bypass line was typically about 0.025 MPa for a flowrate of about 50 dm^3/min. When the slurry was directed through the filter, the pressure drop increased to about 0.1 to 0.25 MPa. The maximum pressure drop established within 30 minutes which became the typical duration of the filtrations.

After filtration, the filter inlet and outlet valves were closed and the filter disconnected from the loop. In this way the hydrate production pressure was maintained in the filter cell. It was necessary to remove the filtrate in the annulus between the filter cup and the wall of the pressure cell. By using a special valve arrangement (Figure 5.3) the filtrate was displaced by gas. The valve arrangement made it possible to maintain the pressure in the filter cell while the filtrate was displaced. The gas had the same composition as the feed gas used during hydrate production in the flow loop. After the filtrate was displaced the filter cell was put in the cold laboratory (≈ 253 K) overnight.

The next day the filters were depressurized and opened. The filter cups were cleaved and samples from the cakes were crushed. To reduce the effect of sample inhomogeneities the sample collected from the filter was larger than the portion eventually transferred to the sample cell. Using sieves from 1 to 10 mm in steps of 1 mm a suitable size range of frozen hydrate was collected. The samples were subject to further analysis in the calorimeter.

A special procedure was used to transfer the samples to the calorimeter sample cell, and the cell to the calorimeter. It was necessary that the samples were kept well below 273 K before the analyzes. This implied that the cell had to be cooled before the sample was introduced to it. It also meant that precautions had to be taken while moving the cell from the cold laboratory to the calorimeter laboratory, since frosting on the cell would give erroneous results. A portable glove compartment was used. It was filled with nitrogen and a special port was made for transfer of the cell to the calorimeter without exposing the cell to surrounding air.

6.3 Calorimetric Method

Levik (1999) described in details the calorimetric experimental work on hydrate up to May 1999. The outcome was the *preliminary* calorimetric method to find Δh_{diss}, n and f. How to find c_p was also described.

The preliminary calorimetric method is reviewed in Section 6.3.2. The underlying experiments and results are presented in Appendix B. The preliminary method is criticized in Section 6.3.3 and modified into a *final* calorimetric method in Section 6.3.4. The final method is argued to be more accurate, but was not validated.

6.3.1 Introductory Experiments

The aim of the introductory experiments was to validate procedures and the performance and calibration of the calorimeter. This was done by measuring c_p for ice. The following procedure was used:

1. Cool the calorimeter to the desired start temperature. Place the ice sample in the calorimeter. Allow time for thermostabilization (no transients in temperature or heat flow).
2. Heat the sample at constant rate. The start temperature should be about 10 K below the cold end of the temperature interval of interest. The stop temperature should be about 10 K above the hot end of the temperature interval of interest.
3. Export the log file with time (t), temperature (T) and heat flow ($\dot{Q}$) to a suitable software for data processing. The sample mass (m) is also a required input.
4. Plot accumulated specific enthalpy, $\Delta h(T)$ (J/g), as a function of temperature. Fit the curve as a virial equation of degree $n+1$ in T.
5. By definition, $c_p = \frac{d\Delta h(T)}{dT}$. Taking the derivative of the accumulated enthalpy equation yields c_p as a virial equation of degree n in T: $c_p = a_0 + a_1 T + a_2 T^2 + a_3 T^3 + \cdots + a_n T^n$.

Using this method on ice samples at ambient pressure, a c_p virial equation was derived. It is plotted in Figure 6.1 together with correlations from the literature. The deviation from literature values was 2% or less - well within the ±3% error band of one of the literature correlations (Ede 1966). This was considered satisfactory.

The enthalpy of ice melting was found to correspond within ±0.5% of the literature value, 6.012 kJ/mol or 333.7 J/g (Weast et al. 1986)[1]. This was considered satisfactory.

Hydrate samples with ice were heated at ambient pressure. It showed that dissociation and ice melting occurred *simultaneously* at about 273 K. Handa

[1] The reference gives the value with unit cal/mol. A conversion factor of 4.1868 was used.

(1986a) reported that krypton hydrate too can show this behavior, where a large portion of the hydrate dissociates around 273 K as the ice melts.

The overall conclusions of the introductory experiments were that literature observations were reproduced, the calorimeter was calibrated with sufficient accuracy and that the procedure to determine c_p virial equations and enthalpy of phase transitions are suitable.

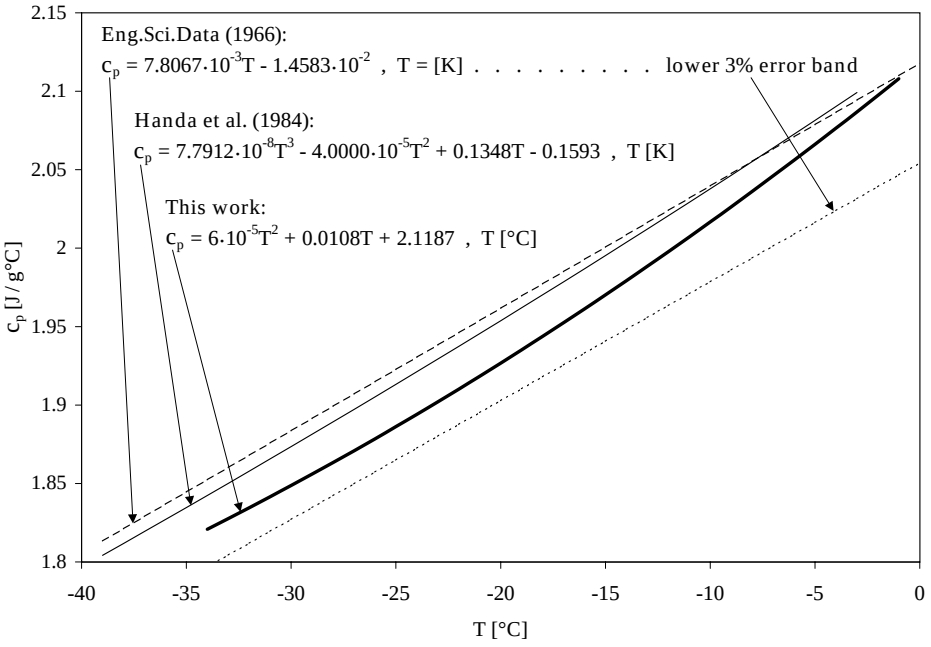

Figure 6.1: Comparison of different virial equations for c_p of ice.

6.3.2 Preliminary Calorimetric Method

The preliminary method is now given step by step. Assume that the hydrate sample is already placed in the calorimeter as explained in Section 6.2. The method involves three heating-cooling cycles or scanning cycles. Each cycle has a specific purpose and each cycle has been optimized with respect to heating rates, cooling rates, duration of isotherms and pressure. The sample is not pressurized during the third cycle. The three cycles are:

Ice conditioning. The pressurized sample is heated above 273 K to allow the free water, which is present as ice, to melt. The gas used to pressurize the sample and the melted water is assumed to reach phase equilibrium. This eliminates thermal effects due to absorption and desorption in the second cycle. See Figure 6.2.

Ice melting. The pressurized sample is heated above 273 K to allow the free water, which is present as ice, to melt. The specific enthalpy of ice melting at the experimental conditions, is known. The amount of free water (ice) and hydrate in the sample may thus be calculated. See Figure 6.3.

Hydrate dissociation. The pressure is relieved and the sample heated above 273 K. This leads to ice melting accompanied by hydrate dissociation at around 273 K. The specific enthalpy of ice melting at the experimental conditions is known. The specific enthalpy of hydrate dissociation may thus be found. See Figure 6.4.

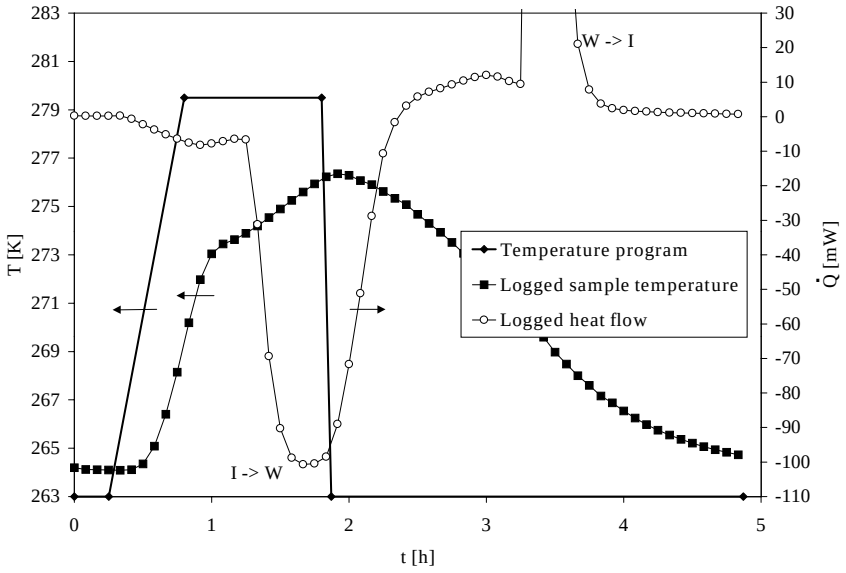

Figure 6.2: Ice conditioning.

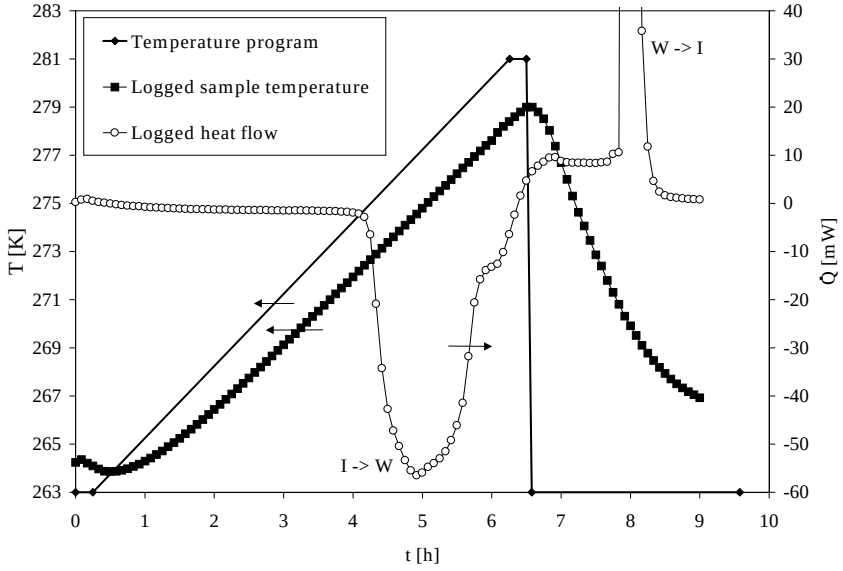

Figure 6.3: Ice melting.

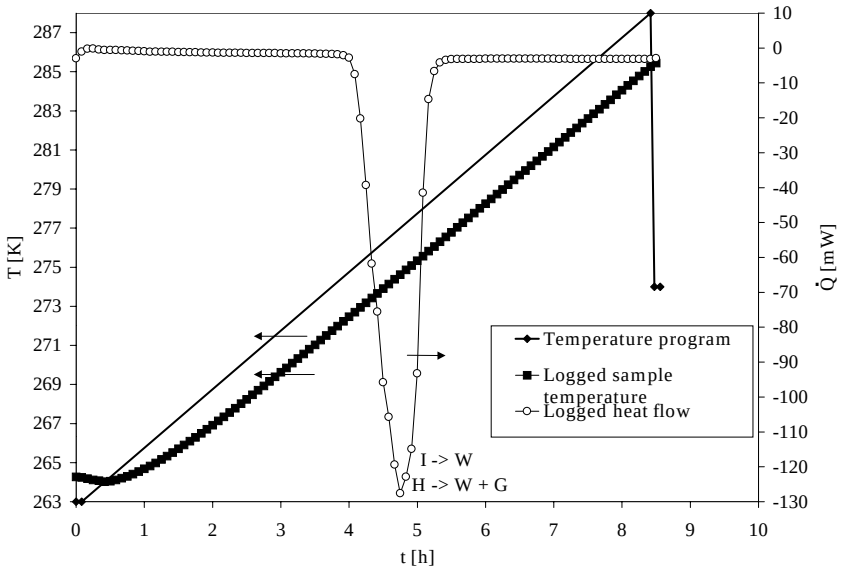

Figure 6.4: Hydrate dissociation.

The calorimeter is operated according to the following procedure. The three cycles are described in detail afterwards along with some comments.

1. Precool the calorimeter to 263 K.
2. Introduce the weighted sample (≈0.9 g) as described in Section 6.2.
3. Pressurize the sample to 1.7 MPa with methane.
4. Allow the calorimeter to thermostabilize (no transients) at 263 K.
5. Invoke the scanning cycle *Ice conditioning* (Figure 6.2).
6. Allow the calorimeter to thermostabilize (no transients) at 263 K.
7. Invoke the scanning cycle *Ice melting* (Figure 6.3).
8. Bleed off the gas in the sample and reference cells to obtain ambient pressure.
9. Allow the calorimeter to thermostabilize (no transients) at 263 K.
10. Invoke the scanning cycle *Hydrate dissociation* (Figure 6.4).
11. Determine the mass of total water (hydrate water + free water) by weighing.

Ice Conditioning

The heating-cooling cycle *Ice conditioning* (Figure 6.2) lasts about five hours. It is important to note that the temperatures that define the different sequences are *program* temperatures and that the *sample* temperature may be quite different, as apparent from Figures 6.2 to 6.4. It is made of the following sequences.

Sequence 1 Isothermal sequence (263 K, 15 minutes). The pressure is about 1.7 MPa. It is seen from Figure 6.5 that at these pressure-temperature conditions the system is located between the hydrate curve for methane and the hydrate forming natural gas. At these conditions there is no formation or dissociation of hydrate. The 15 minute duration is a formal value as the system is given what ever time necessary to thermostabilize before the scanning cycle is invoked.

Sequence 2 Heating sequence (263 K to 279.5 K at 0.5 K/min). The final temperature is such that the ice in a sample of ≈0.9 g has time to melt during Sequence 3. 279.5 K is of course more than the 273 K needed to melt ice, but remember that 279.5 K is the program temperature - the sample does not reach this temperature, as seen in Figure 6.2. A rate of exactly 0.5 K/min is not required, but it is a scanning rate that proved suitable.

Sequence 3 Isothermal sequence (279.5 K, 1 hour). A duration of exactly 1 hour is not necessary. But it is necessary that this isotherm lasts long enough for all ice to melt so the free water may equilibrate with the gas phase. This is the actual conditioning which is a critical element in the overall method. Sequence 3 should not last much longer than necessary to melt the ice. About 1 hour has shown to be about right, as may be seen in Figure 6.2.

Sequence 4 Cooling sequence (279.5 K to 263 K at −4 K/min). The purpose of this sequence is only to freeze the conditioned water. There is no reason to use any other cooling rate than the highest possible; −4 K/min.

Sequence 5 Isothermal sequence (263 K, 3 hours). The temperature is 263 K for the same reasons as described in Sequence 1. The long duration is due to the fact that a *program* cooling rate of −4 K/min is not practically obtainable, as may be seen in Figure 6.2. So for the sample to reach 263 K, three hours or more is necessary. The system is then ready for the next heating-cooling cycle.

Ice Melting

The heating-cooling cycle *Ice melting* (Figure 6.3) lasts about nine hours. It is made of the following sequences.

Sequence 1 Isothermal sequence (263 K, 15 min). This sequence is justified by the same principles as for sequence 1 in the *Ice conditioning* cycle.

Sequence 2 Heating sequence (263 K to 281 K at 0.05 K/min). The initial and final temperature are justified under Sequence 2 for the *Ice conditioning* cycle. The heating rate of 0.05 K/min showed to be suitable as it yielded smooth ice melting peaks.

Sequence 3 Isothermal sequence (279.5 K, 15 min). This sequence only finishes off Sequence 2 smoothly and could be excluded from the temperature program.

Sequence 4 Cooling sequence (279.5 K to 263 K at -4 K/min). The purpose of this sequence is to refreeze the water. As in Sequence 4 in the Ice Conditioning program, there is no reason to use any other cooling rate than the highest possible.

Sequence 5 Isothermal sequence (263 K, 3 h). This sequence starts the thermostabilization at 263 K. The duration is somewhat arbitrary, as it may take longer than 3 hours to obtain thermostabilization.

Hydrate Dissociation

The heating-cooling cycle *Hydrate dissociation* (Figure 6.4) lasts about nine hours. After the *Ice melting* cycle, but before the *Hydrate dissociation* cycle, the pressure has been reduced to ambient and the calorimeter cells are left open to the surroundings. The *Hydrate dissociation* cycle is made of the following sequences.

Sequence 1 Isothermal sequence (263 K, 5 min). This sequence only indicates that the sample is thermostabilized.

Sequence 2 Heating sequence (263 K to 288 K at 0.05 K/min). The final temperature is set at 288 K so that all the hydrate will dissociate and all the ice melt. There is a lag between the program temperature and the sample temperature, such that the sample will never reach 288 K. The heating rate is 0.05 K/min because this was the heating rate in the *Ice melting* cycle. Calorimetric measurements are sensible to effects of heating rate, so the heating rate should be the same in these two scanning cycles.

Sequence 3 Cooling sequence (288 K to 274 K at -4 K/min). In sequence 2, hydrate dissociation and ice melting were completed. During day-time the sample cell could then be weighted to find the mass of total water. But to reduce the evaporation loss if Sequence 2 finished during night-time the sample is cooled to 274 K. Tests have shown that the vaporization loss at 274 K is below the detection limit (0.001 g) after 12 hours.

Sequence 4 Isothermal sequence (274 K, 5 min). The duration of 5 minutes is arbitrary. This is just to indicate that the sample is thermostabilized at this temperature.

6.3.3 Criticism of the Preliminary Method

Errors in the Preliminary Method

To quantify the errors, the method was used in two experiments. These experiments are called Test 8 and Test 11 in Appendix B. The results are given in Table 6.1.

Table 6.1: Experimental results and random errors in calorimeter tests no. 8 and 11. For Test 8 the error intervals were calculated using Gauss' law of random error propagation (Levik 1999). For Test 11 the same random error intervals were assumed. The ideal hydrate number (complete filling) of sII hydrate is $n = 5.67$. The experimental results cover this value.

	Test 8	Test 11	Unit
Structure	sII	sII	
n	4.7 ± 1.8	4.0 ± 1.8	-
Δh°_{diss}	284 ± 9	315 ± 9	J/g
f	59 ± 1	70 ± 1	%mass
$P_{production}$	9.0 ± 0.5	7.0 ± 0.5	MPa
m_{sample}	0.92 ± 0.01	0.900 ± 0.002	g

The n-intervals covered the ideal hydrate number (5.67), but the relative random error in n was about 40%. This error is so large that it makes the preliminary method of little use in hydrate number determination.

The relative random error in Δh_{diss} was about 3%, which is acceptable. But the values 284 and 315 J/g are about half the dissociation enthalpy of 578 J/g estimated from Clausius-Clapeyron calculations (Table 6.2). This is an indication that the preliminary method yields a large systematic error in the dissociation enthalpy measurements.

The relative random error in f is about 1.5% which is satisfactory. The repeatability in f is not good, but this can be explained by sample inhomogeneity. The inhomogeneity may be a draw-back of the sampling procedure, but the difference in f values is not against the calorimetric method.

Assumptions Made in the Preliminary Method

Two critical assumptions were made *before* the development of the preliminary method started:

A big sample which fills the sample cell can be used. This implied that the mass of hydrated gas would be relatively large. Accordingly, weighting would be an easy, direct and accurate way to determine the mass of the gas. But the tests (Appendix B) showed that if the sample mass exceeded about 0.95 g the logged sample temperature exceeded the hydrate equilibrium curve of the hydrate forming gas. This could not be allowed. A consequence of having to use small samples was that the relative random error in n_g became large.

Fractionation during hydrate formation is negligible. It was assumed that the molar mass of the hydrated gas was about the same as the molar mass of the hydrate forming gas. In other words, fractionation was assumed to be negligible. With the knowledge earned later (Chapters 4 and 8) it became obvious that the assumption of negligible fractionation was unrealistic.

Advances of the Preliminary Method

Handa (1986a) reported work on samples with little free water (ice). This method was tried in the present work without success. This is explained by complications due to mass transfer between the free water as it melts in the calorimeter. Despite its shortcomings, the preliminary method was an advancement towards calorimetric analysis of natural gas hydrate with large amounts of ice. The preliminary method had three special features:

- Pressurize the NGH-ice sample with methane.
- Apply an ice conditioning cycle before quantifying the ice (Figure 6.5).
- Operate below the methane hydrate equilibrium curve and above the equilibrium line of the hydrate forming natural gas (Figure 6.5).

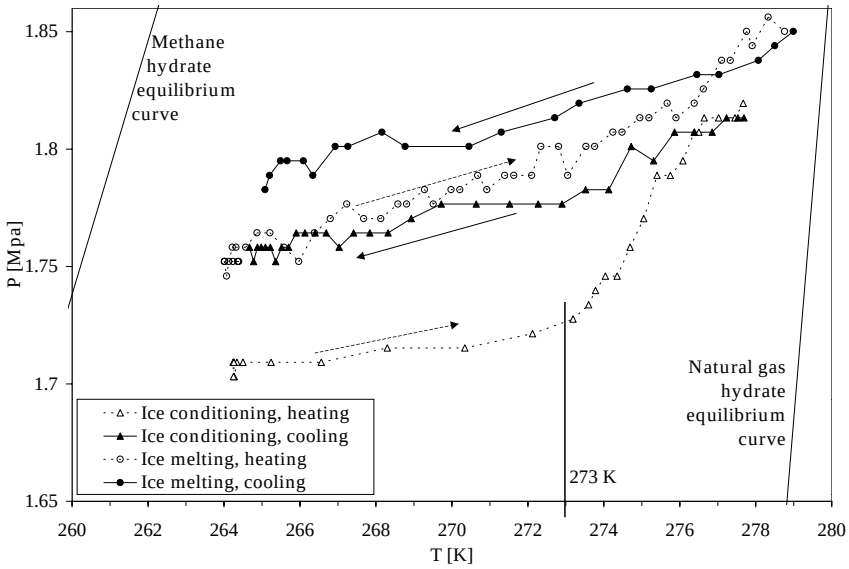

Figure 6.5: Operation lines in the *Ice conditioning* and *Ice melting* cycles. The free water (ice) gives off absorbed gas around 273 K in the heating sequence of the *Ice condition* cycle. This causes a sudden pressure increase.

Since a NGH sample was subject to a pressure exerted by methane, there were two hydrate equilibrium curves of interest; the curve of the hydrate forming natural gas and the curve of methane. It was necessary that the sample pressure was below the methane hydrate forming pressure to avoid methane hydrate formation. But the pressure must be high enough to keep the system above the equilibrium pressure of the natural gas. With these requirements there would be no formation of methane hydrate since the pressure was too low. There would be no dissociation of methane hydrate since no methane hydrate was there. There would be no formation of sII NGH since the content of ethane and propane in the methane was very low. There would be no dissociation of the NGH already present since the pressure of methane, which was the major gas component in the hydrate, was too high. This applied to a pressure range defined by a temperature range, in this case about 263 K to 279 K. In Figure 6.5 it is seen that an initial pressure of 1.7 MPa was suitable.

Because of fractionation the NGH equilibrium curve was below the equilibrium curve of the feed gas. It was therefor conservative practice to operate above the curve of the feed gas.

The free water was saturated in methane, ethane and propane at appreciable partial pressures when it froze to ice. Consequently, there was some desorption when this ice melted in the calorimeter under 1.7 MPa methane. The heat of desorption was registered simultaneously as the heat of ice melting. Accordingly it was not possible to accurately integrate the ice peak. Thus the *Ice conditioning* cycle was proposed.

In the *Ice conditioning* cycle the ice was melted and the water that formed was allowed to equilibrate with the methane above the sample. The sample was then brought back to 263 K. It is seen in Figure 6.5 how the pressure suddenly increases because of desorption at about 273 K during the heating sequence of the *Ice condition* cycle. In the next cycle, the *Ice melting* cycle, the ice melted again. This time the water that formed at 273 K was already equilibrated with the gas. Consequently there was almost no desorption of gas from the water. The peak was due to melting alone and could be integrated accurately. The specific enthalpy of the melting process were determined in separate experiments (Appendix B.2.3, Test 8).

6.3.4 Final Calorimetric Method

An Alternative Approach

It is necessary to modify the preliminary calorimetric method. A new method should be devised where a big sample is used. The procedure should be robust towards the composition of the hydrated gas. Two modifications are proposed:

1. In the *Ice conditioning* and *Ice melting* cycles, melt the ice *isothermally* at 274 K.
2. Measure the pressure increase during hydrate dissociation to determine the amount (moles) of hydrated gas.

Modification 1 makes it possible to use a big sample which fills the calorimeter cell (≈ 8 cm^3). Since the ice melting takes place during isothermal operation the sample temperature will always be above the feed gas equilibrium curve even if the sample mass exceeds about 0.9 g.

Modification 2 requires that the gas which liberates during dissociation causes a pressure increase. This increase must be small, thus a gas expan-

sion chamber is connected to the calorimeter as in the apparatus of Handa (Figure 2.4). The volume of the whole system (calorimeter cells, expansion chamber and tubing) must be calibrated. The amount (moles) of hydrated gas is calculated using equation 2.8.

Calorimeter Operation

A big sample which completely fills the calorimeter sample cell will be analyzed. Three cycles will be used, just as in the preliminary method. The *Ice conditioning* and *Ice melting* cycles are subject to the same change; instead of melting the ice during a scanning sequence, the ice is melted during an isotherm at 274 K. The duration of this sequence will have to be based on experience. It is also possible to stop the isotherm manually after the melting peak is completed and then cool the sample to complete the cycle.

The *Hydrate Dissociation* cycle is carried out as in the preliminary method, with the exception that in stead of dissociating in an open system, the system is now closed. The gas that liberates during the dissociation causes the pressure to increase. The pressure increase is measured. Since the system volume is calibrated, the amount (moles) of gas can be calculated. Because of the expansion chamber the pressure increase is not very large and the system is kept in a low pressure region to ensure smooth dissociation. This is the principle used by Handa (1986a).

To collect data for c_p determination the sample is heated at a constant rate over the temperature interval of interest. Section 6.3.1 describes how $c_p(T)$ is found. To find $c_{p,hyd}$ it is necessary to subtract the contribution of the ice. This can be done since the mass of ice is found and since $c_{p,ice}(T)$ is known from Section 6.3.1.

Calculation Procedure

Amount of free water, f (%mass):

$$f = \frac{m_{ice}}{m_{sample}} 100 \tag{6.1}$$

where

$$m_{ice} = \frac{\Delta H_{1.7MPa,ice}}{\Delta h_{1.7MPa,ice}} \tag{6.2}$$

The subscript $_{1.7}$ refers to the methane pressure 1.7 MPa during the ice melting process.

Hydrate number, n (-):

$$n = \frac{n_{w,hyd}}{n_g} \tag{6.3}$$

where

$$n_{w,hyd} = n_{w,tot} - n_{ice} = \frac{m_{w,tot}}{M_w} - n_{ice} \tag{6.4}$$

and n_g is found by equation 2.8:

$$n_g = \frac{(P_f - P_i - P_w)(V_t - V_w)}{RT_g + B(P_f - P_i - P_w)}$$

To find the volume average of the gas temperature, T_g, an extension of equation 2.9 is suggested; equation 6.5. It includes a contribution from the reference cell, since the reference cell contributes to the total system volume.

$$T_g = \frac{V_1 T_r + \frac{1}{2}V_2(T_c + T_r) + T_c(V_S - V_w) + \frac{1}{2}V_2'(T_c + T_r) + T_c V_R}{V_{tot} - V_w} \tag{6.5}$$

where V_2' corresponds to V_2 except the latter is for the sample cell and the first for the reference cell. The rest of the symbols are the same as for equation 2.9.

Specific enthalpy of hydrate dissociation, Δh_{diss} (J/mol):

$$\Delta h_{diss} = \frac{\Delta H_{diss}}{n_g} \tag{6.6}$$

Specific heat capacity, c_p (J/gK), is found according to the procedure described in Section 6.3.1.

$$\begin{aligned} c_p &= \frac{d\Delta H(T)}{dT} \\ &= \frac{d}{dT}(a + a_0 T + a_1 T^2 + a_2 T^3 + \cdots + a_{n+1} T^n) \\ &= a_0 + a_1 T + a_2 T^2 + a_3 T^3 + \cdots + a_n T^n \end{aligned} \tag{6.7}$$

6.4 Properties Estimates

To estimate thermophysical and compositional properties of natural gas hydrate, the models and correlations found in the literature (Chapter 2) were used. The calculations and assumptions are given in Appendix C. The results are collected in Table 6.2.

Table 6.2: Estimated thermophysical and compositional properties of sII natural gas hydrate.

Property	Value	Remark
C1:C2:C3	89:6:5 %mol	assumption
n	6	assumption
M_{NG}	18.24 g/mol	
Δh°_{diss}	73.0 kJ/mol	Clausius-Clapeyron
Δh°_{diss}	578 J/g	=(73 kJ/mol)·1000/($M_{NG}+18n$)
c_p	2.28 J/gK	(Groisman 1985)
c_p	287 J/molK	=(2.28 J/gK)·($M_{NG}+18n$)
λ	0.373 W/Km	for ρ=700 kg/m^3, (Groisman 1985)
dl/ldT	$52 \cdot 10^{-6}$ K^{-1}	(Sloan 1998, p.64)

6.5 Discussion

6.5.1 Calorimetric Method

Most literature report how Δh_{diss}, n and f are found for *single*-guest hydrates with very *low* ice content. This work focuses on analyses of *multi*-guest hydrates with very *high* ice content. Handa (1988b) reported analysis on a natural gas hydrate sample with ice (NGH8 in Table 2.2). It was not possible to determine the ice contents of this sample. Consequently, n and Δh_{diss} could not be determined either. If all cages in NGH8 were occupied, then it contained about 20 %mass of ice. Full occupancy is not possible, so the ice content must have been below 20 %. To compare, the samples in the present work contained about 40-70 %mass ice.

The contribution of the present work is to expand Handa's method (Handa 1986a) to make it more suitable for samples of mixed hydrates with large amounts of ice. From the calorimeter tests (Appendix B) it was concluded that the heat of ice melting depends on the pressure at which the ice formed,

the pressure at which the ice is melted and the composition of gas used to pressurize the ice during the analysis. More specifically; when ice froze under 6-9 MPa natural gas and melted under a 1.7 MPa methane, processes took place that had a thermal response. Two processes could be important: desorption of natural gas and PV work. It was not possible to make meaningful corrections for these effects. Effects related to the presence of hydrate are less likely, since similar effects were seen in water-nitrogen systems without any hydrate (Appendix B.2.2).

To get around the complications that arose from desorption, it was suggested that the calorimeter method should have an extra heating-cooling cycle before the actual analysis. The purpose of this extra cycle is to condition or pretreat the sample, or actually the ice in the sample. This was achieved by melting the ice at a suitable pressure and allowing the water to equilibrate with the gas and then refreeze the water. This cycle was called the *Ice conditioning* cycle. Then, during the *Ice melting* cycle the ice melted under a gas with which it was equilibrated at the PT conditions at the melting point. The specific enthalpy of ice melting for these conditions were found in separate experiments. Then the mass of free water in the sample could be calculated.

It was also concluded from the tests that to pressurize the sample with the hydrate forming natural gas introduced errors because of a complicated and not fully understood thermal response around the melting point. Hydrate formation seemed to take place. Instead of pressurizing with natural gas it was decided to pressurize with methane. A suitable pressure, as mentioned above, was a pressure below the hydrate curve of methane and above the hydrate curve of the hydrate forming gas. For the temperature interval of interest, 1.7 MPa was a suitable pressure, as illustrated in Figure 6.5.

Getting around the problems associated with the high ice content in this way; pressurizing natural gas hydrate with methane and operating between the corresponding equilibrium curves, is one of the main results of the present work. It is also suggested that the *Ice melting* cycle includes an isotherm at 274 K. It must last long enough for all ice to melt. This will allow large samples and the random errors will be reduced accordingly.

6.5.2 Hydrate Sampling

In this section it is suggested why filtration of hydrate-in-water slurries is so difficult. It is then proposed how filtration could be carried out.

Filtration Mechanism

Hydrate was separated from the hydrate-in water slurries by inline filtration. The samples that were obtained contained large amounts of free water. Filtration of hydrate slurries is known to be difficult. It is difficult to grow large hydrate crystals with good filtration characteristics. Light, feathery crystals which form compacted beds are quite common (Mullin 1994, p.360). The same behavior was observed in numerous hydrate production and filtration experiments.

The poor filtration properties could be explained if there is no build-up of a proper filter cake. What happens instead is perhaps the build-up of a hydrate plug in the filter. This hypothesis is based on the fact that the filter cloth more or less resembles a hydrate plug; a stationary flow restriction. The slurry will continue to build the "plug" (the filter cloth) already there. Accordingly, the material that fills the filter cup will have similarities to hydrate plugs. For example, the water content may be very high, as measured in the present work. Filtration is then a way of collecting plug samples. Therefor this work becomes relevant for plug related topics. For example, the plug dissociation characteristics, which are intimately related to the thermophysical and compositional properties, are important in flow remediation.

Washing Agent

It may be possible to remove the water in the filter cake by some washing agent. The washing agent will have to meet these criteria:

- It must be a water soluble liquid.
- It must be volatile for temperatures well below 273 K.
- It must be sub-critical at pressure-temperature conditions at the hydrate process.

- It should not be a hydrate former.
- It must not have a destabilizing effect on the hydrate.

It is suggested that 1-butanol may be used. But since 1-butanol is a hydrate inhibitor, its effect on the hydrate stability may be undesirable. It meets the other criteria. The idea is that after filtration the filter is flushed with 1-butanol at the operating pressure and temperature. In theory, the water in the filter will gradually be replaced by the alcohol. In the end the alcohol could be displaced by gas in the ordinary and proven manner. Then the filter is cooled to about 250 K to stabilize the hydrate. When the filter is opened the cake will be pasty instead of solid and ice-like. The paste is spread in a thin layer at about 250 K and left for the alcohol to evaporate. The remaining product will be dry, pure hydrate.

6.6 Conclusions

- A calorimetric method was developed for analyzing natural gas hydrate that contain large amounts of free water (ice). The advances compared to previous works are:
  1. Natural gas hydrate is pressurized with methane and the system is operated at PT-conditions that are below the methane hydrate curve and above the natural gas hydrate hydrate curve.
  2. In a sample conditioning step the ice is equilibrated with the gas used to pressurize the sample.
- Standard hydrate dissociation enthalpy was measured. The values were lower than expected.
- Hydrate number was measured. The relative error was large.
- Free water was measured. The values were reasonable and errors were regarded acceptable.
- Improvements of the method was suggested to reduce the errors in dissociation enthalpy and hydrate number.
- Specific heat capacity for ice was fitted as a virial equation in T. The correspondence to literature measurements was good.
  $c_{p,ice} = 6 \cdot 10^{-5} T^2 + 0.0108T + 2.1187$ for $-34\ ^\circ\mathrm{C} < T < -1\ ^\circ\mathrm{C}$.

Chapter 7

Metastability - Results

7.1 Introduction

The first purpose of the work reported in this chapter was to develop calorimetric methods to quantify metastability of natural gas hydrate. An isothermal method can be used to measure the rate of very slow dissociation processes. It quantifies how (if) the amount of natural gas hydrate changes during storage.

The second purpose of the work reported in this chapter was to develop a climate laboratory where the storage conditions could be controlled. The storage apparatus is described in Chapter 5.5.

7.2 Isothermal Calorimetry Method

There was no evidence found in the literature (Chapter 3) that metastable hydrate can exist indefinitely. Accordingly, it was assumed that metastability properties of hydrate can be described in terms of *kinetic metastability*; the sample undergoes steady dissociation, but the rate of dissociation is so low that the hydrate persists for long times. It follows that metastability can be quantified by the rate of dissociation, which in turn can be correlated to storage conditions and sample characteristics. An isothermal calorimetric method based on the principles outlined in Section 3.4 was developed.

The sample was transferred to the calorimeter as described towards the end

of Section 6.2. Since the calorimeter was operated in isothermal mode, it could be said that the samples were stored in the calorimeter at well defined and constant pressure and temperature. After the initial thermostabilization, a steady heat flow signal, $\dot{Q}$ (W), was collected. The signal was weak due to the very low rate of dissociation. The signal was corrected by subtracting the blank signal, or else a relatively large error would result. The collected signal, $\dot{Q}$ (W), was referred to the initial sample mass to find the specific heat flow, $\dot{q}$ (W/g). By convention, a negative heat flow corresponds to heat flow *to* the sample.

The procedure was tested in two series of experiments. Temperature (T) and sample diameter (D) were the independent variables.

7.2.1 Effect of Temperature

The results from the temperature effect experiments are shown in Figure 7.1. Three experiments were done at temperatures of 272, 268 and 238 K using particles with $D \approx 1$ mm. A high temperature gave a large heat flow to the sample, and the dissociation rate was relatively high. It was also seen that the collected heat signals at 268 and 238 K were fairly constant, except they fluctuated somewhat. This indicated constant rates of dissociation. The heat signal collected at 272 K varied more.

The data in Figure 7.1 provided a basis for estimating the rate of dissociation. It was necessary to estimate the amount of free water in the samples. It had been found in previous experiments that $f = 40$ %mass was a reasonable assumption. The correlation $\Delta h_{diss} = 215.59 \cdot 10^3 - 394.945T$ (J/kg) for 248 K $< T <$ 273 K (Selim and Sloan 1990) was used to find Δh_{diss}. For $T = 268$ K the correlation yields 110 J/g. The rate of hydrate dissociation was calculated using the relation

$$r_{diss} = \frac{-3600\dot{q}}{0.4\Delta h_{diss}} \tag{7.1}$$

where the constant 0.4 is due to the assumption that $f = 40$ %mass. It is also useful to put a number on the degree of conversion or dissociation, α, after a time interval of interest, for example 240 hours (10 days). If r_{diss} remains constant, then $\dot{q}$ remains constant, and then

$$\alpha = \frac{-\dot{q}t}{\Delta h_{diss}} \tag{7.2}$$

Results from r_{diss} and α calculations are presented in Table 7.1.

Table 7.1: Quantification of NGH metastability. α_{240h} values are extrapolations.

Sample	T (K)	D (mm)	$\approx \dot{q}$ (mW/g)	r_{diss} (1/h)	α_{240h}
Granulate	238	≈ 1	> 0	-	-
Powder	268	< 1	-0.035	0.0029	0.27
Granulate	268	≈ 1	-0.014	0.0011	0.11
Granulate	268	≈ 10	-0.027	0.0022	0.21
Granulate	272	≈ 1	-0.25	0.020	1

7.2.2 Effect of Sample Diameter

The effect of diameter (D) is shown in Figure 7.2. Three experiments were carried out on particles with diameters of < 1 mm, ≈ 1 mm and ≈ 10 mm at a temperature of 268 K. No correspondence between D and $\dot{q}$ was found. The data were corrected by subtracting blank data obtained at 268 K. r_{diss} and α values are presented in Table 7.1.

7.3 Discussion

7.3.1 Rate Limitations

An important issue regarding kinetic metastability is to determine if the rate represents intrinsic kinetics, or if the rate is limited by heat or mass transfer processes. During the isothermal calorimetric experiments the calorimeter was operated at a defined temperature set point. Due to dissociation, a heat flow in the order of magnitude 0.1 W was supplied by the calorimeter to maintain the temperature setpoint. In other words, the heat was supplied as a consequence of dissociation. An adiabatic system would probably self-cool to a lower temperature, as observed by Ershov and Yakushev (1992).

The calorimeter may supply heat flows of about 0.5 W which is about 5 times the heat flow in the experiments. This makes it unlikely that rate limitations

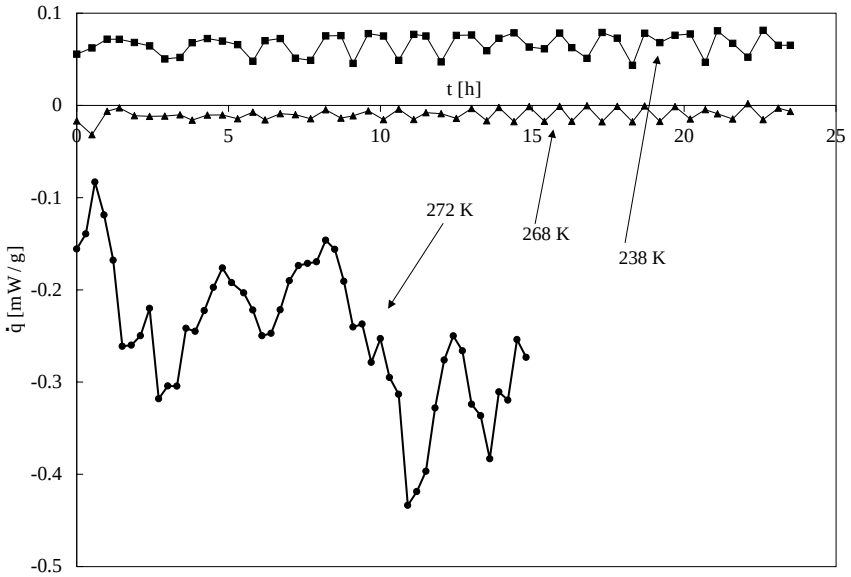

Figure 7.1: Effect of temperature on NGH metastability. $D \approx 1$ mm.

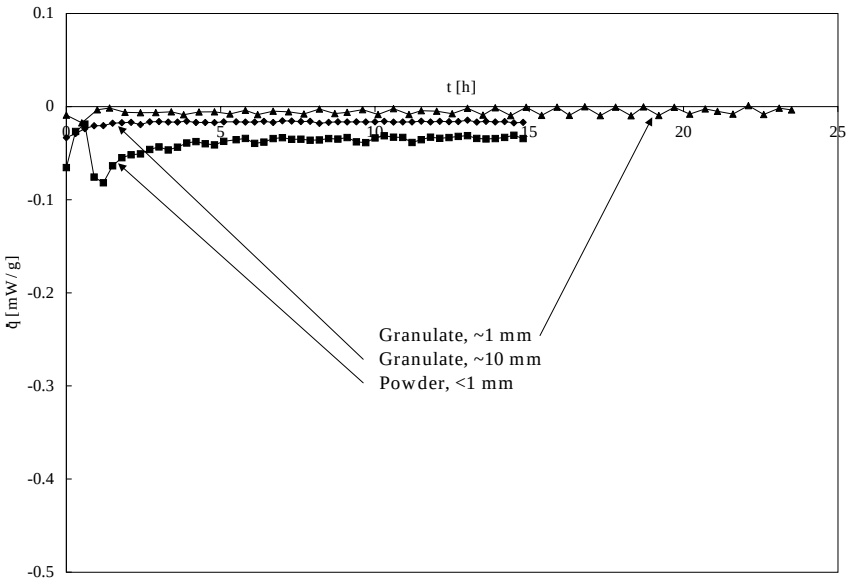

Figure 7.2: Effect of sample diameter on metastability. $T = 268$ K.

are due to limitations in the heat transfer. There were large amounts of ice in the system. As suggested in the literature, the ice could make it difficult for the gas to escape. Consequently, the dissociation rate could be limited by mass transfer.

7.3.2 Effect of Temperature and Sample Size

The isothermal method was tested in too few experiments to develop meaningful correlations and to quantify the errors. However, when r_{diss} values are plotted (Figure 7.3) to illustrate the combined effects of D and T, it seems clear that the temperature effect is much more pronounced than the diameter effect, in the D and T ranges used here.

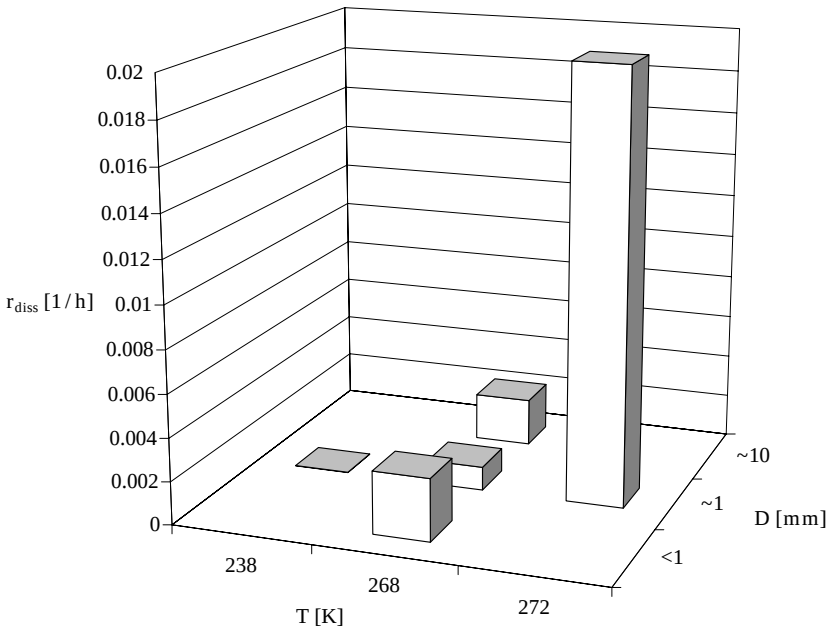

Figure 7.3: Combined effect of temperature and diameter on dissociation rate.

If the three experiments at 268 K are compared, there seems to be no correspondence between sample size and the dissociation rate. From $D < 1$ mm to $D \approx 1$ mm the rate decreased from 0.0029h^{-1} to 0.0011h^{-1}. This was

expected. But increasing D further, from ≈ 1 mm to ≈ 10 mm, caused the rate to increased to 0.0022. This was not expected. It is not known whether the deviating behavior is due to random error or sample inhomogeneities. The latter seems more likely, since to determine r_{diss} it was assumed that all samples contained 40 %mass free water (ice). This assumption could easily cause errors of 10% or more in the r_{diss} values.

Despite the inaccuracies, the results seemed reasonable. For $D \approx 1$ mm, at 268 K the estimated degree of conversion (α) after 10 days was only 0.11 while at 272 K the sample was completely dissociated by this time. It was confirmed that even at a relatively high temperature of 268 K, natural gas hydrate has metastability properties that justifies further work with the hydrate process for storage and transport of natural gas.

7.3.3 Effect of Pressure

The isothermal method can be used at any pressure, for example ambient pressure when using calorimeter cells that are open to the surrounding atmosphere. In the experiments reported here, closed cells were used, and accordingly the pressure increased as more and more hydrate dissociated.

The effect of the gauge pressure on the dissociation rate was insignificant. This is evident since the $\dot{q}$ curves are about flat if the fluctuations are ignored. If the increasing pressure had caused a shift (decrease) of the dissociation rate, this would have been reflected in a proportional shift in $\dot{q}$ which would approach zero. But on the contrary, the only experiment with a shift ($T = 272$ K, $D \approx 1$ mm) showed an unsteady *increase* in the dissociation rate.

The fact that the effect of temperature on the dissociation rate is as expected, further supports that there was no significant effect of the gauge pressure on dissociation rate in these experiments. But it should be noted that if an experiments last significantly longer than in this work, the gauge pressure will have an effect, according to theory.

7.3.4 Blank Run

Experiments were carried out at 272, 268 and 238 K. All $\dot{q}$ data were corrected by subtracting a blank run carried out at 268 K. The resulting curve for 238 K was disregarded, since it showed a positive value, $\dot{q} \approx +0.05$ mW/g

(Figure 7.1). This could at a first glance be taken as an indication of hydrate formation, but that was not possible. A likely explanation is that the blank signal recorded at 268 K over compensated the measurements at 238 K.

A similar type of over compensation, but oppositely directed and smaller, was probably encountered in the curve for 272 K. This error is assumed insignificant. To obtain better accuracy the blanks should be run at the same temperature as the corresponding experiments, but there was only time to do one blank (268 K).

7.3.5 Micro Regimes

An important visual observation was made on the hydrate samples from the fractionation laboratory. Small, white regions sometimes developed *inside* the samples. The hypothesis is set forth that this was caused by the formation of small gas bubbles around hydrate agglomerates which partially dissociated to gas and ice. This would create micro regimes where the pressure was higher than the ambient, perhaps as high as the equilibrium pressure at the storage temperature.

The consequence is that the hydrate inside the samples is subject to storage conditions that favor long-time storage. It may be that a large fraction of the hydrate was subject to conditions at or close to phase equilibrium, even if the bulk material is stored at ambient pressure. The formation of an *ice layer* on the sample *surface* has been observed and is reported in the literature (Chapter 3). But no reports describing the experimental observation of *gas bubbles inside* the samples were found.

Raman spectroscopy could perhaps be used to study this further. It may be that the signals from hydrated guests gradually decrease, while the signals from ex-guests in small gas bubbles gradually increase. Eventually the signals may even out due to enhanced hydrate stability resulting from the pressure exerted by the gas in the bubbles.

7.3.6 Other Comments

The heat signal for the experiment at 272 K showed larger fluctuations than the others. This could be so because the system was close to the ice melting point, so the ice became less able to stabilize the hydrate. It could also be that sample inhomogeneities gave the large fluctuations as zones with more

or less hydrate dissociated. This is to rely on the hypothesis that the ice stabilizes the hydrate.

The three-cycles method proposed in Section 6.3.4 can be used to find the hydrate number. First, a fresh sample is analyzed to find the hydrate number to have a reference value. Then, samples are subject to metastable storage at controlled conditions (temperature, relative humidity) in the climate laboratory. Finally, the stored samples are analyzed to find the hydrate number after storage. The hypothesis is that the changes in the hydrate number are negligible during storage of hydrate. This is likely, since the escape tendency of guest molecules is extremely low when they are not liberated at the surface of a dissociating sample. The guest would have to escape from its cage, diffuse through the hydrate phase and perhaps through some ice too. This process is negligible for all practical purposes.

7.3.7 Speculations on Metastability

Metastability of natural gas hydrate is not well understood, although a number of authors propose (Section 3.2) that an ice layer forms on the sample and inhibits the dissociation process. In the following it is suggested how a solid mixture approach may be useful in understanding hydrate metastability.

Metal alloys that are quenched rapidly may consist of many phases in a solid mixture. Such phases are often thermodynamically unstable but persist because they are metastable. To pursue this approach it may be useful to consult the metallurgic and solid materials literature, notably Adams and Kaufman (1997), Gaskell (1994) and Godreche (1992). It is also known that if two polymer solutions are mixed and the solvent evaporated, then a polymer mixture forms that may be thermodynamically unstable. The mixture may persist because the polymer chains are sterically fixed. The polymer mixture is metastable.

The analogy to frozen hydrate with free water (ice) is that the two phases make a solid mixture too. It may be that if an unstable phase (hydrate) is caught in a matrix of a stable phase (ice), this promotes metastable behavior of the unstable phase. Hypothesis: *Metastability of NGH is due to stabilization by a thermodynamically stable ice matrix.* This implies that a certain amount of free water (ice) is necessary to obtain metastability.

The resemblance to the ice layer theory in the literature is obvious. An ice layer or an ice matrix is in effect the same; a barrier between the hydrate and the surrounding gas phase. The difference is that the ice layer forms with time as a portion of the hydrate dissociates. The ice matrix is originally there and no initial dissociation is required. In popular terms, the price to pay for stabilization by an ice layer is the gas that initially evolves. This gas is lost or requires handling. The price for stabilization of an ice matrix is a reduced bulk gas content compared to pure hydrate.

7.4 Conclusions

- An isothermal calorimetry method was developed to study metastability of natural gas hydrate with ice for temperatures below 273 K.
- Metastability of natural gas hydrate with ice was demonstrated at 268 K.
- Rate of dissociation decreases with decreasing temperature.
- Rate of dissociation seems to be limited by mass transfer.
- Visual observations indicated that gas bubbles may form inside the samples to create micro-regimes of elevated pressure. This may have an effect on the stability of the hydrate.

Chapter 8

Fractionation - Results

8.1 General Fractionation Model

A general fractionation model, including a functional relation between fractionation and the driving force (subcooling), is proposed. It is based on three hypotheses:

H1 When operating with zero driving force (on the equilibrium line), the largest possible fractionation takes place.

H2 When operating with infinite driving force, no fractionation takes place.

H3 Between these extremes, the fractionation as function of the driving force changes exponentially.

It is not practicable to operate a system on the equilibrium line (H1). The exact position of any equilibrium line is unknown. Even if it was exactly known, it would be necessary to have pressure and temperature regulation with zero error bands, which is impossible. In the apparatus used in this work, the composition of the gas in the reactor changes as propane is depleted and methane is being enriched. Consequently, the hydrate equilibrium line of the gas shifts upwards in the pressure-temperature plane. It follows that the system behavior at the boundary where the driving force is zero can not be determined experimentally. The best thing that can be done is to do experiments with small, yet significant, driving forces ($\Delta T = 2\mathrm{K}$).

Consequently, at the boundary where the driving force is zero, the assumption above (H1) has to be made.

It is impossible, indeed without any physical meaning, to do experiments with infinite driving force (H2). For an equilibrium temperature T_{eq}, the highest practical driving force in the apparatus used is $\Delta T = T_{eq} - 273$. A larger driving force would bring the system below 273 K where the water freezes to ice. The best thing that can be done is to do experiments close to, yet above, 273 K. For an infinite driving force the assumption above (H2) has to be made. Following this line of thought, complete suppression of fractionation is not possible in practical operations.

The functional relation (H3) between fractionation and the driving force must be consistent with H1 and H2. Thus, the content of any component in the hydrate as the driving force (ΔT) approaches zero is the equilibrium content, $C_{i,eq}$ (H1). This value follows from the theory of Section 4.1.2, and can be calculated using CSMHYD (Sloan 1998), for example. When the driving force approaches infinity, the composition of the hydrate gas approaches the composition of the feed gas, which is known (H2).

It follows that the functional relation for fractionation starts at a finite value between 0 and 100 %mol for $\Delta T = 0$, and approaches the feed gas composition asymptotically for increasing driving forces. An exponential term is assumed to describe this behavior.

Fractionation is known to be component dependent and pressure dependent. It is believed to be system dependent too. Accordingly, the function must contain a system dependent empirical constant, $k(P, i)$. For a system with n guests, exponential expressions are deduced for $n - 1$ guests. The last equation is the mass balance which closes at 100 %mol. For the system in the present work with methane, ethane and propane as guests, the three hypotheses can now be formulated in mathematical terms:

H1	$C_{i,diss} = C_{i,eq} = \theta_{i,eq} \cdot 100$	$\Delta T = 0$
H2	$C_{i,diss} = C_{i,feed}$	$\Delta T = \infty$
H3-a	$C_{i,diss} = (C_{i,feed} - C_{i,eq})e^{-k(P,i)/\Delta T} + C_{i,eq}$	$0 < \Delta T < \infty$, i = C1, C3
H3-b	$C_{C2,diss} = 100 - (C_{C1,diss} + C_{C3,diss})$	$0 < \Delta T < \infty$, i = C2

The most important equation is the one labeled H3-a. It expresses how the hydrate content of guest type i depends on the content of guest i in the feed gas, pressure and driving force. This equation contains equations H1 and H2;

Equation H3-a yields $C_{i,eq}$ for $\Delta T = 0$, as in Equation H1. Equation H3-a yields $C_{i,feed}$ for $\Delta T = \infty$, as in Equation H2. $C_{i,eq}$ in Equation H3-a is equal to $\theta_{i,eq} \cdot 100$, and when $\theta_{i,eq}$ is substituted using equation 4.3, Equation 8.1 results. To completely write out the equation calls for further substitutions using the equations in Section 4.1.2.

$$C_{i,diss} = \left(C_{i,feed} - 100 \left(\frac{16\theta_{s,i} + 8\theta_{l,i}}{16 \sum_i \theta_{s,i} + 8 \sum_i \theta_{l,i}} \right)_{eq} \right) e^{-k(P,i)/\Delta T} + C_{i,eq} \tag{8.1}$$

8.2 Methods

The purpose of this work was to investigate the effect of driving force on fractionation, notably to evaluate the suitability of the proposed fractionation model. To accomplish this, the driving force was varied by operating at different pressures and temperatures. The driving force was expressed in terms of subcooling relative to the hydrate equilibrium curve for the feed gas. The experiments can be grouped in terms of driving force. 2, 4, 8, 12 and 16 K subcooling were used. Experiments can also be grouped in terms of operation pressure. 3.0, 4.5, 6.0 and 7.5 MPa were used. With these sets of driving forces and operating pressures, a set of operating temperatures is implicitly defined.

Figure 8.1 shows the CSMHYD equilibrium curve for the feed gas and the curves for the planned driving forces. The operation points lie where the curves for the planned driving forces intercept the planned isobars. Each experiment was numbered as shown in the figure.

The apparatus was described in Section 5.6. To produce hydrate, distilled water (80 cm^3) was brought in contact with natural gas (5 %mol ethane and 3 %mol propane in methane). But before feeding the gas, the air in the reactor and air that was dissolved in the water was removed by evacuating the reactor ($\approx$5 Pa) for 20 minutes or more. Then the reactor was cooled to the operating temperature, while pressurized with the gas to somewhat below the equilibrium pressure for this temperature. The magnetic stirrer was started (about 400 RPM). When the desired temperature was reached, the data logger was started and the reactor pressurized to the operating pressure. The reactor was operated for about four hours. The pressure-

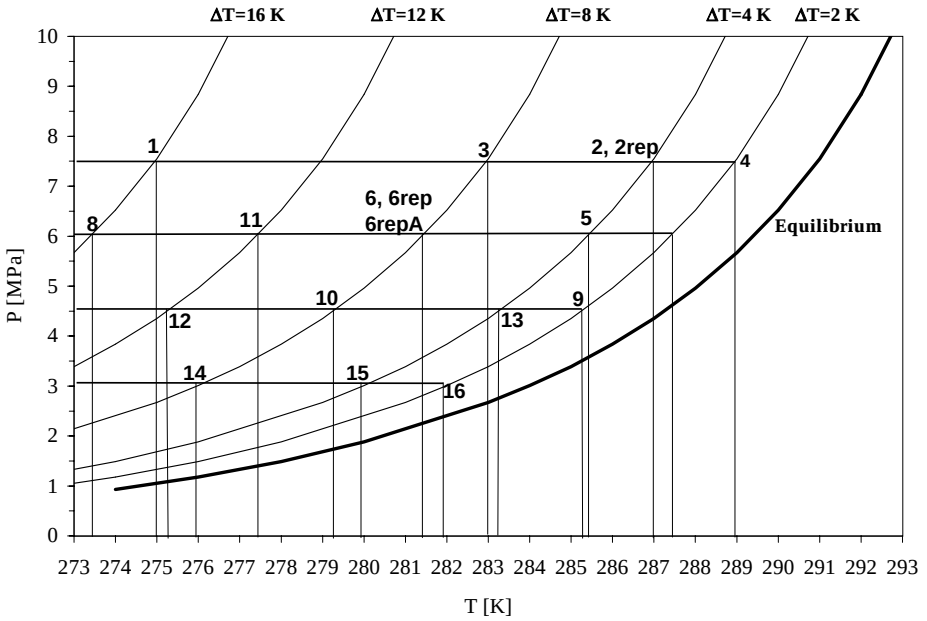

Figure 8.1: Plan for the fractionation experiments. The equilibrium curve is for a gas with ethane (5 %mol) and propane (3 %mol) in methane and is calculated using CSMHYD (Sloan 1998).

temperature course during an experiment (no. 2, P=7.5 MPa, T=287 K, ΔT=4 K) is illustrated in Figure 8.2. Afterwards, a sample of the gas in the reactor was analyzed by gas chromatography. The results are reported as $C_{i,reac}$ in Tables 8.1 to 8.4. Then the reactor was refrigerated (252 K) overnight. Note that due to fractionation, the composition of the gas phase in the reactor changed during the experiments. This is discussed later.

The next day the reactor was quickly depressurized to ambient pressure. It took about half a minute or less, depending on the initial reactor pressure. The reactor was opened, and hydrate quickly scraped into the precooled dissociation cell. The cell was closed immediately. The sample transfer took place in the freezer at around 252 K.

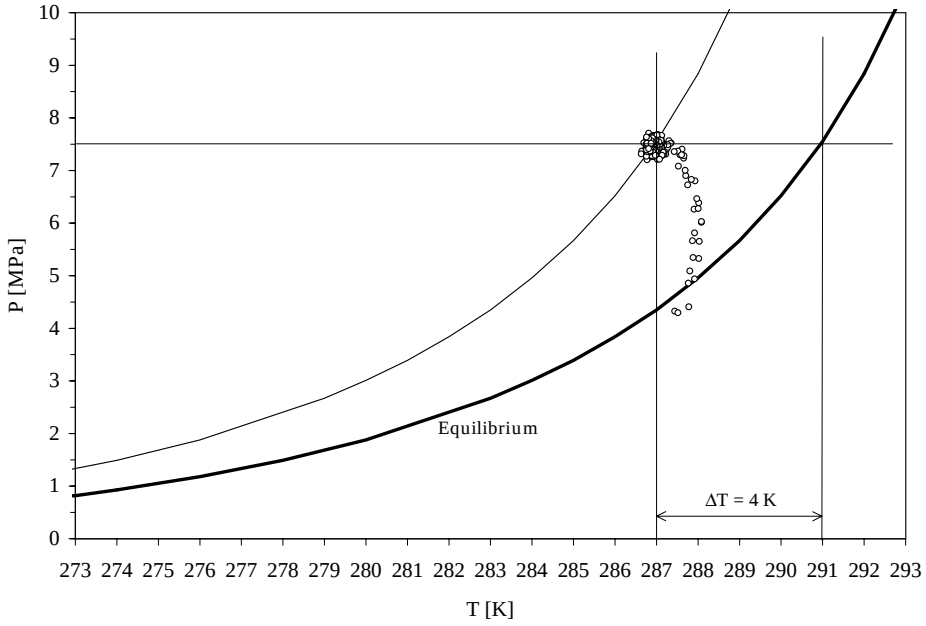

Figure 8.2: Pressure-temperature course during experiment no. 2 with P=7.5 MPa and ΔT=4 K. The cluster of data points around the PT set point contains about 450 measurements collected during nearly 4 hours.

8.3 Measurements

Tables 8.1 to 8.4 give the results of all the gas chromatograph measurements. $C_{i,reac}$ (%mol) is the content of gas i in the reactor when the hydrate production was stopped after 4 hours operation. $C_{i,diss}$ (%mol) is the content of gas component i in the gas from a completely dissociated sample. $C_{i,reac}$ and $C_{i,diss}$ were normalized to 100 %mol. A three dimensional plot illustrates the combined effects of driving force and pressure on methane fractionation (Figure 8.3).

Table 8.1: Composition of reactor gas and gas from dissociated samples. Hydrate production pressure was 7.5 MPa.

		$C_{i,reac}$ (%mol)			$C_{i,diss}$ (%mol)		
Run no.	ΔT (K)	CH_4	C_2H_6	C_3H_8	CH_4	C_2H_6	C_3H_8
4	2	93.4	4.6	2.0	76.6	10.1	13.2
4	2				76.0	9.6	14.4
2	4	94.5	4.1	1.4	85.6	6.9	7.6
2	4				84.8	7.4	7.8
2rep	4	93.2	4.5	2.3	75.6	9.3	15.1
3	8	92.5	4.8	2.7	85.1	7.5	7.4
1	16	92.2	5.0	2.9	88.9	6.0	5.1

Table 8.2: Composition of reactor gas and gas from dissociated samples. Superscript * indicates gross errors. Hydrate production pressure was 6.0 MPa.

		$C_{i,reac}$ (%mol)			$C_{i,diss}$ (%mol)		
Run no.	ΔT (K)	CH_4	C_2H_6	C_3H_8	CH_4	C_2H_6	C_3H_8
7	2	92.4	4.9	2.8	83.5	6.8	9.7
5	4	93.1	4.5	2.4	76.8	10.7	12.5
6	8	*90.8	*5.4	*3.8	84.4	7.7	7.9
6rep	8	92.7	4.8	2.6	84.6	7.8	7.6
6repA	8	92.6	4.8	2.7	84.3	7.9	7.7
6repA	8				84.0	8.0	8.0
11	12	92.2	5.0	2.8	88.4	5.9	5.6
11	12	92.1	5.0	2.9			
8	16	92.3	4.9	2.8	89.3	5.6	5.1
8	16				89.5	5.6	5.0

Table 8.3: Composition of reactor gas and gas from dissociated samples. Hydrate production pressure was 4.5 MPa.

		$C_{i,reac}$ (%mol)			$C_{i,diss}$ (%mol)		
Run no.	ΔT (K)	CH_4	C_2H_6	C_3H_8	CH_4	C_2H_6	C_3H_8
9	2	93.1	4.8	2.1	76.1	8.9	15.0
13	4	93.4	4.5	2.1	76.6	10.2	13.3
10	8	92.9	4.7	2.4	82.4	8.4	9.2
12	12	92.4	4.9	2.7	89.0	5.6	5.4
12	12				88.9	5.6	5.5

Table 8.4: Composition of reactor gas and gas from dissociated samples. Hydrate production pressure was 3.0 MPa.

		$C_{i,reac}$ (%mol)			$C_{i,diss}$ (%mol)		
Run no.	ΔT (K)	CH_4	C_2H_6	C_3H_8	CH_4	C_2H_6	C_3H_8
16	2	93.3	4.7	2.0	73.0	9.3	17.7
15	4	94.7	4.1	1.2	75.5	10.7	13.8
14	8	93.9	4.3	1.8	79.3	9.6	11.1

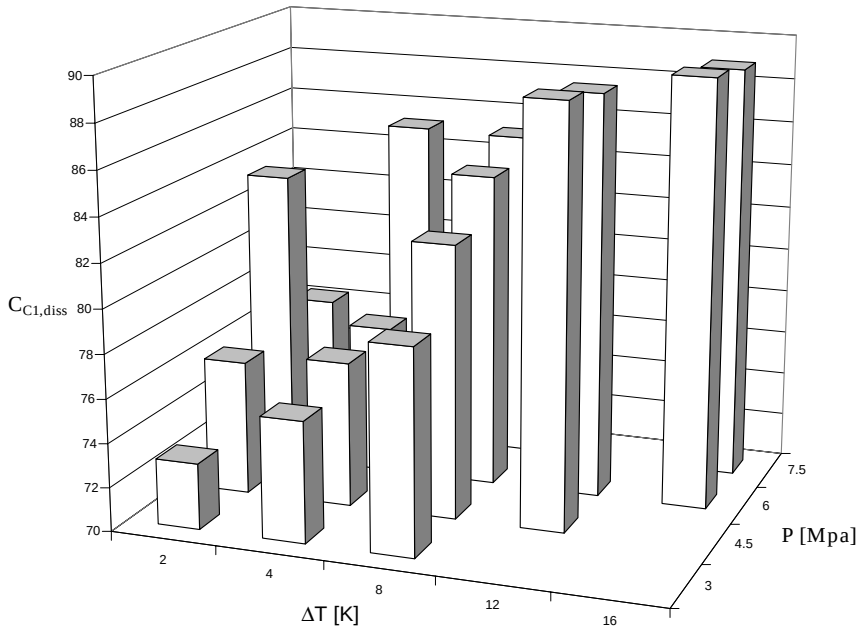

Figure 8.3: Concentration of methane in gas from dissociated hydrate samples as function of operation pressure and driving force. The plot illustrates that driving force and pressure should be high to suppress fractionation.

8.4 Interpretation of Measurement Results

8.4.1 Driving Force Threshold

Hypothesis

Earlier observations made in the NTNU Hydrate Laboratory indicated that there is a connection between the hydrate formation conditions and the hydrate composition. Hypothesis:

- There exists a driving force threshold beyond which the fractionation is insignificant.

Findings

It is known that fractionation occurs for small driving forces. Thus, to check the hypothesis, it was necessary to do only one experiment using the largest driving force possible. If insignificant fractionation was observed, then the hypothesis could be regarded true. But if significant fractionation was observed, the hypothesis needed not be regarded false. It would only mean that with the available apparatus it was not possible to achieve a driving force large enough to suppress fractionation.

The largest driving force that could be obtained was 17 K subcooling. However, the largest subcooling used in the experiments was 16 K. It was assumed that this relatively small difference of 1 K had no impact on the conclusion regarding a driving force threshold. Two experiments were carried out with 16 K subcooling; experiment no. 1 (P=7.5 MPa, T=275 K) and no. 8 (P=6.0 MPa, T=273.5 K), see Tables 8.1 and 8.2. Fractionation was observed in both experiments. The hydrate produced in experiment no. 1 had a normalized methane content of 88.9 %mol which is a reduction of 3.1 %mol compared to the feed gas with 92 %mol methane. The gas from the dissociated hydrate contained 5.1 %mol propane, while the feed gas contained 3 %mol. For experiment no. 8 the figures were about the same. The hypothesis of insignificant fractionation for large driving forces remains unsupported.

8.4.2 System Specific Fractionation Model

Generally, the average reactor gas composition, $\overline{C}_{i,reac}$, was taken as the average of the initial reactor gas composition and the final reactor gas composition. In symbols: $\overline{C}_{i,reac} = (C_{i,feed} + C_{i,reac})/2$. H1 applies when $\Delta T = 0$, and there are no $C_{i,reac}$ values available in this case. $C_{i,reac}$ values have to be estimated. This is done graphically in Figures D.1 and D.2 for methane and propane, respectively. The estimation for ethane follows from the mass balance; $\sum C_{i,reac} = 100$ %mol. $\overline{C}_{i,reac}$ and $C_{i,eq}^{CSMHYD}$ values for $\Delta T = 0$ are given in Table 8.5.

Table 8.5: Average composition of the gas in the reactor ($\overline{C}_{i,reac}$) for $\Delta T = 0$ as found in Figures D.1 and D.2, and simulated composition of the corresponding equilibrium hydrate ($C_{i,eq}^{CSMHYD}$). Values are normalized to 100 %mol. These are estimates, and the many decimals are not significant but are given here for traceability. Average ethane content of the reactor gas is $\overline{C}_{C2,reac} = 100 - (\overline{C}_{C1,reac} + \overline{C}_{C3,reac})$.

	$\overline{C}_{i,reac}$ (%mol)				$C_{i,eq}^{CSMHYD}$ (%mol)			
P (MPa)	CH_4	C_2H_6	C_3H_8	Sum	CH_4	C_2H_6	C_3H_8	Sum
7.5	92.825	4.600	2.575	100	69.13	3.63	27.24	100
6.0	92.825	4.600	2.575	100	68.00	3.52	28.48	100
4.5	92.950	4.650	2.400	100	66.93	3.61	29.46	100
3.0	93.775	4.425	1.800	100	66.26	4.10	29.63	99.99

As seen in Figures D.1 and D.2, the reactor gas composition data for $\Delta T = 2$ K deviate from the pattern established by the other data. The same observation is made for the hydrate composition data in Figures 8.5 and 8.6. Three important questions arise. The questions must be treated in the following order and they must be treated at this point, since the answers have consequences for the fractionation modeling.

- Are the deviations significant?
- How can the deviations be explained?
- Should the deviating data have influence on the k-values?

Answers to these questions are proposed in the following. Data points in Figures 8.4 to 8.7 show that for $\Delta T > 4$ K fractionation is suppressed if ΔT

is increased. But a less clear (Figure 8.6) or even contradicting (Figure 8.5) behavior is seen in that a driving force of 2 K may cause less fractionation than a driving force of 4 K. Figure D.2 shows that for 3.0 MPa operation pressure, the reactor gas at the end of experiments is richer in propane for $\Delta T = 2$ K than for $\Delta T = 4$ K and also for $\Delta T = 8$ K. This is noteworthy, even if the hydrate composition did not deviate form the overall trend in this case. A similar pattern was seen for methane at 3.0 MPa. On this background, the deviations for $\Delta T = 2$ K are regarded significant.

It is observed that as the driving force becomes smaller than 4 K, then fractionation may be suppressed compared to larger driving forces. This is contrary to expectations. The behavior may be explained by kinetic effects. In case of a small driving force, about 2 to 4 K and smaller, the degree of conversion is low due to a long induction time (stochastic) and a low gas consumption rate (deterministic). Consequently little gas is (may be) consumed, which implies a small change in the gas composition. Following this line of though, at the limit of zero driving force there would be no gas consumption. Then the gas composition at the end of an experiment would be equal to the feed gas composition, and no fractionation would be observed. But this is only because the system does not reach equilibrium during the four hours the experiments last. This behavior is likely to be highly apparatus dependent. On this basis the deviating data for $\Delta T = 2$ K are not processed further and has no influence on the model. The data points are labeled "&" in Figures 8.4 to 8.7. This line of though is supported by the experimental results of Khokhar (1998) who found that when the driving force (subcooling) was increased 47% the water conversion increased up to 450%. A summary of the three answers is then:

- The deviations at $\Delta T = 2$ K are significant.
- The deviations are explained by kinetic phenomena.
- The deviating data are not given influence on the modeling.

k-values were determined for methane and propane. Least squares plots with $\sum(\text{model}(k, \Delta T) - \text{data}(\Delta T))^2$ on the ordinate and k on the abscissa were made for each pressure (Figures D.3 to D.10, page 159). $k(P, i)$ was read from these plots. The procedure was repeated eight times (8=2x4, 2 components and 4 pressures). Expressions for $C_{C1,diss}$ and $C_{C3,diss}$ could then be written out explicitly for each pressure (Table 8.6). The same procedure

could be used for ethane, but then the mass balance would in general not close at $\sum C_{i,diss} = 100$ %mol. To achieve this, the content of ethane in the hydrate was instead found by subtracting the values for methane and propane from 100, according to hypothesis H3-b. Methane and propane show the strongest fractionation tendency which is the reason these components were modeled rather than ethane. Table 8.6 summarizes the results of the modeling, notably the model equation (Equation 8.1) is outwritten using system dependent values for $k(P,i)$, C_{eq} and C_{feed}. Figures 8.4 to 8.7 show how simulations compare to data. The legends are as follows:

● ━━━ Methane (C1)
○ ——— Ethane (C2)
△ - - - - Propane (C3)

Table 8.6: The fractionation model written out for methane and propane at different pressures. For each pressure, ethane is simulated by subtracting the methane and propane concentrations from 100.

Pressure (MPa)	Component	$C_{diss} = (C_{feed} - C_{eq})e^{-k(P,i)/\Delta T} + C_{eq}$
7.5	CH_4	$C_{diss} = (92 - 69.13)e^{-2.00/\Delta T} + 69.13$
6.0	CH_4	$C_{diss} = (92 - 68.00)e^{-3.07/\Delta T} + 68.00$
4.5	CH_4	$C_{diss} = (92 - 66.93)e^{-3.18/\Delta T} + 66.93$
3.0	CH_4	$C_{diss} = (92 - 66.26)e^{-3.99/\Delta T} + 66.26$
7.5	C_3H_8	$C_{diss} = (3 - 27.24)e^{-1.11/\Delta T} + 27.24$
6.0	C_3H_8	$C_{diss} = (3 - 28.48)e^{-1.69/\Delta T} + 28.48$
4.5	C_3H_8	$C_{diss} = (3 - 29.46)e^{-1.82/\Delta T} + 29.46$
3.0	C_3H_8	$C_{diss} = (3 - 29.63)e^{-1.93/\Delta T} + 29.63$

8.4.3 Simulations

To get an idea about what to expect for higher pressures, a simulation was carried out for 9.0 MPa. k-values for methane and propane were assigned by extrapolating linear regression lines in Figure D.11 on page 163. It was found that $k_{C1,9.0MPa} \approx 1.5$ and $k_{C3,9.0MPa} \approx 1.0$. The feed gas composition is unchanged; 3 %mol propane and 5 %mol ethane in methane. Normalized equilibrium concentrations of the different components in the hydrate, $C_{i,eq}$, were found by CSMHYD simulations. The input to the CSMHYD code was

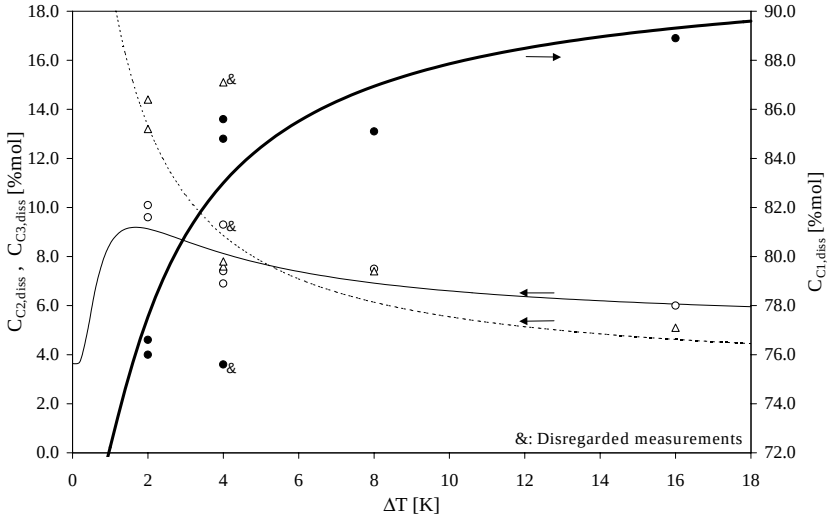

Figure 8.4: Simulations and measurements at 7.5 MPa.

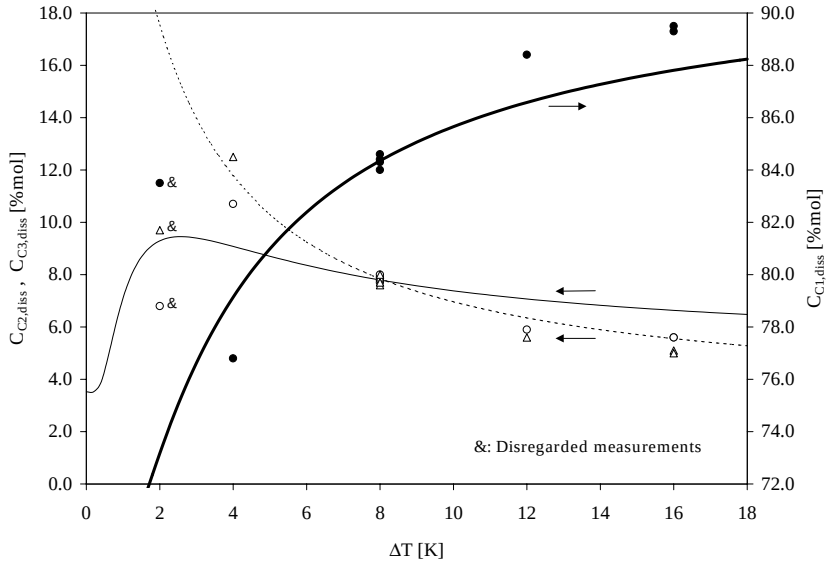

Figure 8.5: Simulations and measurements at 6.0 MPa.

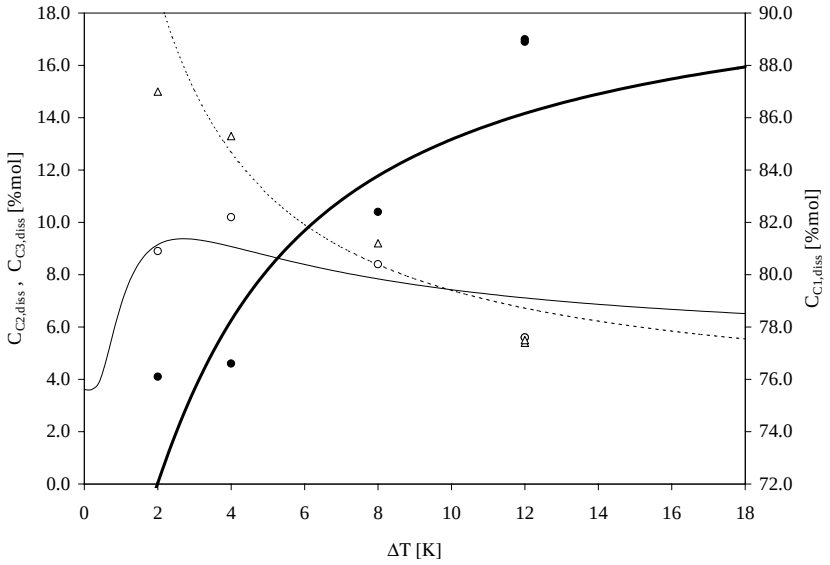

Figure 8.6: Simulations and measurements at 4.5 MPa.

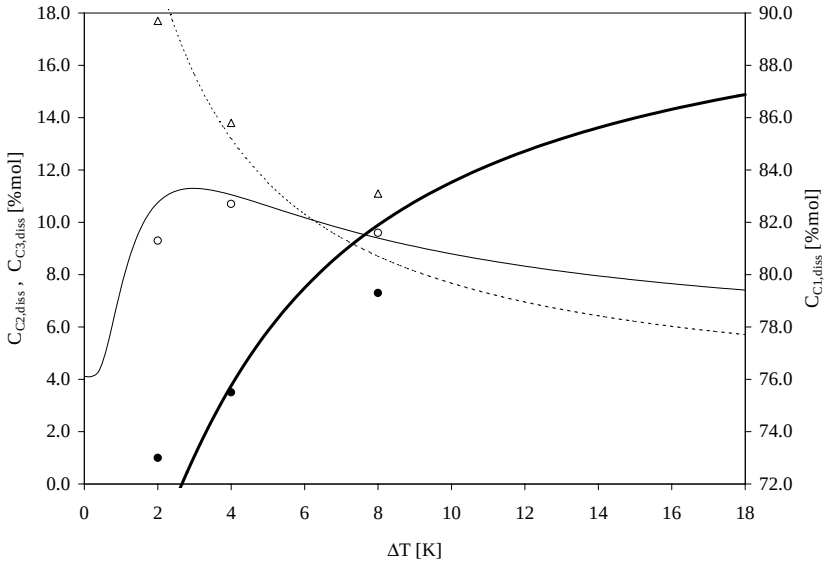

Figure 8.7: Simulations and measurements at 3.0 MPa.

feed gas composition and pressure (9.0 MPa). This yielded an equilibrium hydrate composition as follows: methane: 69.41 %mol, ethane: 3.63 %mol, propane: 26.96 %mol.

The fractionation simulation at 9.0 MPa is shown in Figure 8.8. The simulation for 7.5 MPa, known from Figure 8.4, is shown for comparison. By going from an operation pressure of 7.5 MPa to 9.0 MPa, fractionation is further suppressed.

Simulations could be done for any other reasonable pressure. k-values could be found graphically, as for 9.0 MPa. For the sake of completeness, Figure D.11 gives correlations that could be used instead. But given the scatter of the points from which the correlations were derived, the graphical estimate is equally good.

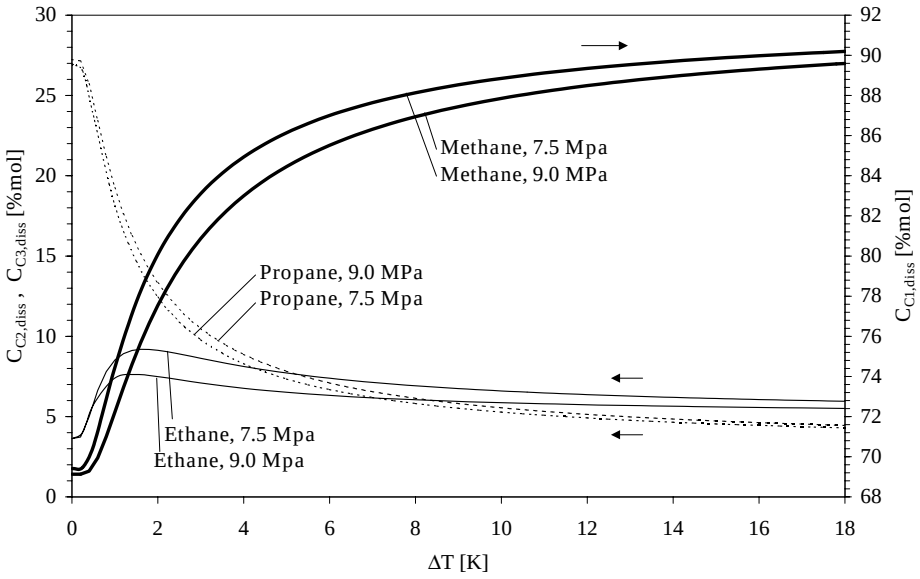

Figure 8.8: Extrapolation of the fractionation model to simulate fractionation at 9.0 MPa. The simulation at 7.5 MPa is shown for comparison.

8.5 Discussion

8.5.1 Fractionation Model

Suitability

To evaluate the suitability of the fractionation model, it is necessary to first state its purpose. The purpose of the model is to predict hydrate composition in cases where the driving force is not small, i.e. the subcooling is larger than 2 K. The reason for excluding the range where the driving force is small is that the focus is on fractionation suppression. But it is seen that in some coincident cases the model predictions are just as good (or bad) for $\Delta T = 2$K as for larger subcoolings (Figures 8.4 and 8.7).

The suitability is evaluated by comparing simulations to data for $\Delta T \geq 4$K. The only reason for excluding $\Delta T = 2$K is that the interest is in system behavior for the larger subcoolings. A rigorous approach using statistical methods is not used - there are too few data to determine error bands that are both narrow and have a satisfactory statistical significance. Instead, representative errors are determined in a simpler way.

$\overline{\Delta}_{i,abs}$ is the average absolute difference between the model and the measurements (all measurements except for $\Delta T = 2$K and the one set of measurements at 7.5 MPa and $\Delta T = 4$K with gross error). $\overline{\Delta}_{i,rel}$ is the relative error. The relative error for methane is given with reference to the average of all methane measurements (except for $\Delta T = 2$ K and the one set of measurements at 7.5 MPa and $\Delta T = 4$K with gross error). The average of all ethane measurements and of all propane measurements were found in the same way. This gave the following reference values: methane: 84.3 %mol, ethane: 7.6 %mol, propane: 8.1 %mol.

Table 8.7 is referred to. The absolute errors are not very different for methane, ethane and propane. It is interesting to note that the absolute error is smaller for ethane even if ethane is modeled such that both the methane and propane errors propagate to the ethane error. The explanation is that the errors made in methane and propane simulations partially cancel each other when used to express ethane fractionation; $C_{C2,diss} = 100 - (C_{C1,diss} + C_{C3,diss})$. The absolute errors being comparable makes the relative errors for ethane and propane about an order of magnitude larger than that for methane. This reflects the fact that in the hydrate, absolute

methane content was about an order of magnitude higher than ethane and propane contents.

Table 8.7: Representative errors made during fractionation simulations.

i	$\overline{\Delta}_{i,abs}$ (%mol)	$\overline{\Delta}_{i,rel}$ (%)
CH_4	± 1.1	± 1
C_2H_6	± 0.68	± 9
C_3H_8	± 1.1	± 14

Assumptions

The estimations of $\overline{C}_{C1,reac}$ and $\overline{C}_{C3,reac}$ made in Figures D.1 and D.2 were not obvious, but some sort of average concentration had to be assessed. An error was introduced that is difficult to quantify in a good manner, but Figures 8.4 to 8.7 show that the chosen approach was reasonable.

The model is not reliable for small driving forces, $\Delta T \leq 2$K. This has been explained already by kinetic phenomena; long induction time and low rate of gas conversion. This explanation is supported by three different observations, all which indicate that there was little hydrate in the samples that showed deviating hydrate composition.

Sample consistency. Hydrate samples in the reactor were normally easy to carve or crush with a screw driver, but deviating samples were hard, compact and difficult to carve or crush. They were ice-like.

Sample popping. Hydrate samples normally popped spontaneously during reactor depressurization and flakes of hydrate bounced off when carved. Samples with deviating compositions were dead.

Gas content. When allowed to dissociate in the dissociation cell, it showed that the samples with deviating composition contained extraordinarily little gas.

The focus of the present work is not kinetics, but the effect of driving force on fractionation, notably at large driving forces. Thus efforts were not put into further description or modeling of the behavior for small driving forces.

It could be said that in the present work the term "nominal driving force with reference to the feed gas composition" is more appropriate than "driv-

ing force". The reason is that during the course of the experiments the composition of the gas in the reactor changed due to fractionation. Accordingly, the hydrate equilibrium curve of the gas made a shift towards higher pressures and lower temperatures. This caused the driving force to become smaller. In the treatment of the results this is not accounted for.

Implications

An important implication to the design of an industry-scale process for NGH production, is that it may be necessary to purge methane. Methane can be recycled too, meaning that the concentration of methane in the reactor will be higher than in the feed gas. Methane purge will then be smaller, but still necessary. This is so because it is not possible to operate at steady state such that all methane enters the hydrate phase. Theory in Section 4.1.2 describes this, and the experimental results in the present work showed significant fractionation for all pressure-temperature pairs.

8.5.2 Calibration and Measurement Errors

The gas chromatograph was calibrated according to the external standard method. The gas used for calibration was the same gas mixture that was used to produce the hydrate. The nominal composition of this gas was 5 %mol ethane and 3 %mol propane in methane. The real composition according to the ISO 9000 analysis certificate from the supplier (Air Products France) were known within an error of ±0.100 %rel and ±0.060 %rel for ethane and propane, respectively.

Because experiment no. 6 had intermediate pressure and temperature values, this experiment was done three times and four hydrate samples were analyzed to quantify the random error of $C_{i,diss}$. The standard deviations were 0.25, 0.13 and 0.18 %mol for methane, ethane and propane, respectively. These values were small enough to proceed. The operation point, see Figure 8.2, had random and systematic errors in pressure and in temperature as follows.

$$\begin{aligned} \delta P_{random} &\approx \pm 0.2\text{MPa} \quad &&\gg \delta P_{systhematic} \\ \delta T_{systematic} &\approx 1\text{K} \quad &&\gg \delta T_{random} \end{aligned}$$

These are intervals that cover about 90% of all the operation pressures and temperatures that spread around the set values. The intervals were narrow enough to proceed. These error intervals may be borne in mind when studying Figures 8.4 to 8.7.

In experiment number 6, the $C_{i,reac}$ values seemed to indicate that the gas phase in the reactor was enriched in propane (from 3.0 to 3.8 %mol), while depleting methane (from 92.0 to 90.8 %mol). These values contradict the trend established by the other measurements and must be disregarded. A possible explanation is that the gas chromatograph loop was insufficiently flushed after the analysis of a dissociated hydrate sample, which was rich in propane (> 3.0 %mol) and lean in methane (< 92.0 %mol).

8.6 Conclusions

- A model to describe fractionation was proposed.
- The model simulates experimental hydrate composition data within an absolute error of about ± 1 %mol.
- The absolute errors convert into relative errors of about 1% for methane, which is present in high concentrations. The relative errors are about 10% for ethane and propane, which are present in lower concentrations.
- To suppress fractionation a large driving force should be used, operating at a high pressure.
- It was not possible to achieve insignificant fractionation with the present apparatus. With 16 K driving force at 7.5 MPa, the methane content of hydrate was about 89 %mol, while the feed gas contained 92 %mol methane. The corresponding figures for propane are 5 %mol and 3 %mol, respectively.
- It was indicated that a large-scale process for natural gas hydrate production will need methane purge and possibly methane recycling.

Chapter 9

Discussion

9.1 Advances and Shortcomings

Three topics were given attention in the present work; thermal and compositional properties of NGH (Chapter 6), metastability of NGH below 273 K (Chapter 7) and fractionation in NGH formation (Chapter 8).

Compositional properties refers to the content of ice and the total content of gas in the hydrate. The composition of the hydrated gas was treated separately in the work on fractionation. Details were discussed at the end of Chapters 6 to 8. This chapter has a broader perspective.

9.1.1 Thermal and Compositional Properties

The present work benefited from the numerous publications of Handa. Still, developing a calorimetric method to analyze hydrate samples to determine h°_{diss}, n and f was challenging. By the time the experimental work was stopped the development was coming to an end, but the method was not validated. This is the major shortcoming of the present work.

The advances were the introduction of the *Ice conditioning* cycle and operating between the hydrate equilibrium lines of methane and the natural gas. It was actually the ice that was conditioned, or pretreated, before the analysis. The purpose was to eliminate the thermal response when ice that froze at a natural gas pressure of about 6-9 MPa melted at a methane pressure

of 1.7 MPa. This was explained in more detail in Sections 6.3.2. With the proposed improvements in Section 6.3.4 it should be possible to analyze hydrate samples that contain large amounts of free water (ice). It is necessary to mount an expansion chamber on the calorimeter (Figure 2.4).

9.1.2 Metastability

The treatment of metastability in this work considers metastability as a kinetically controlled transition; Hydrate $\rightarrow$ Ice + Gas. This is a natural approach since it has never been documented that metastable hydrate persists indefinitely. But it can persist for long times, weeks or even years, and this is what makes it possible to store and transport hydrate at ambient pressure if the temperature is below 273 K.

In this work it was an important objective to quantify the metastability properties. This was done by measuring the rate of dissociation during metastable storage. The isothermal calorimetric method suggested in Section 7.2 is one way of doing this. The working equations of this method, Equations 7.1 and 7.2 contain on the specific enthalpy of hydrate dissociation, Δh_{diss}, and the amount of free water, f. Thus, the accuracy of the isothermal calorimetry method depends on the accuracy of the scanning calorimetry method used to find Δh_{diss}. The isothermal and the scanning methods must be seen as part of a whole. The isothermal method without the input from the scanning method is suitable to compare the *relative* effects of storage temperature on the stability properties.

9.1.3 Fractionation

In contrast to the flow loop and the calorimeter, the fractionation apparatus was simple and experiments were carried out routinely. A fractionation model was developed. At the boundary of zero driving force, the model coincides with van der Waals-Platteeuw theory. For increasing driving force, the system is described by an exponential term which includes a system dependent constant. It was postulated that for an infinite driving force, the composition of the hydrated gas equals the composition of the hydrate forming gas. The experiments showed a satisfactory repeatability, making it possible to assign meaningful values to the system dependent constant (Table 8.6). When the model was used to simulate the system it was accurate within $\approx \pm 1\%$ absolute, which was regarded satisfactory.

9.2 Further Work

It is suggested to continue the present work in three ways:

- Complete the development of the three-cycles scanning calorimetric method for determination of h°_{diss}, n and f. This includes connecting an expansion chamber to the calorimeter before the final experimental work.
- Produce hydrate with no or little ice and study the metastability properties of this hydrate. This will help understand the role of ice.
- In the context of a industry-scale hydrate process operating at steady state, it would be interesting to upgrade the fractionation apparatus such that the composition of the gas phase is constant throughout an experiment.

Chapter 10

Conclusions

- A flow loop with a CSTR reactor and inline filters was constructed for the production and sampling of natural gas hydrate. The design pressure was 1.2 MPa and the design temperature range was 273-293 K. The purpose was to obtain data and operational experience for the design of a pilot plant.
- A scanning calorimetry method was suggested as a way to find the specific enthalpy of hydrate dissociation, the hydrate number and the amount of free water (ice) for natural gas hydrate. The method was developed to analyze samples that contain large amounts of ice. Improvements to reduce the error of the method were proposed.
- An isothermal calorimetric method was suggested as a way to determine the low rates of hydrate dissociation during metastable storage, at ambient pressure and for temperatures below 273 K. This is a method to quantify the metastability properties of natural gas hydrate. Metastability was confirmed for 268 K.
- It was shown that increasing driving force and pressure suppresse fractionation. A model was suggested which describes fractionation as an exponential function of the subcooling (driving force). The accuracy is about $\pm 1\%$ absolute. The model coincides with van der Waals-Platteeuw theory in the case of zero driving force.

References

Aaldijk, L. (1971). *Monovariante Gashydraatevenwichten in Het Stelsel Xenon-Water*. Ph. D. thesis, Technical University of Delft, Delft. (in Dutch).

Adams, T. and M. Kaufman (1997). *Stable Versus Metastable Phase Equilibria in Faceted/Nonfaceted Systems*, Volume Chemistry and Physics of Nanostructures and Related Non-Equilibrium Materials. The Minerals, Metals and Alloys Society.

Andersson, V. (1999). *Flow Properties of Natural Gas Hydrate Slurries - an Experimental Study*. Ph. D. thesis, Norwegian University of Science and technology, Department of Petroleum Engineering and Applied Geophysics, Trondheim.

Bamford, C. and C. Tipper (Eds.) (1980). *Reactions in the Solid State*, Volume 22 of *Comprehensive Chemical Kinetics*. Amsterdam: Elsevier.

Barrer, R. and A. Edge (1967). Gas hydrates containing argon, krypton and xenon: Kinetics and energetics of formation and equilibria. *Proc. Roy. Soc., Ser. A 300*, 1–24.

Barrow, G. (1979). *Physical Chemistry*. McGraw-Hill. ISBN 0-07-Y66170-7.

Berecz, E. and M. Balla-Achs (1983). *Gas Hydrates*, Volume 4 of *Studies in Inorganic Chemistry*. Amsterdam: Elsevier. ISBN 0-444-99675-5.

Buffett, B. and O. Zatsepina (1999). Metastability of gas hydrate. *Geophysical Research Letters 26*(19), 2981–2984.

Calvet, E. and H. Prat (1963). *Recent Progress in Microcalorimetry*. Oxford: Pergamon Press.

Chao, K.-C. and R. Greenkorn (1975). *Thermodynamics of Fluids - An Introduction to Equilibrium Theory*, Volume 4 of *Chemical Process-*

ing and Engineering. New York: Marcel Dekker. L.F. Albright, R.N. Maddox and J.J. McKetta(Eds.).

Chersky, N., A. Groisman, L. Nikitina, and V. Tsarev (1982). Results of the first experimental measurements of netural gas hydrate heat of decomposition (in russian). *Doklady Akademii Nauk SSSR 265*, 185–189.

Cook, J. and D. Leaist (1983). An exploratory study of the thermal conductivity of methane hydrate. *Geophys Rsch Lett 10*(5), 397–399.

Currier, J. and E. Schulson (1982). The tensile strenght of ice as a function of grain size. *Acta Metall. 30*, 1511–1514.

de Forcrand, R. (1923). *Compt. Rend. 176*, 355.

de Forcrand, R. (1925). *Compt. Rend. 181*, 15.

de Roo, J., C. Peters, R. Lichtenthaler, and G. Diepen (1983). *AIChE J. 29*, 651.

Deaton, W. and E. Frost (1946). Number 8 in U.S. Bureau of Mines Monograph. U.S. Bureau of Mines.

Debenedetti, P. (1996). *Metastable Liquids - Concepts and Principles*. Princeton: Princeton University Press.

Dymond, J. and E. Smith (1980). *The Virial Coefficients of Gases*. London: Clarendon Press.

Ebinuma, T., T. Uchida, and H. Narita (1999, 18-22 July). Stability and dissociation behaviors of gas hydrates at low temperature relating to a new technology of natural gas storage. In G. Holder (Ed.), *paper submitted to the Third Intl. Conf. on Natural Gas Hydrates*, Salt Lake City.

Ede, A. (1966). Specific heat capacity at constant pressure of water substance. In *Engineering Sciences Data*, pp. 4–8. London: Engineering Sciences Data Unit. Item no. 68008.

Ershov, E. and V. Yakushev (1992). Experimental research on gas hydrate decomposition in frozen rocks. *Cold Regions Science and Technology 20*, 147–156.

Ewing, G. and L. Ionescu (1974). *J. Chem. Eng. Data 19*, 367.

Fleyfel, F. and E. Sloan, Jr. (1991, 11-16 August). Prediction of natural gas hydrate dissociation enthalpies. In *Proceedings of the first International Offshore and Polar Engineering Conference*, Volume I, Edin-

burgh, pp. 447–453. The International Society of Offshore and Polar Engineers. ISBN 0-9626104-6-1.

Frost, E. and W. Deaton (1946). *Oil Gas J. 45*, 170.

Galwey, A. (1985). Solid state decompositions: The interpretation of kinetic and microscopic data and the formulation of a reaction mechanism. *Thermochim. Acta 96*, 259–275.

Gaskell, D. (1994). *Introduction to the Thermodynamics of Materials*. Washington D.C.: Taylor and Francis.

Glasstone, S. and D. Lewis (1960). *Elements of Physical Chemistry* (2 ed.). London: Macmillan.

Godreche, C. (Ed.) (1992). *Solids Far From Equilibrium*. Cambridge: Cambridge University Press.

Groisman, A. (1985). *Thermophysical Properties of Gas Hydrates*. Moscow: Nauka.

Groisman, A. and A. Savvin (1988). Phase equilibrium conditions, heat capacities and heats of gas hydrate dissociation. *Modelling, Simulation & Control (B) 17*(1), 15–24.

Gudmundsson, J. (1990). Method and equipment for production of gas hydrate (in norwegian). Norwegian patent. Pat. no. 172080.

Gudmundsson, J., V. Andersson, O. Levik, and M. Parlaktuna (1998, 20-22 October). Hydrate concept for capturing associated gas. In *SPE European Petroleum Conference*, The Hague. Society of Petroleum Engineers. SPE paper 50598.

Gudmundsson, J. and A. Børrehaug (1996, 2-6 June). Frozen hydrate for transport of natural gas. In J. de Swaan Aarons and J. Monfort (Eds.), *Proc. 2nd Intl. Conf. on Natural Gas Hydrates*, Toulouse, pp. 415–422. National Polytechnical Institute.

Gudmundsson, J. and M. Parlaktuna (1991). Gas-in-ice: Concept evaluation. Technical report, Department of Petroleum Engineering and Applied Geophysics, Norwegian University of Science and Technology, Trondheim.

Gudmundsson, J. and M. Parlaktuna (1992, 29 March - 2 April). Storage of natural gas hydrate at refrigerated conditions. In *AIChE Spring Natl. Meeting*, New Orleans. AIChE.

Gudmundsson, J., M. Parlaktuna, and A. Kohar (1994, February). Storing natural gas as frozen hydrate. *SPE Production and Facilities*, 69–73.

Gudmundsson, J., M. Parlaktuna, O. Levik, and V. Andersson (1999, 18-22 July). Laboratory for continuous production of natural gas hydrates. In G. Holder (Ed.), *Proc. 3rd Intl. Conf. on Natural Gas Hydrates*, Salt Lake City. N.Y. Academy of Sciences.

Hammerschmidt, E. (1934). Formation of gas hydrates in natural gas transmission lines. *Industrial and Engineering Chemistry 26*(8), 851–855.

Handa, Y. (1986a). Calorimetric determinations of the compositions, enthalpies of dissociation, and heat capasities in the range 85 to 270 K for clathrate hydrates of xenon and krypton. *J. Chem. Thermodynamics 18*, 891–902.

Handa, Y. (1986b). Composition dependence of thermodynamic properties of xenon hydrate. *J. Phys. chem. 90*, 5497–5498.

Handa, Y. (1986c). Compositions, enthalpies of dissociation, and heat capasities in the range 85 to 270 K for clathrate hydrates of methane, ethane, and propane, and enthalpy of dissociation of isobutane hydrate, as determined by a heat-flow calorimeter. *J. Chem. Thermodynamics 18*, 915–921.

Handa, Y. (1988?a). Calorimetric studies of laboratory synthesized and naturally occurring gas hydrates. Technical report, Division of Chemistry, National Research Council of Canada, Ottawa.

Handa, Y. (1988b). A calorimetric study of naturally occuring gas hydrates. *Ind. Eng. Chem. Res. 27*(5), 872–874.

Handa, Y. and J. Cook (1987). Thermal conductivity of xenon hydrate. *Journal of Physical Chemistry 91*(25), 6327–6328.

Handa, Y., R. Hawkins, and J. Murray (1984). Calibration and testing of a Tian-Calvet heat-flow calorimeter, enthalpies of fusion and heat capasities for ice and tetrahydrofuran hydrate in the range 85 to 270 K. *J. Chem. Thermodynamics 16*, 623–632.

Happel, J., M. Hnatow, and H. Meyer (1994). The study of separation of nitrogen from methane by hydrate formation using a novel apparatus. In E. Sloan, Jr., J. Happel, and M. Hnatow (Eds.), *Proc. Intl. Conf. on Natural Gas Hydrates*, Volume 715 of *Ann. NY Acad. Sci.*, New York, pp. 412–424. ISBN 0-89766-847-2.

Höhne, G., W. Hemminger, and H. Flammersheim (1996). *Differential Scanning Calorimetry*. Berlin: Springer-Verlag. ISBN-3-540-59012-9.

Holder, G. and S. Godbole (1982). Measurement and prediction of dissociation pressures of isobutane and propane hydrates below the ice point. *AIChE Journal 28*(6), 930–934.

Holder, G. and G. Grigoriou (1980). *J. Chem. Thermodynamics 12*, 1093.

Holder, G. and V. Kamath (1982). *J. Chem. Thermodynamics 14*, 1119.

Holder, G. and D. Manganiello (1982). Hydrate dissociation pressure minima in multicomponent systems. *Chemical Engineering Science 37*(1), 9–16.

Holder, G., S. Zetts, and N. Pradhan (1988). Phase behaviour in systems containing clathrate hydrates. *Reviews in chemical Engineering 5*, 1–70.

Istomin, V. (1999). On possibility of superheating of natural gas hydrates and other aqueous crystalline solids. *Russian Journal of Physical Chemistry 73*(11), 1887–1890.

Istomin, V. and V. Yakushev (1992). *Gas Hydrates in Natural Conditions (in Russian)*. Moscow: Nedra.

Jhaveri, J. and D. Robinson (1965). *Can. J. Chem. Eng. 43*, 75.

Khokhar, A. (1998). *Storage Properties of Natural Gas Hydrates*. Ph. D. thesis, Norwegian University of Science and Technology, Trondheim.

Kobayashi, R. and J. Lievois (1988, March). Development of a generalized, automated, high pressure heat flux calorimeter and its application to measure the heats of dissociation and hydrate numbers of methane hydrates. Technical report, Rice University, Dept. of Chemical Engineering, Houston.

Levik, O. (1999). Calorimetric analysis of natural gas hydrate. Technical report, Norwegian University of Science and Technology, Department of Petroleum Engineering and Applied Geophysics, Trondheim.

Makogon, Y. (1997). *Hydrates of Hydrocarbons*. Tulsa: PennWell. ISBN 0-87814-718-7.

Maksimov, A. (1996). Experimental studies. Technical report, Moscow.

Marshall, D., S. Saito, and R. Kobayashi (1964). *AIChE J. 10*, 202.

McLeod, H. and J. Campbell (1961). *J. Pet. Technol. 222*, 590.

Michel, B. (1978). Strenght of polycrystalline ice. *Canadian Journal of Civil Engineering 5*(3), 285–300.

Mullin, J. (1994). *Crystallization* (3 ed.). Oxford: Butterworth-Heinemann. ISBN 0-7506-1129-4.

Nagayev, V., A. Gritsenko, and V. Murin (1979). Determination of heat of CO_2 hydrate formation. In *Trans. 8th All-Russian Conf. on Calorimetry and Chem. Thermodynamics (in Russian)*.

Ng, H. and C. Borman (1999). Hydrate phase composition for multicomponent gases. project 976, DB Robinson Research Ltd., Edmonton.

Parent, J. (1948, January). *The Storage of Natural Gas Hydrate*, Volume bulletin no. 1 of *Institute of Gas Technology Research Bulletins*. Chicago: Institure of Gas Technology.

Parlaktuna, M. and J. Gudmundsson (1991, December). Gas-in-ice, production and stability. Technical report, Norwegian University of Science and Technology, Department of Petroleum Engineering and Applied Geophysics, Trondheim.

Parrish, W. and J. Prausnitz (1972). Dissociation pressures of gas hydrates formed by gas mixtures. *Ind. Eng. Chem. Process Des. Develop. 11*(1), 26–35.

Petersen, J. (1997). Performance of equipment and data acquisition in the hydrate laboratory. Master's thesis, Norwegian University of Science and Technology, Department of Petroleum Engineering and Applied Geophysics, Trondheim.

Reamer, H., F. Selleck, and B. Sage (1952). *Pet. Trans. AIME 195*, 197.

Ripmeester, J., C. Ratcliffe, and J. Tse (1988). *J. Chem. Soc. Faraday Trans. 84*, 3731.

Roberts, O., E. Brownscombe, L. Howe, and H. Ramser (1941). *Pet. Engr. 12*, 56.

Rouher, O. and A. Barduhn (1969). *Desalination 6*, 57.

Rueff, R., E. Sloan, Jr., and V. Yesavage (1988, September). Heat capasity and heat of dissociation of methane hydrates. *AIChE J. 34*(9), 1468–1476.

Schneider, G. and J. Farrar (1968, January). Res. develop. progr. rept. no. 292. Technical report, Office of Saline Water.

Selim, M. and J. E. Sloan (1990, May). Hydrate dissociation in sediment. *SPE Reservoir Engineering*, 245–251.

Skovborg, P. and P. Rasmussen (1993). On the dissociation enthalpies of gas hydrates. In *IVC-SEP: Phase Equilibria and Separation Processes*. Lyngby (Denmark): Department of Chemical Engineering, Denmark Technical University.

Sloan, Jr., E. (1998). *Clathrate Hydrates of Natural Gases* (2 ed.). New York: Marcel Dekker. ISBN 0-8247-9937-2.

Sloan, Jr., E. and F. Fleyfel (1992). Hydrate dissociation enthalpy and guest size. *Fluid Phase Equilibria 76*, 123–140.

Sonntag, R. and G. van Wylen (1982). *Introduction to Thermodynamics* (2 ed.). New York: Wiley. ISBN 0-471-09719-5.

Stackelberg, M. (1949). *Naturwiss 36*, 359.

Stern, L., S. Circone, S. Kirby, J. Pinkston, and W. Durham (1999, 18-22July). Dissociation kinetics and phase stability of pure methane hydrate at 0.1 mpa. In G. Holder (Ed.), *abstract submitted to the Third Intl. Conf. on Natural Gas Hydrates - Gas Hydrates and Challenges for the Future*, Salt LakeCity.

Stoll, R. and G. Bryan (1979). Physical properties of sediments containing gas hydrates. *J. Geophys Rsch 84*, 1629–1634.

Sum, A., R. Burruss, and E. Sloan, Jr. (1996, June 2-6). Measurements of clathrate hydrates properties via raman spectroscopy. In J. Monfort (Ed.), *Proc. 2nd International Conference on Natural gas Hydrates*, Toulouse, pp. 51–58. National Polytechnical Institute - ENSIGC.

Tian, A. (1923). Microcalorimeter with compensation by peltier and joule effects. *Bull. Soc. Chim. Fr. 33*(4), 427.

Uchida, T. and I. Hayano (1964). *Repts. Govt. Chem. Ind. Res. Inst. Tokyo 59*, 382.

Uchida, T., T. Hirano, T. Ebinuma, H. Narita, K. Gohara, S. Mae, and R. Matsumoto (1999). Raman spectroscopic determination of hydration number of methane hydrates. *AIChE Journal 45*(12), 2641–2645.

van der Waals, J. and J. Platteeuw (1959). Clathrate solutions. *Adv. Chem. Phys. 2*, 1–57.

Weast, R., M. Astle, and W. Beyer (Eds.) (1986). *CRC Handbook of Chemistry and Physics* (66 ed.). Boca Raton: CRC Press. ISBN-0-8493-0466-0.

Yakushev, V. and V. Istomin (1991, September). Gas-hydrates self-preservation effect. In *Proc. IPC-91 Symp.*, Sapporo, pp. 136–140.

Zakrzewski, M. and Y. Handa (1993). Thermodynamic properties of ice and tetrahydrofuran hydrate in confined geometries. *J. Chem. Thermodynamics 25*, 631–637.

Zeng, J., L. Fan, and J. Schlup (1998). Critical thermodynamic analysis of differential scanning calorimetry for studying chemical kinetics. *Journal of Thermal Analysis 51*, 205–218.

Appendix A

Collection of Δh°_{diss} and n measurements in the Literature

Table A.1 gives standard (P=101.325 kPa) enthalpies of hydrate dissociation, Δh°_{diss}. Values for NGH1 to NGH7 were originally published by Chersky et al. (1982) and Groisman (1985) at pressures of 1-14 MPa, i.e. *not* standard state. Sample NGH9 contained free water that could not be quantified. Instead, an enthalpy interval was calculated based on the assumptions of no free water and 20 %mass free water.

Table A.1: Experimental Δh°_{diss} values. *:Unreasonable value, 5.67 is the theoretical minimum. †:Not standard state.

Guest	Δh°_{diss} kJ/mol	n -	T K	Transition	Reference
sII NGH1	77.3†	6.7	273	h→w+g	(Maksimov 1996)
sII NGH2	72.5†	6.6	278	h→w+g	(Maksimov 1996)
sII NGH3	72.1†	6.3	283	h→w+g	(Maksimov 1996)
sII NGH4	73.9†	6.2	286	h→w+g	(Maksimov 1996)
sII NGH5	70.9†	6.1	288	h→w+g	(Maksimov 1996)
sII NGH6	71.4†	6.1	289	h→w+g	(Maksimov 1996)
sII NGH7	68.8†	5.95	293	h→w+g	(Maksimov 1996)
sII NGH9	27.8-33.1	0-20 %mass ice	220-260	h→i+g	(Handa 1988b)

Table A.1: Experimental Δh°_{diss} values. *:Unreasonable value, 5.67 is the theoretical minimum. †:Not standard state.

Guest	Δh°_{diss} kJ/mol	n -	T K	Transition	Reference
sI NGH8	17.50	$CH_4 \cdot 5.91H_2O$	273	h→i+g	(Handa 1988b)
CH_4	54.19 ± 0.28	6.00 ± 0.01	273.15	h→w+g	(Handa 1986c)
CH_4	54.36	7.00	273.15	h→w+g	(Roberts et al. 1941)
CH_4	67.85	6.3	273.15	h→w+g	(de Roo et al. 1983)
CH_4	55.12		273.15	h→w+g	(Deaton and Frost 1946)
CH_4	55.07		273.15	h→w+g	(McLeod and Campbell 1961)
CH_4	53.41		273.15	h→w+g	(Marshall et al. 1964)
CH_4	18.13 ± 0.27	6.00 ± 0.01	160-210	h→i+g	(Handa 1986c)
CH_4	19.06	7.18	273.15	h→i+g	(Frost and Deaton 1946)
CH_4	23.37	7.4	273.15	h→i+g	(de Roo et al. 1983)
C_2H_6	71.80 ± 0.38	7.67 ± 0.02	273.15	h→w+g	(Handa 1986c)
C_2H_6	69.71	7	273.15	h→w+g	(Roberts et al. 1941)
C_2H_6	73.88		273.15	h→w+g	(Deaton and Frost 1946)
C_2H_6	86.32		273.15	h→w+g	(Reamer et al. 1952)
C_2H_6	76.09		273.15	h→w+g	(Holder and Grigoriou 1980)
C_2H_6	25.70 ± 0.37	7.67 ± 0.02	190-250	h→i+g	(Handa 1986c)
C_2H_6	23.75		273.15	h→i+g	(Frost and Deaton 1946)
C_3H_8	129.2 ± 0.4	17.0 ± 0.1	273.15	h→w+g	(Handa 1986c)
C_3H_8	109.1		273.15	h→w+g	(Reamer et al. 1952)
C_3H_8	126.9		273.15	h→w+g	(Frost and Deaton 1946)
C_3H_8	27.00 ± 0.33	17.0 ± 0.1	210-260	h→i+g	(Handa 1986c)
C_3H_8	27.91	17.95	275.15	h→i+g	(Frost and Deaton 1946)
C_3H_8	28.30		273.15	h→i+g	(Holder and Kamath 1982)
C_3H_8	26.68		273.15	h→i+g	(Holder and Godbole 1982)
i-C_4H_{10}	133.2	17 assumed	273.15	h→w+g	(Handa 1988a)
i-C_4H_{10}	132		273.15	h→w+g	(Uchida and Hayano 1964)
i-C_4H_{10}	122.4		273.15	h→w+g	(Rouher and Barduhn 1969)
i-C_4H_{10}	131		273.15	h→w+g	(Schneider and Farrar 1968)
i-C_4H_{10}	31.07 ± 0.20	17 assumed	273.15	h→i+g	(Handa 1988a)
i-C_4H_{10}		31.31	273.15	h→i+g	(Holder and Godbole 1982)

Table A.1: Experimental Δh°_{diss} values. *:Unreasonable value, 5.67 is the theoretical minimum. †:Not standard state.

Guest	Δh°_{diss} kJ/mol	n -	T K	Transition	Reference
$(CH_3)_3CH$	133.2 ± 0.3	17	273.15	h→w+g	(Handa 1986c)
$(CH_3)_3CH$	132		273.15	h→w+g	(Uchida and Hayano 1964)
$(CH_3)_3CH$	122.4		274.2	h→w+g	(Rouher and Barduhn 1969)
$(CH_3)_3CH$	131		273.15	h→w+g	(Schneider and Farrar 1968)
$(CH_3)_3CH$	31.07 ± 0.20		230-260	h→i+g	(Handa 1986c)
$(CH_3)_3CH$	31.31		256.5	h→i+g	(Holder and Godbole 1982)
CO_2	57.98 ± 7%		281	h→w+g	(Nagayev et al. 1979)
Kr	56.3	5.0*	273.15	h→w+g	(de Forcrand 1923)
Kr	58.2		273.15	h→w+g	(Stackelberg 1949)
Kr	56.20 ± 0.25	6.10	273.15	h→w+g	(Handa 1986a)
Kr	19.54 ± 0.24	6.10	273.15	h→i+g	(Handa 1986a)
Kr	20.5	6.0	273.15	h→i+g	(Barrer and Edge 1967)
Xn	63.23 ± 0.19	6.29	273.15	h→w+g	(Handa 1988a)
Xn	61.96 ± 0.19	5.90	273.15	h→w+g	(Handa 1986a)
Xn	69.2	6.6	273.15	h→w+g	(de Forcrand 1925)
Xn	69.9		273.15	h→w+g	(Stackelberg 1949)
Xn	61.67 ± 0.84	6.0	273.15	h→w+g	(Aaldijk 1971)
Xn	64.0	6.0	273.15	h→w+g	(Ewing and Ionescu 1974)
Xn	26.50 ± 0.17	5.90	273.15	h→i+g	(Handa 1986a)
Xn	25.43 ± 0.17	6.29 ± 0.03	273.15	h→i+g	(Handa 1986b)
Xn	24.0	6.0	211-268	h→i+g	(Barrer and Edge 1967)
Xn	25.79 ± 0.41	6.0	263-273	h→i+g	(Aaldijk 1971)

Table A.2: Composition of the samples NGH1 to NGH8 referred to in Tables 2.3 and A.1.

Sample	CH_4	C_2H_6	C_3H_8	i-C_4H_{10}	O_2	N_2	$M + 18n$ (g/mol)
NGH1	52.5	2.79	39.1	2.22	3.19	0.16	149.5
NGH2	62.1	2.36	29.73	1.69	3.96	0.20	145.7
NGH3	64.14	2.35	27.57	1.56	4.17	0.21	138.8
NGH4	65.02	2.39	26.62	1.50	4.26	0.22	135.9
NGH5	65.51	2.42	26.08	1.47	4.32	0.23	134.9
NGH6	65.73	2.43	25.82	1.45	4.34	0.23	134.8
NGH7	66.66	2.49	24.77	1.39	4.45	0.23	130.9
NGH8	99.93	0.01	0.01	0.05			

Appendix B

Experiments and Findings Leading to the Preliminary Calorimetric Method

B.1 Alternative Schemes for a Calorimetric Method

Heat has to be supplied to dissociate hydrate . The total heat is in part due to dissociation of the hydrate itself, but also due to melting of the free water present as ice. In the introductory experiments (Section 6.3.1) the samples were heated at ambient pressure. This yielded a single peak at about 273 K. This peak represented both ice melting and hydrate dissociation. The main challenge in calorimetric analysis of NGH was to develop a method that enables the separation of these two heat contributions.

It was clear that the sample had to be pressurized by a gas. The hydrate forming natural gas was the first choice. Trial and error was important as the work proceeded. Three principal schemes were pursued. For the next two paragraphs, note that the specified temperatures and scanning rates were only the *initial assumptions*.

Schemes 1 and 3. The sample was heated under pressure. This yielded one peak around 273 K (ice melting) and one peak at a higher temperature (hydrate dissociation). In Scheme 1 the scanning rate was increased from 0.01 K/min to 4 K/min after the ice peak. In Scheme 3 the scanning rate was constant at 0.05 K/min.

Scheme 2. The sample was first heated under pressure to produce an ice melting peak at 273 K. Then the sample was refrigerated again and the pressure relieved. During the second heating sequence at ambient pressure one peak due do combined ice melting and hydrate dissociation was seen at 273 K. The scanning rate was 0.05 K in both heating sequences.

B.2 Individual Tests

Two issues were addressed: First, it was required that the thermal response due to ice melting and hydrate dissociation were well separated. Second, it was necessary to gain a quantitative understanding of how to interpret the heat signals detected for each process (melting and dissociation). A number of tests were carried out to find ways to meet these two requirements. Selected tests are presented in detail in the following. They are treated in the same order as they were carried out, thus the progress of system understanding is also communicated.

B.2.1 Tests with Natural Gas

Test 1, Scheme 3 modified, Figure B.1

This was a modification of Scheme 3 where an isothermal sequence was used between the peaks. Natural gas was used to pressurize the sample 2.1 MPa. The gas composition was the same as during hydrate formation; ethane (5 %mol) and propane (3 %mol) in methane. The idea was that by using the hydrate forming gas to establish pressure, this would impose the least disturbances on the hydrate system. The isotherm between the two peaks allowed complete ice melting before further heating and subsequent hydrate dissociation.

Peak separation was good, but the drawback was that the baseline shifted when going from scanning mode to isothermal mode. This complicated the peak integration. Since accurate integration is essential, this way of separating the peaks was abandoned. When the data were processed, an unreasonable low hydrate number was found, n=1.33, while the ideal (theoretical minimum) hydrate number is 5.67. Base line shift may explain this in part, but there is more to it, as will be demonstrated.

Test 2, Scheme 3, Figure B.2

In this test the same NG mixture as in Test 1 was used to pressurize the sample (3.0 MPa), but now the isotherm in the scanning cycle was omitted. The sample was heated from 253 K to almost 313 K at a heating rate of 0.05 K/min. The low start temperature was to make sure the base line had stabilized before the first peak (ice). The high stop temperature was to make sure that the last peak (hydrate) should come to a completion.

Peak separation was not good, but when the data were analyzed, a reasonable hydrate number was found; n=6.05. The ideal hydrate number is 5.67. The specific enthalpy of hydrate dissociation was Δh_{diss}=534.2 J/g. This way of treating the sample yielded promising results, but little confidence was put in the results since the peak separation was not good. The exothermic response between the peaks could be explained by hydrate formation. It was concluded that the procedure in this test was unreliable.

Test 3, Scheme 3, Figure B.3

The pressure was 8.0 MPa. This was not a feasible procedure as the thermogram was full of undesirable peaks with considerable exothermic and endothermic integrals. One reason for the complicated peak pattern is probably due to desorption of natural gas from the water that formed as the ice melted. Desorption is explained since the ice froze at around 9 MPa which is about 1 MPa higher than the pressure used in this test. Hydrate probably formed too.

B.2.2 Tests with Nitrogen

Test 4, Scheme 3, Figure B.4

Pressurizing with natural gas was not successful. It was decided to try pressurize with nitrogen. Nitrogen too is a hydrate former, but not at the pressure-temperature conditions applied during these tests. The peak separation was not good. In this test the heating rate was 0.05 K/min. Lower rates yielded even poorer separation. Tests with higher heating rates were not tried.

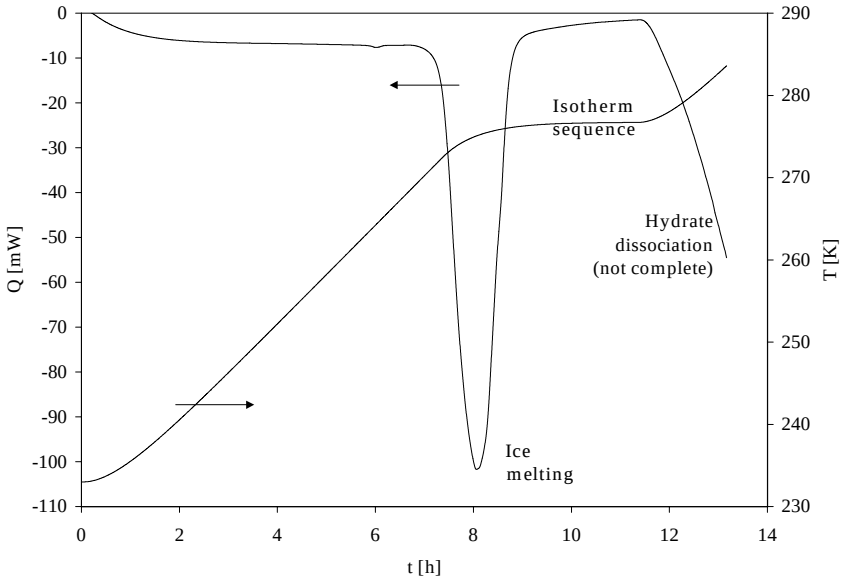

Figure B.1: Test 1, thermogram.

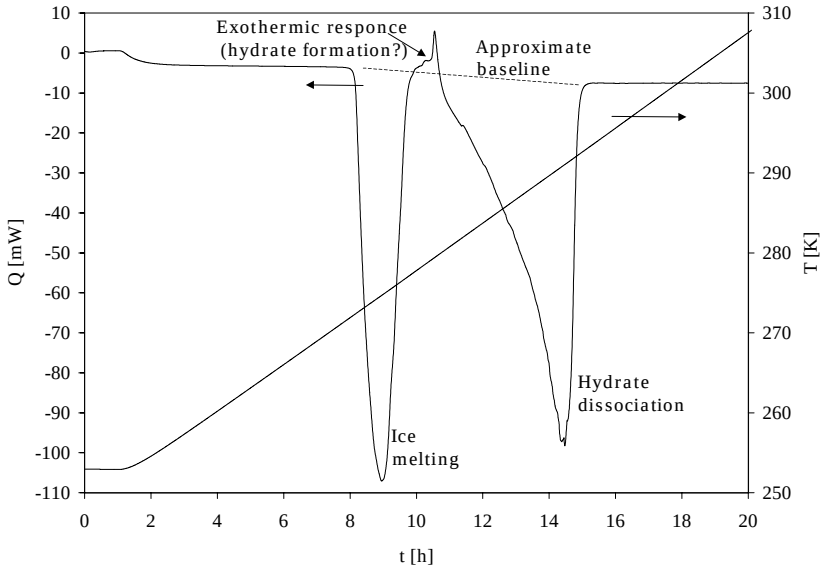

Figure B.2: Test 2, thermogram.

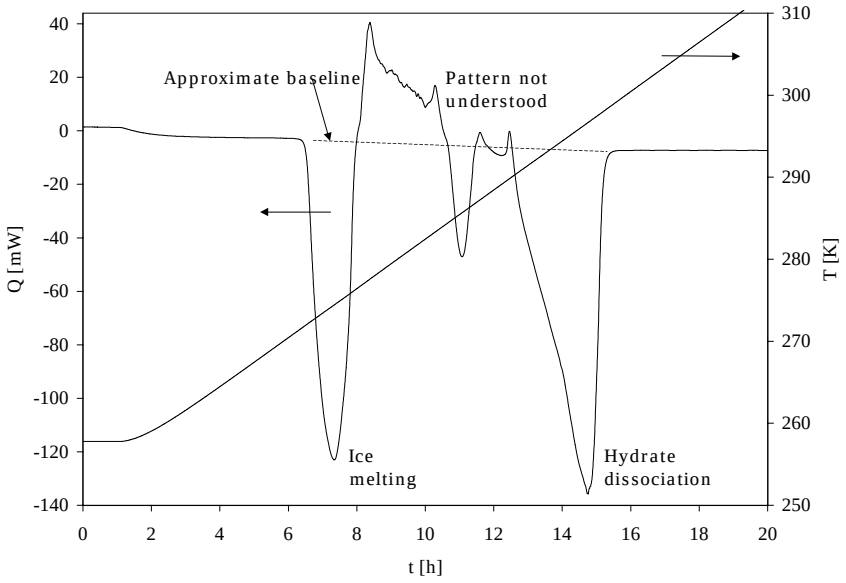

Figure B.3: Test 3, thermogram.

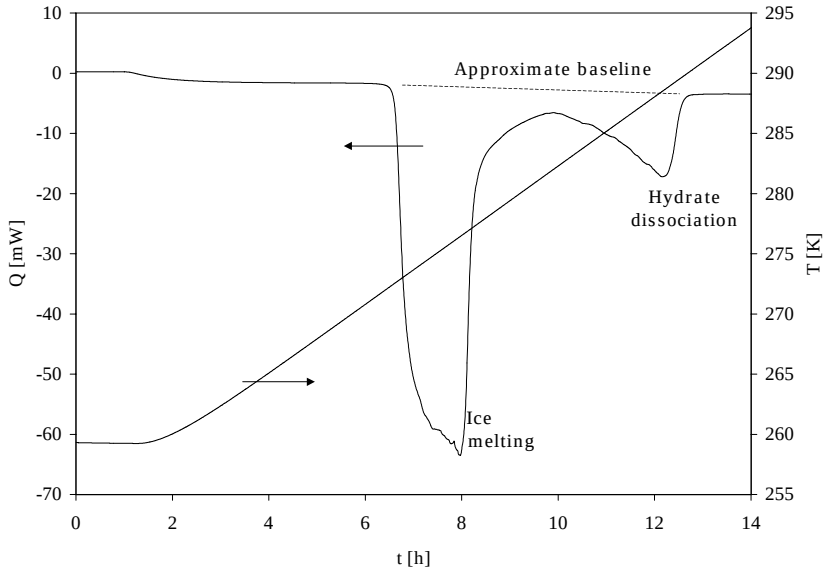

Figure B.4: Test 4, thermogram.

Test 5, Scheme 1

The thinking now was that a very slow heating rate past the ice peak would give a good peak separation but without base line shift as with isotherms (Test 1). From the above tests and from the literature (Höhne et al. 1996) it was known that higher heating rates yield narrower peaks. Thus a scanning cycle was tried where the sample was heated at 0.01 K/min past the ice peak and then heated at the highest possible rate past the hydrate peak.

The peak separation was good and there are no apparent sources of error such as peaks in addition to the two expected peaks. Still an unreasonable hydrate number was obtained, n=1.73.

Test 6: Investigation of the Effect of Nitrogen Absorption, Figure B.5

It was expected that nitrogen would be absorbed by the free water when the ice melted. But it was assumed that the thermal effects due to absorption could be ignored. It seemed now that this assumption did not hold, as the results so far were unreasonable. The two peaks in the thermograms had to have a more complex origin than only ice melting and hydrate dissociation. Experiments were carried out to investigate this issue further.

To get a reference measurement, a sample of ice prepared from pure but not degassed water, was melted in the calorimeter at ambient pressure in an open cell. This yielded an enthalpy of melting equal to 334.44 J/g. This deviated only -0.2% from the literature value of 333.7 J/g (Weast et al. 1986).

Degassed water was used during hydrate production. During tests 4 and 5 the hydrate samples were pressurized with nitrogen. The next experiment was therefore to make ice from degassed water and melt a sample of this ice under nitrogen pressure. The deviation from 333.7 J/g was as large as -23.2% and -23.0% in experiments performed at initial nitrogen pressures of 5.05 MPa and 5.00 MPa, respectively. The reproducibility of these two experiments were good. The peaks were smooth. How the pressure developed is shown in Figure B.5. It is seen how pressure decreased due to absorption of nitrogen. Since the density of ice is about 90% of the water density, the sample contraction upon melting will contribute to the pressure reduction. How absorption and sample contraction compare was not calculated.

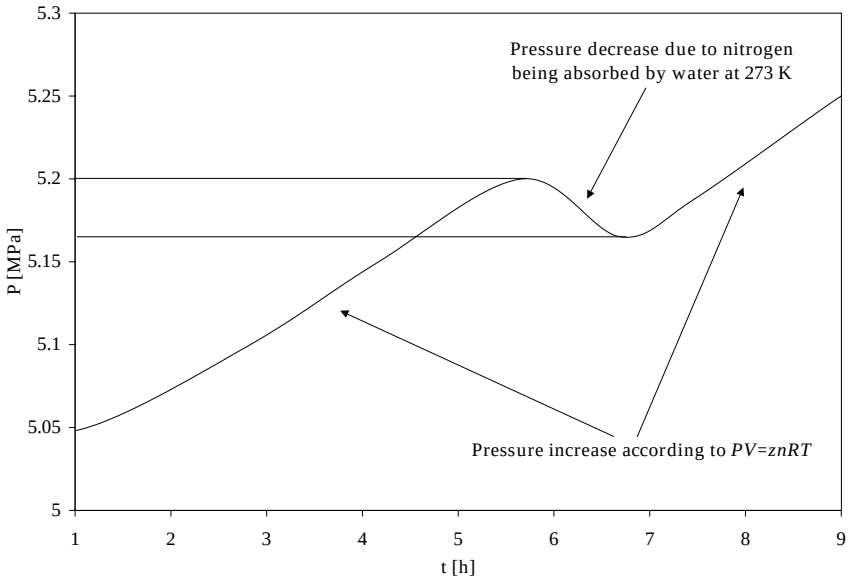

Figure B.5: Test 6. Up to 273 K the pressure increased according to $PV = znRT$. At 273 K there was a sudden drop as nitrogen was absorbed by the water. Upon further heating the pressure continues to increase.

The following had been shown. When a sample of ice prepared from degassed water is melted under a nitrogen atmosphere of 5.0 MPa, the specific heat of melting is 256.5 ± 0.5 J/g. This has important consequences for hydrate number calculations - so far, a melting enthalpy of 333.5 J/g had been used in calculations, under the assumption that thermal effects of nitrogen absorption were negligible. This assumption failed. A different value had to be used.

This also had consequences as far as the procedure it self is concerned. It was assumed that nitrogen would also absorb in the water that was formed when the hydrate dissociated under nitrogen pressure. Further complications regarding data analysis follows. This tends to favor Scheme 2, where only ice is melted under pressure, while hydrate is dissociated at ambient pressure.

Test 7, Scheme 2, Figure B.6

During the first cycle the sample was pressurized. The peak was due to ice melting. The peak was neat, so the integration did not pose any problems. The sample was then refrozen and the pressure was taken down to ambient and the calorimeter cells left open to the surrounding air. In the second cycle there also was one single peak (Figure B.6). It was due to combined ice melting and hydrate dissociation. Test 7 was repeated, and worked fine as far as operation and peak separation are concerned. The desorption of gas from the melted ice has to be accounted for when integrating the ice melting peak. This illustrates the need for some "fundamental" data:

- Enthalpy of melting when ice from degassed water is melted at elevated pressure.
- Enthalpy of melting when ice formed at elevated pressure pressure is melted at ambient pressure.

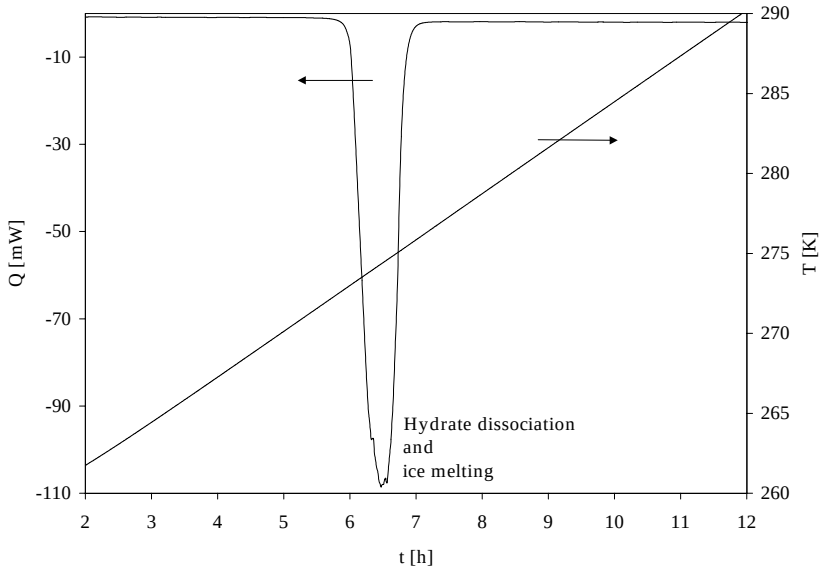

Figure B.6: Test 7, *Hydrate dissociation* cycle.

B.2.3 Tests with Methane

Test 8, Scheme 2 extended

Tests 1 to 7 showed that natural gas and nitrogen caused complications due to absorption and desorption, and probably hydrate formation in the case of natural gas. The idea now was to pressurize the sample with methane. But still the melting of the ice (free water) will be accompanied by absorption/desorption. The corresponding thermal effect contributed to the melting peak. This contribution could not be quantified. Thus, it was proposed to extend Scheme 2 by applying a *sample conditioning* step.

Sample conditioning refers to melting the ice that formed under an elevated natural gas pressure, to allow the water phase with the dissolved natural gas to equilibrate with methane. Thus, the part of the sample that actually was conditioned or pretreated, was the ice. After the conditioning, the sample was refrozen.

In a second cycle, the sample was heated once again to melt the ice. Now the ice melted under a gas with which it was equilibrated as it froze. Accordingly, the thermal effect of absorption/desorption was negligible and the peak was due to melting only. To calculate the amount of free water it was necessary to know the specific enthalpy of ice melting when freezing and melting took place at the same pressure. This value was determined in separate experiments to be 342.63 J/g for a methane pressure of 1.7 MPa. It was assumed that the uncertainty is $\pm 0.5\%$, as in earlier ice melting experiments.

The pressure 1.7 MPa was chosen as follows. The sample needed to be pressurized above the hydrate curve for the NG used to produce the hydrates. At the same time, the pressure had to be below the hydrate curve for methane. This should make the system non-reactive - it was assumed that hydrate will neither form nor dissociate. The pressure was needed to melt the ice without dissociating the hydrate. This governed the temperature interval of interest. The water could not be heated above 276 K. The lowest temperature is about 263 K. If the hydrate curves are consulted (Figure 6.5) it is seen that an initial pressure of 1.7 MPa was appropriate.

Effects due to ethane and propane in the free water are assumed negligible for the following reasons. The ice contains ethane corresponding to an ethane partial pressure of about $0.05P_{production}$. The origin of 0.05 is that the NG used to produce the hydrate contains 5 %mol ethane. A similar argument

can be set forth for propane, which was present at 3 %mol in the NG. Nearly all of the ethane and propane in the water that formed during the sample conditioning will desorb in order to attain phase equilibria. Only negligible amounts of sII hydrate may form during the following cooling sequence, if at all. Further, the system was operated in a pressure-temperature region where methane hydrate do not form. In short, the driving forces for absorption/desorption and hydrate formation/dissociation are negligible after the conditioning step.

What remained was to dissociate the hydrate to find the specific enthalpy of dissociation. This could be done either at some elevated pressure (1.7 MPa) by just continuing the heating of the sample. Alternatively, the sample could be refrozen while still pressurized and the system depressurized to ambient pressure before dissociation. The latter alternative was chosen since it is the least involving, and sources of error are reduced. Note that when NGH is dissociated in the NGH chain, this will also take place at ambient pressure. It is known from the introductory experiments (Section 6.3.1) that in this case, hydrate dissociation will be accompanied by ice melting and that the peak will show at about 273 K. The heat contribution from ice melting and desorption of absorbed gases, notably methane, can be calculated. Specific enthalpy of dissociation is then found from the mass and energy balance. What is needed is the enthalpy of melting at ambient pressure of ice that formed under 1.7 MPa methane. This value was determined experimentally in a separate test as 344.38 J/g.

The results of Test 8 were reasonable ($n = 4.7 \pm 1.8$, $f = 59 \pm 1\%$), but the random error in n was large. This could be reduced by using a more accurate balance when measuring the sample mass and by increasing the sample mass. Both means would reduce the random errors.

Test 9 and 10, Scheme 2 extended

These tests were carried out according to the same procedures as in Test 7, but with a more accurate balance; ± 0.002 g in stead of ± 0.01 g. The sample mass was increased from about 0.92 g to 1.100 g (Test 9) and 1.001 g (Test 10). Because of the higher sample masses the ice melting peaks became wider and the criterion of not heating the sample above the hydrate equilibrium line, was violated. It was concluded that a sample mass of about 0.95 g was the highest feasible.

Test 11, Scheme 2 extended

This test was carried out just as Test 8 except now the pressure was 1.7 MPa (it was 1.5 MPa in Test 8). The sample had been stored at 224 K for 7 weeks and at 257 K for 2 days. The hydrate number was low, but if the same uncertainty interval as in Test 8 was assumed, then the error interval covered the ideal hydrate number. The specific enthalpy of hydrate dissociation was 315.8 J/g. The amount of free water was 70 %mass. The thermograms looked as in Figures 6.2 to 6.4 which were collected during the same type of test.

Appendix C

Thermal and Compositional Properties - Estimates

The models and correlations reported in the literature (Chapter 2) are now used to estimate thermophysical and compositional properties of sII natural gas hydrate. The numbers are mostly estimated independently of each other and may not be fully consistent. The results are collected in Table 6.2.

Composition

The hydrated gas is assumed to consist of methane (89 %mol), ethane (6 %mol) and propane (5 %mol). This is about the same hydrate composition as obtained during run 1 in the fractionation experiments where the $P = 7.5$ MPa and $T = 275$ K, giving a driving force of $\Delta T = 16$ K. The average molar mass of the hydrated gas is then 18.24 g/mol.

The hydrate number is assumed to be n=6. This is a reasonable assumption as the ideal hydrate number is 5.67, and since a considerable driving force ($\Delta T = 16$ K) is a relevant assumption.

Enthalpy of Dissociation

Δh°_{diss} is estimated in Figure C.1 using the Clausius-Clapeyron equation around $P = 1.01$ MPa. Phase equilibrium data are simulated using CSMHYD (Sloan 1998) and assuming a natural gas of ethane (5 %mol) and propane (3 %mol) in methane.

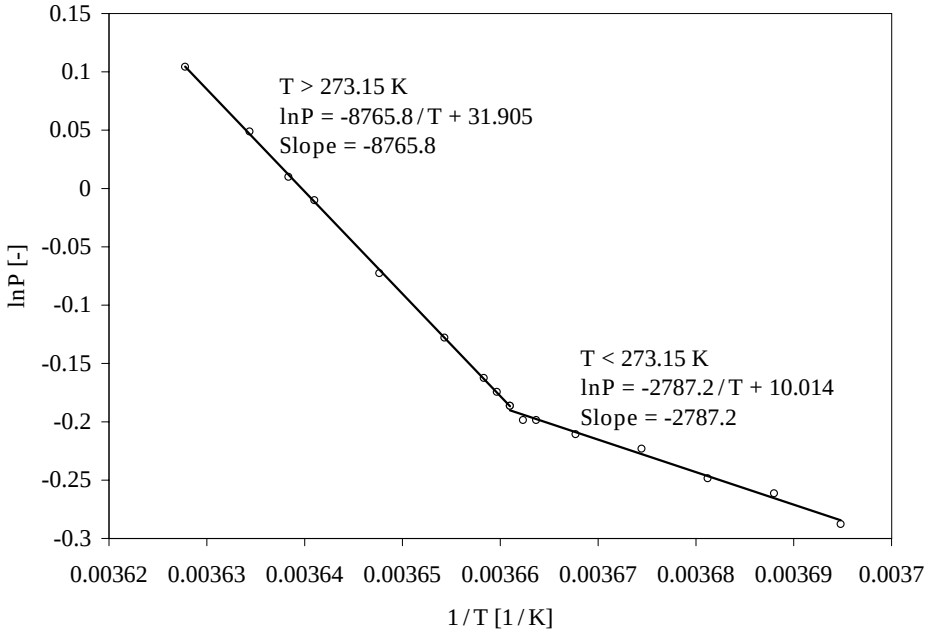

Figure C.1: Clausius-Clapeyron plot around 101,325 Pa. The phase equilibrium data are for a gas of ethane (5 %mol) and propane (3 %mol) in methane and were obtained using CSMHYD.

Assuming $z \approx 1$ gives for $T = 274.8$ K and $P = 1.01$ MPa:
$\Delta h^{\circ}_{diss} = -zaR \approx -1(-8785)8.413$ J/mol $= 73.0$ kJ/mol.
Multiplying by $1000/(M_{NG} + 18n)$, using $n = 6$ and $M = 18.24$ g/mol (assumptions made above), this converts into 578 J/g. This is a relevant estimate for sII natural gas hydrate.

Using the equilibrium values $M_{NG} \approx 27$ g/mol and $n \approx 7.4$ obtained by CSMHYD, 73 kJ/mol converts into 456 J/g. This shows that the formation conditions, notably the driving force, has a big impact on Δh_{diss} (J/g) via the average molar mass of the hydrated gas, M_{NG}. For $T < 273.15$ K, the slope is -2787.2 K. Then, $\Delta h_{diss} = -zaR \approx -1(-2787.2)8.314$ J/mol $=$ 23 kJ/mol. The way Δh_{diss} suddenly changes at $T = 273.15$ K is reflected in the change of slope in the Clausius-Clapeyron plot.

The Δh_{diss} (kJ/mol) values obtained above compare to experimental values in the literature. Maksimov (1996) reported 68.8-77.3 kJ/mol for sII NGH above 273.15 K. It has been shown here, how a Clausius-Clapeyron simulation yielded an intermediate value; 73.0 kJ/mol. Handa (1988b) reported 27.8-33.1 kJ/mol for sII NGH below 273.15 K. The deviation between the lower value (27.8 kJ/mol) and the Clausius-Clapeyron prediction (23 kJ/mol) is about 20%. Using the guest size dependent model (Section 2.4.2) by Sloan and Fleyfel (1992) the value $\Delta h_{diss} = 79$ kJ/mol ($T > 273$ K) is found.

The correlation by Selim and Sloan (1990) in Section 2.4.4 yields $\Delta h_{diss} = 446.12 \cdot 10^3 - 132.638 \cdot 274.8 = 410$ J/g. This value differs -29% from 578 J/g obtained above, and -10% from the value 456 J/g, also obtained above but assuming equilibrium values of M_{NG} and n. The deviations may be explained since this correlation applies to hydrate in sediment. The correlation is not ment to apply to bulk hydrate. The correlation is based on Clausius-Clapeyron calculations and using equilibrium data, which is probably why it compares better to 456 J/K. Also note that the correlation is given for natural gas hydrate, without specifying the composition of the hydrate or the hydrate forming gas.

An intresting thing can be seen if the Δh_{diss} values in Table 2.3 are corrected for the hydrate number variations. Let the value $n = 6.7$ for sample NGH1 be the reference, since it applied in the case where the pressure was lowest (1.1 MPa) and closest to standard pressure. Table C.1 is referred to. For NGH7, Δh_{diss} becomes $\frac{6.7}{5.95} \cdot 68.8$ kJ/mol $= 77.4$ kJ/mol, which is close to the value 77.3 kJ/mol for sample NGH1. The largest deviation from the reference value (77.3 kJ/mol) is 4.8% (NGH2) and with an average deviation of 1.9%. The corresponding numbers for the original data are 11.0% and 7.4%, respectively. This shows how the variations in the hydrate number largly account for the variations in Δh_{diss} (kJ/mol). This reflects that breaking the hydrogen bonds in the lattice accounts for a large portion of Δh_{diss}. Another intresting manipulation of the Δh_{diss} data in Table 2.3 is to multiply by $1000/(M_{NG} + 18n)$ to convert from kJ/mol to J/g. The largest deviation from the reference value (517 J/g) is 5.2% (NGH4) and with an average deviation of 2.5%.

Table C.1: Conversion of Δh_{NGH} data given by Chersky et al. (1982) and Groisman (1985).

Sample	$M_{NG}+18n$ g/mol	n -	Measured kJ/mol	for n_{ref}=6.7 kJ/mol	Converted J/g
NGH1	149.5	6.7	77.3	77.3	517
NGH2	145.7	6.6	72.5	73.6	498
NGH3	138.8	6.3	72.1	76.7	519
NGH4	135.9	6.2	73.9	79.9	544
NGH5	134.9	6.1	70.9	77.9	526
NGH6	134.8	6.1	71.4	78.4	530
NGH7	130.9	5.95	68.8	77.4	526

Specific Heat Capacity; c_p

Specific heat capacity, c_p, is estimated using the correlation by Groisman (Equation 2.25): $c_p = \frac{4.5R+18{\cdot}6(2.3+8.4732{\cdot}10^{-3}(274.8-273.15))}{18.24+18{\cdot}6} = 2.28$ J/gK, which transforms into 287 J/molK.

Thermal Conductivity; λ

Thermal conductivity, λ, is estimated using the correlation by Groisman (Equation 2.27). It is necessary to estimate the hydrate density and a value of 700 kg/m^3 is assumed. This yields: $\lambda = -0.21+8.33\cdot10^{-4}\cdot700$ W/Km = 0.373 W/Km. The density may be too low, but the correlation is not valid for higher densities.

Thermal Expansivity; $\frac{dl}{ldT}$

The thermal expansivity for sII natural gas hydrate was given in Table 2.10 as $52\cdot10^{-6}$ K^{-1}.

Appendix D

Determination of Fractionation Model Parameters

Average Reactor Gas Composition for Zero Driving Force

To develop the fractionation model it was necessary to estimate the average reactor gas composition in case of $\Delta T = 0$. This is done in Figures D.1 and D.2 for methane and propane, respectively.

k-value Determination

The fractionation model includes a system dependent constant k. k-values were determined for methane and propane in least squares plots with

$$\Sigma(\text{model}(k, \Delta T) - \text{data}(\Delta T))^2$$

on the ordinate and k on the abscissa for each pressure. The model expresses the content of ethane in the hydrate as $C_{2,diss} = 100 - (C_{C1,diss} + C_{C3,diss})$ to make the mass balance close at 100 %mol. Concequently, the k-values for ethane are not needed. The plots follow in Figures D.3 to D.10.

Extrapolation of $k(P, i)$ to 9.0 MPa

The model was extrapolated to $P = 9.0$ MPa. k-value estimates for methane and propane were found graphically in Figure D.11.

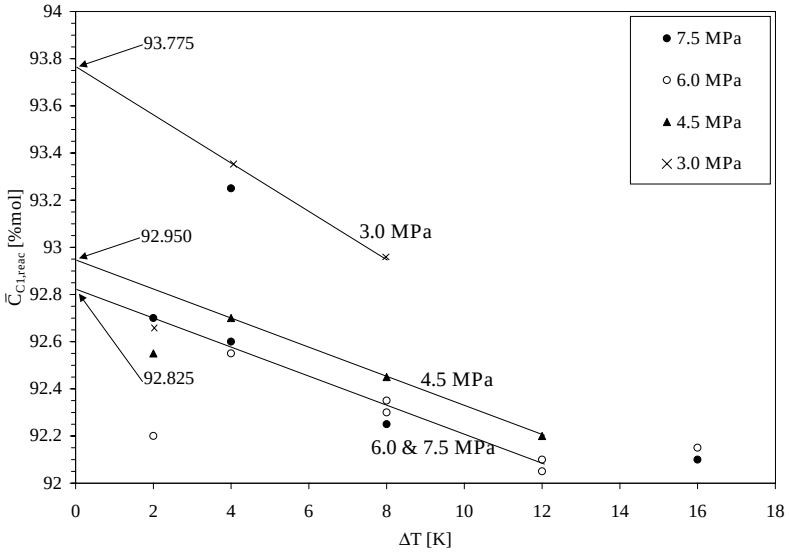

Figure D.1: Extrapolation of $\overline{C}_{C1,reac} = (C_{C1,feed} + C_{C1,reac})/2$ to $\Delta T = 0$. $C_{C1,reac}$ is the gas phase concentration of methane at the end of an experiment.

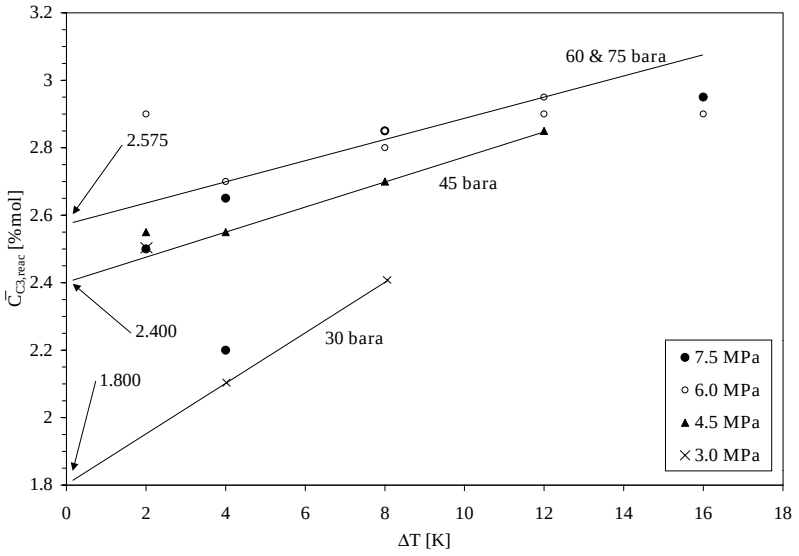

Figure D.2: Extrapolation of $\overline{C}_{C3,reac} = (C_{C3,feed} + C_{C3,reac})/2$ to $\Delta T = 0$. $C_{C3,reac}$ is the gas phase concentration of propane at the end of an experiment.

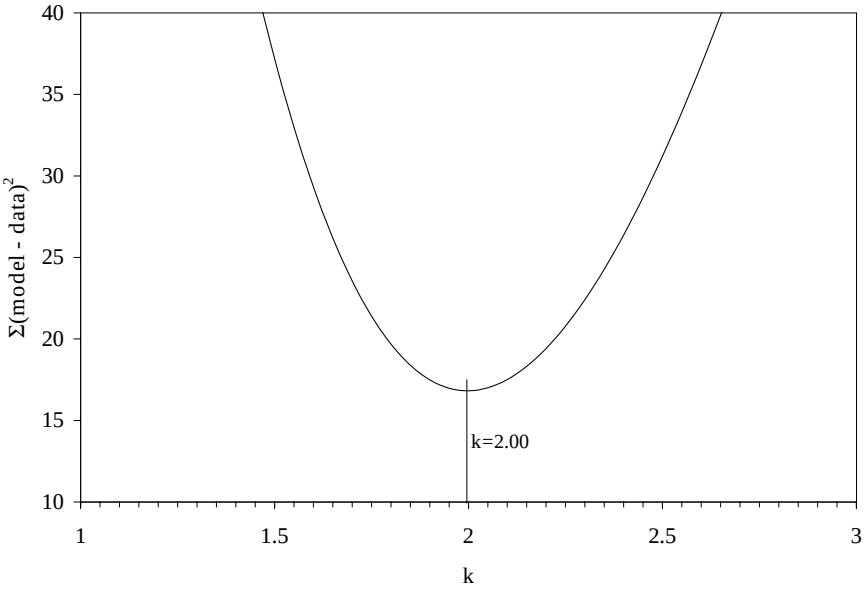

Figure D.3: Finding the system dependent k-value for methane at 7.5 MPa.

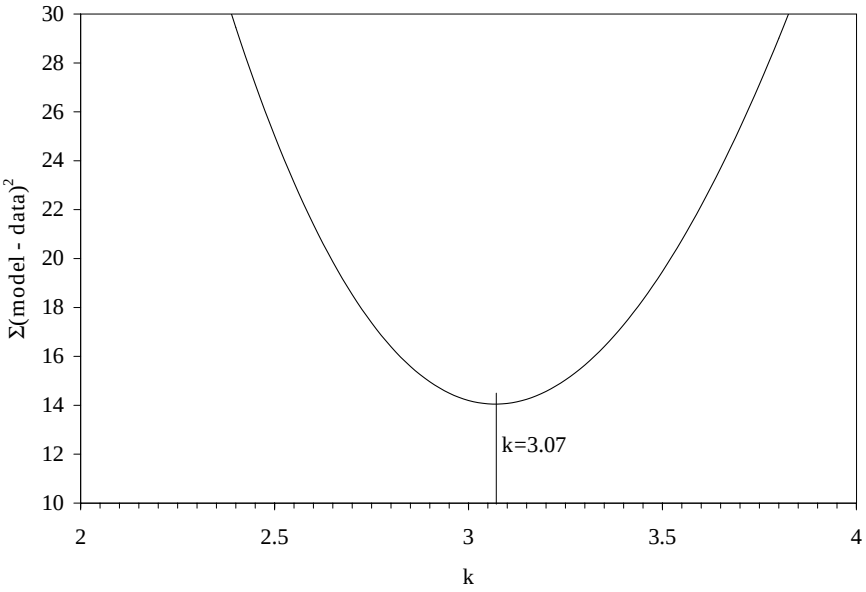

Figure D.4: Finding the system dependent k-value for methane at 6.0 MPa.

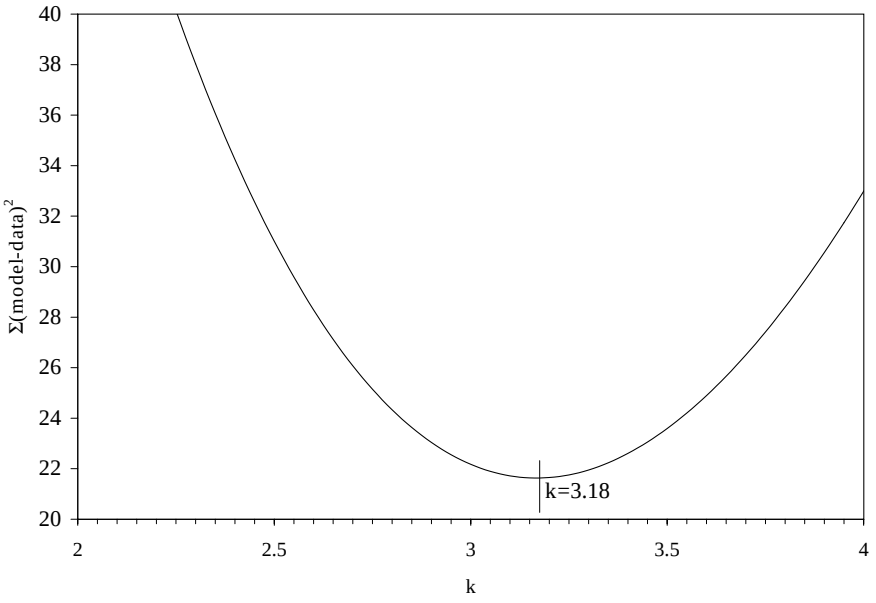

Figure D.5: Finding the system dependent k-value for methane at 4.5 MPa.

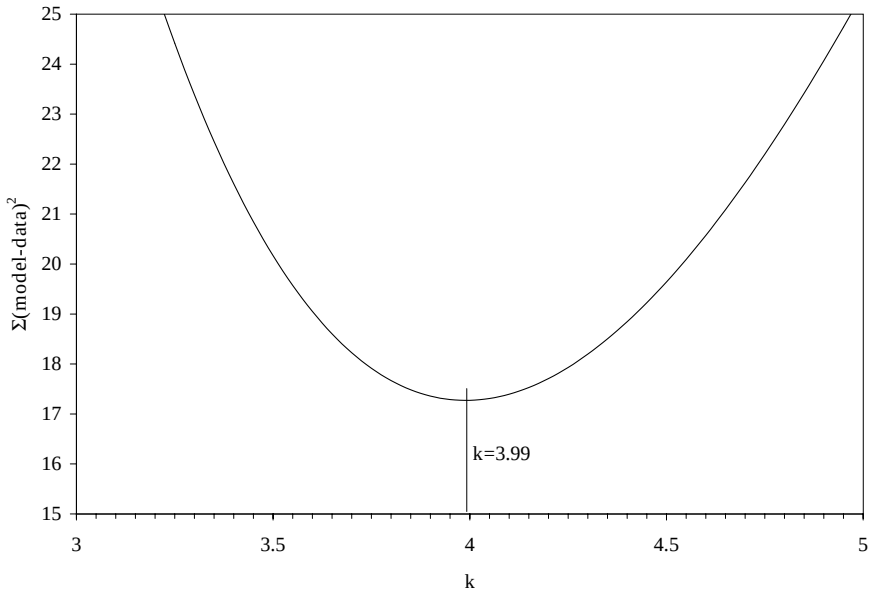

Figure D.6: Finding the system dependent k-value for methane at 3.0 MPa.

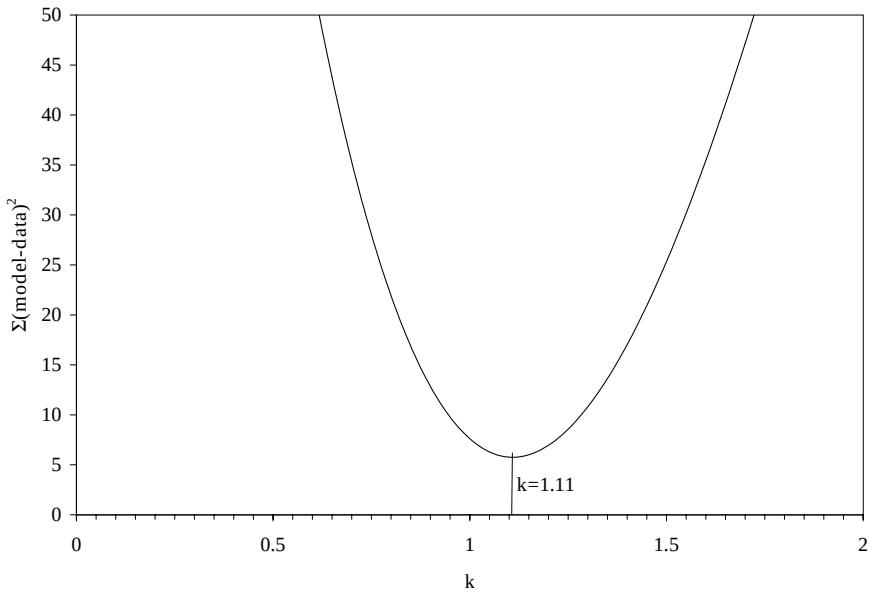

Figure D.7: Finding the system dependent k-value for propane at 7.5 MPa.

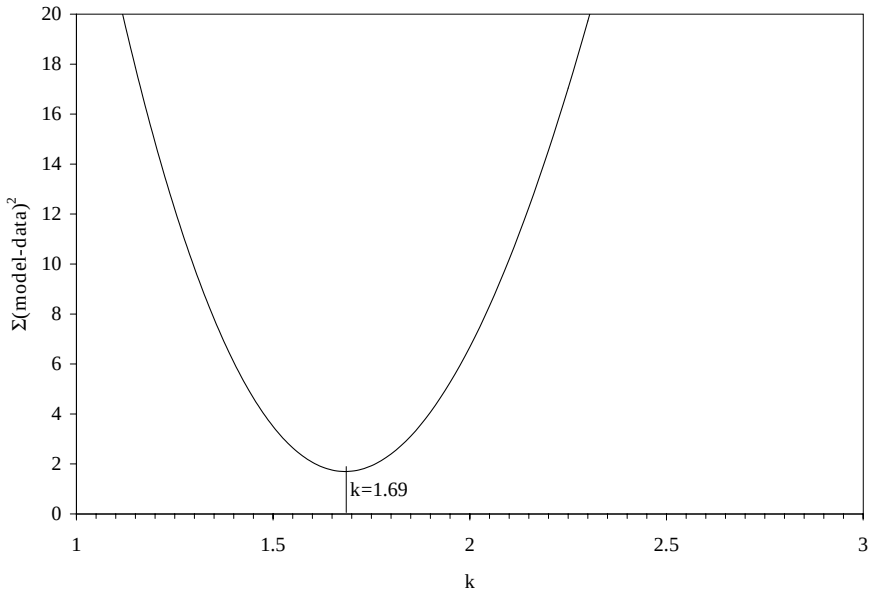

Figure D.8: Finding the system dependent k-value for propane at 6.0 MPa.

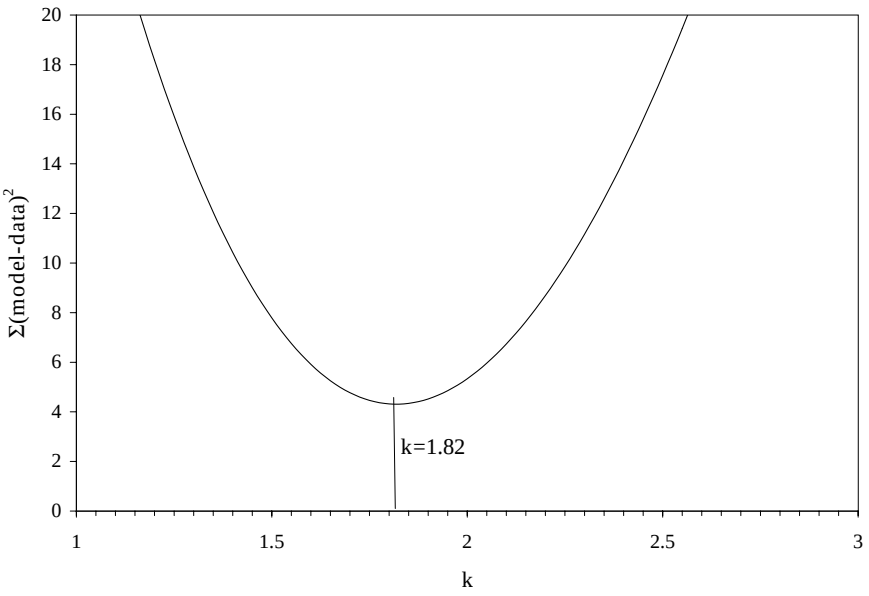

Figure D.9: Finding the system dependent k-value for propane at 4.5 MPa.

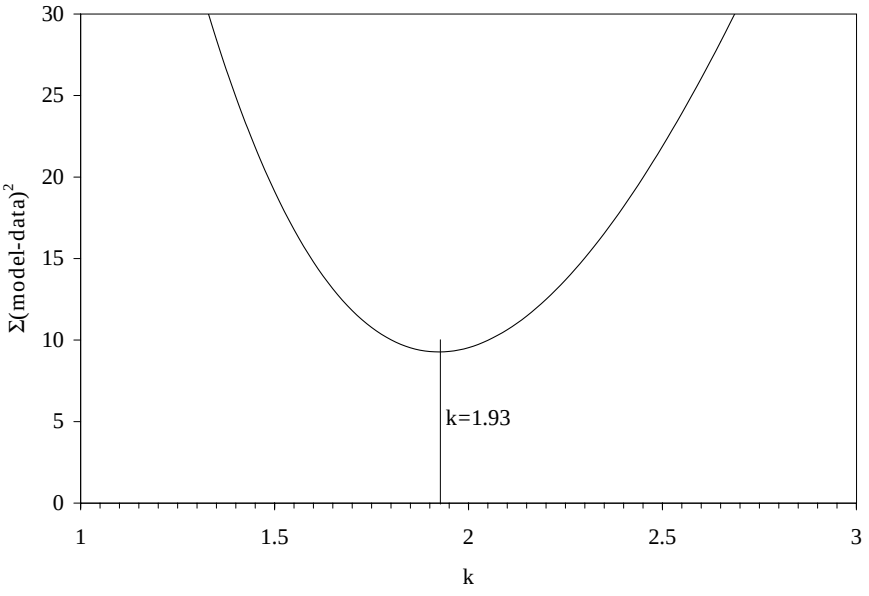

Figure D.10: Finding the system dependent k-value for propane at 3.0 MPa.

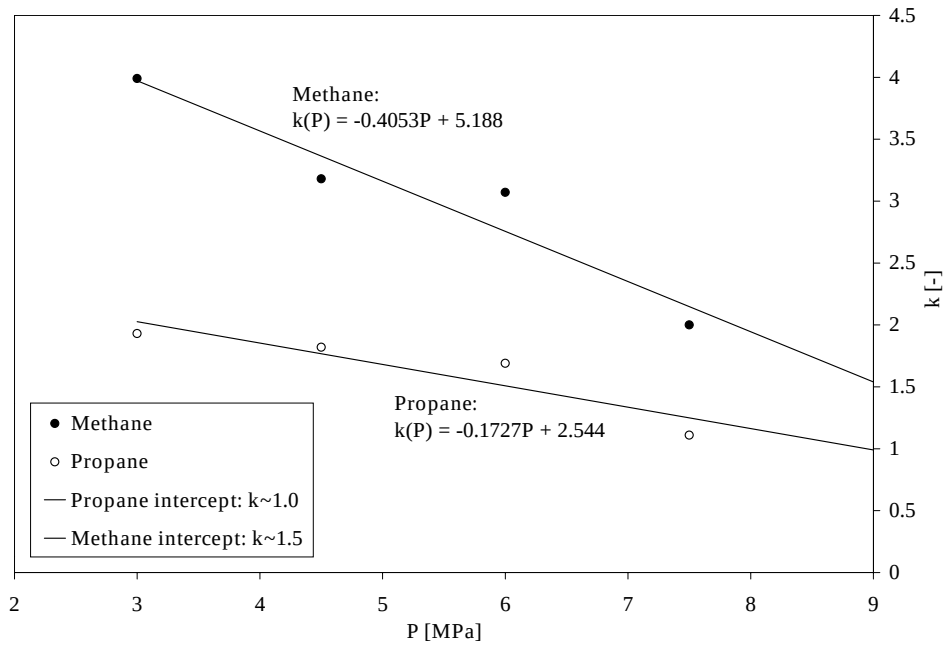

Figure D.11: Linear regression (extrapolation) of experimental k-values at 3.0, 4.5, 6.0 and 7.5 MPa to estimate k-values at 9.0 MPa.

Appendix E

List of Publications

The following publications were made as part of the present work:

Gudmundsson, J.S., Andersson, V., Levik, O.I. and Parlaktuna, M.: Natural Gas Hydrates: A new Gas-Transportation Form, J. Petrol. Technol. **51**(4):66-67, 1999.

Gudmundsson, J.S., Andersson, V., Durgut, I., Levik, O.I. and Mork, M.: NGH on FPSO - Slurry Process and Cost Estimate, SPE Annual Technical Conference and Exhibition, Houston, 3-6 October 1999. SPE paper 56629.

Levik, O.I. and Gudmundsson, J.S.: Calorimetry to Study Metastability of Natural Gas Hydrate at Atmospheric Pressure and Temperatures below 0 °C, 3rd. Intl. Conf. on Gas Hydrates, Salt Lake City, 18-22 July, 1999.

Gudmundsson, J.S., Andersson, V., Levik, O.I. and Mork, M.: Hydrate Technology for Capturing Stranded Gas, 3rd. Intl. Conf. on Gas Hydrates, Salt Lake City, 18-22 July, 1999.

Gudmundsson, J.S., Parlaktuna, M., Levik, O.I. and Andersson, V.: Laboratory for Continuous Production of Natural Gas Hydrates, 3rd. Intl. Conf. on Gas Hydrates, Salt Lake City, 18-22 July, 1999.

Gudmundsson, J.S., Andersson, V., Levik, O.I. and Parlaktuna, M.: Hydrate Concept for Capturing Associated Gas, SPE European Petroleum conference, The Hague, 20-22 October, 1998, SPE paper 50598.

Gudmundsson, J.S., Andersson, V. and Levik, O.I.: Gas Storage and Transport Using Hydrate, Proc. Offshore Mediterranean Conference, Ravenna, 19-21 March, **2**:1075-1083, 1997.